DEVELOPMENT OF GAS-PHASE ION/ION REACTIONS FOR CHARACTERIZING PROTEIN AND PEPTIDE IONS

by

Anthony Marcel Pitts-McCoy

A Dissertation

Submitted to the Faculty of Purdue University

In Partial Fulfillment of the Requirements for the degree of

Doctor of Philosophy

Department of Chemistry

West Lafayette, Indiana

August 2021

THE PURDUE UNIVERSITY GRADUATE SCHOOL
STATEMENT OF COMMITTEE APPROVAL

Dr. Scott A. McLuckey, Chair

Department of Chemistry

Dr. Corey Thompson

Department of Chemistry

Dr. Hilkka Kenttamaa

Department of Chemistry

Dr. Jean Chmielewski

Department of Chemistry

Approved by:

Dr. Christine Hrycyna

Dedicated to my family and friends, my success is our success.

&

To my Uncle Keith McCoy and my Grandparents Walter and Georgia Pitts, I hope to be a blueprint to the younger generation as you were to me.

ACKNOWLEDGMENTS

This work was possible because of dedicated family, friends, and mentors who drive and inspire me to continue to grow. I want to thank my parents, Tracey and Robaire who raised me to understand the value of education as a steppingstone to chase my dreams. I want to thank my Grandmothers Alicia and Georgia for unknowingly inspiring my love of chemistry through their love of cooking for our family. You all provided, disciplined, and were my first teachers. To my Grandfathers Walter and Paul, thank you for showing the importance of service to others. To brothers and sister Antuan, Robbie, and Georgia, thank you for all your love, support, and competition (I'm winning). To my closest friends Daryel, Diamond, Kiara, Jeremy, Tiara, Kendall, and Chrismond, thank you for the support and love. Y'all are so dope. The memories we share never need to be shared with anyone else but will always be cherished (DnD).

To my Chicago State Family, Dr. Mardis, Dr. Goss, and Dr. LeSuer, thank you for showing me how far chemistry could take me. You have expanded my view on what is possible through hard work and good science. I want to acknowledge some of people I have met throughout my scientific career. I want to thank Diane Mankin, Anabel Laza, and Tim Clopp. I met you all on my journey to Purdue and you have all worked to maintain our friendship throughout the years. These simple acts always encouraged me, and you all are fantastic in your own ways.

During my time at Purdue, there have been so many people who have offered encouraging words or kind gestures it would be impossible to name them all. Chris Pulliam and Stella Betancourt, thank you both for all your mentorship. Your kindness and willingness to embrace me is what brought me to Purdue. You showed me that I can belong in any room, but I must put the work in. Thank you Tsdale, you always surprised me and helped me grow as a scientist, but always reminded me where I came from. To John Andjaba, thank you for putting up with all my antics and being a great roommate and a better friend. It has been an honor to grow with you. To Ms. Natasha Harris, you have been a fundamental part of my support system here at Purdue. You have put me in rooms with giants and there is no way I can thank you for all you have done for me. To Reena B. and Tamika, thank you both for every kind word, helping hand, and hard lesson. You two truly have black girl magic. To Dr. Chmielewski, Nicole Escorcia, Jocelyn Nardo, Atheena Jenkins, Jennifer Garcia, and Ana Morales, Kristos Negron, Edwin Gonzalez, working with you

all in the CDI helped me to remain steadfast pursuing goals that I hold very close to my heart. I hope the next generation of students follow your lead and continue the pursuit of equality and inclusion.

I must acknowledge my group members current and former who I've learned so much from. I must thank Fei Fei, Nan, Mack, Eric, Dave, Josh, and Andrew, you all have offered so much advice and great conversations. I must acknowledge Elissia and Chris, you two have been essential to my success here at Purdue and a few hangovers. Thank you for all the great times and memories. To De'Shovon and Abdi I appreciate every moment I was able to act as a mentor to you both. It has been a blessing to watch you both grow and become leaders in our group and the department. To His-Chun and Jay, I have learned so much from you and I hope you continue to teach younger students. To Kim, Alex, Angie, Sam, Nicole, Nick, Zach, and Sarah I want to wish you the best of luck as you continue on your journey.

I would like to thank my committee for all their support and advice throughout the years. I would like to acknowledge my advisor Scott for all the great insight you have given me. I am truly grateful for the group culture you've cultivated and the opportunity to be a part of (in my opinion) the best group in the university. There are many names of people who I may have forgotten to mention but I appreciate you too. Please charge this absence to my head not my heart. Thank you.

TABLE OF CONTENTS

LIST OF FIGURES 10
ABSTRACT 14
CHAPTER 1. INTRODUCTION TO GAS-PHASE ION/ION CHEMISTRY AND MASS SPECTROMETRY 15
1.1 Electrospray 15
1.1.1 History 15
1.1.2 Ionization Mechanism 16
1.1.3 Taylor Cone 17
Models 18
1.1.4 Nanospray 18
1.2 Mass Analyzers 19
1.2.1 Quadrupoles 19
Design 19
Ion Trapping and Stability 19
Ion Isolation 20
Mass Analysis and Detection 21
1.2.2 Time of Flight 21
Design 21
1.2.3 Hybrid instruments 22
Sciex 4000 Triple Quadrupole 22
Sciex 5600 TripleTOF 23
1.3 Tandem MS 23
1.3.1 Collisional Activation 24
1.3.2 Ion Trap CID 24
Beam-type CID 24
Dipolar Direct Current CID 24
1.3.3 Peptide Fragmentation 25
1.4 Ion/ion Reactions 26

1.4.1 Mutual storage of oppositely charged ions 27
1.4.2 Gas-Phase Covalent Modification 28
1.4.3 Applications 28
1.5 Conclusions 29
1.6 References 30
1.7 Figures 38
CHAPTER 2. GAS-PHASE ION/ION CHEMISTRY AS A PROBE FOR THE PRESENCE OF CARBOXYLATE GROUPS IN POLYPEPTIDE CATIONS 44
2.1 Introduction 44
2.2 Experimental 47
2.2.1 Materials 47
Reagent synthesis 47
Peptide methyl esterification 47
Carboxyl O^{18} Labeling 47
2.2.2 Mass Spectrometry 48
2.3 Results and Discussion 48
2.3.1 HOBt-TMAB and Ac-AADAADAA-Ome 48
2.3.2 Sulfobenzoyl HOBt and Ions Derived from YGRAR 49
2.3.3 Sulfobenzoyl HOBt and YRARG 52
2.3.4 Sulfobenzoyl HOBt and Ubiquitin $[M+7H]^{7+}$ 53
2.4 Conclusions 54
2.5 References 56
2.6 Figures 60
CHAPTER 3. GAS PHASE CROSS-LINKING OF PROTEIN COMPLEXES VIA ION/ION REACTIONS 79
3.1 Introduction 79
3.2 Experimental 80
3.2.1 Materials 80
Ubiquitin 80
Trypsin and Aprotinin 80
Reagents 80

3.2.2 Mass Spectrometry 81
3.3 Results and Discussion 81
3.3.1 Ubiquitin 81
3.3.2 Trypsin & Aprotinin 83
3.4 Conclusions 83
3.5 References 85
3.6 Figures 87
CHAPTER 4. DEVELOPMENT OF NEGATIVE MASS ANALYSIS OF MACROMOLECULAR ANALYTES VIA MULTIPLY CHARGED ION ATTACHMENT (N-MAMA-MIA) FOR MASS DETERMINATION OF PROTEIN COMPLEXES 95
4.1 Introduction 95
4.2 Experimental 99
4.2.1 Materials 99
Sample preparation for native mass spectrometry of bio-complexes 99
Reagent preparation 99
4.2.2 Mass spectrometry 99
4.2.3 Simulation 100
Results and Discussion 101
4.2.4 β-Galactosidase 101
4.2.5 GroEL Chaperonin 102
4.2.6 Ribosome 30S/50S 103
4.3 Conclusion 105
4.4 References 107
4.5 Figures 109
CHAPTER 5. CHARGE INVERSION OF LARGE PROTEIN COMPLEXES VIA MASS ANALYSIS OF MACROMOLECULAR ANALYTES VIA MULTIPLY-CHARGED ION ATTACHMENT(MAMA-MIA) 125
5.1 Introduction 125
5.2 Experimental 126
5.2.1 Materials 126
Sample preparation for native mass spectrometry of bio-complexes 126

Reagent preparation 127
5.2.2 Mass Spectrometry 127
5.3 Results and Discussion 127
5.3.1 Cesium iodide for instrument calibration 127
5.4 Conclusions 128
5.5 References 129
5.6 Figures 131
LIST OF PUBLICATION 136
VITA 137

LIST OF FIGURES

Figure 1.1. Generic electrospray ionization set up 38

Figure 1.2 Mathieu stability diagram showing stability of ion in a quadrupolar field 39

Figure 1.3 A schematic of a Sciex 4000 QTRAP modified for ion/ion reactions 40

Figure 1.4 A schematic of a Sciex 5600 TripleTOF modified for ion/ion reactions 41

Figure 1.5 Schematic of the quadrupole mass analyzer along the x axis with DDC CID available on the Sciex 5600 TripleTOF in q0 and q2..... 42

Figure 1.6 A schematic of the nomenclature system of protonated peptides and proteins when activated in mass spectrometry 43

Figure 2.1 Product ion spectra derived from (a) Ion-ion reaction between [Ac-ADAADAA-Ome-2H]$^-$ and [TMAB-HOBt]$^+$ (b) CID of complex [M-2H+(TMAB-HOBt)]$^-$ (c)CID of [M-2H+TMAB]$^-$ Formation of the [M-H-H_2O]$^-$ (indicated by the blue outline)..... 60

Figure 2.2 Reaction between the carboxylate group in a doubly-deprotonated Ac-AADAADAA-Ome with deprotonation at both the aspartic acid side chains with a positively charged TMAB HOBt 61

Figure 2.3 Distribution of 18O heavy labeled [YGRAR+2H]2+ b) isolation of mass corresponding to the exchange of 2 heavy oxygens 62

Figure 2.4a.) Ion-ion reaction spectrum showing formation of a) [YGRAR+2H+Sulfobenzoyl HOBt]+ b.) [YGRAR-OMe+2H+Sulfobenzoyl HOBt]+ c.) [O18-YGRAR+2H+Sulfobenzoyl HOBt]+ and d.) [ac-YGRAR+2H+Sulfobenzoyl HOBt]+. 63

Figure 2.5 Ion trap CID of the complexes [M+2H+SB-HOBt]$^+$ generated via ion/ion reactions between deprotonated SB-HOBt and doubly protonated (a) YGRAR, (b) YGRAR-OMe, (c) O^{18}-YGRAR, and (d) ac-YGRAR. (Shaded regions indicate where [M+2H+Sulfobenzoyl]$^+$ would be formed.) ↙ indicates parent ion 64

Figure 2.6 Different charge site isomers of [M+2H+Sulfobenzoyl HOBt]+..... 65

Figure 2.7 Reaction between the carboxylate group in a doubly-charged YGRAR with protonation at the N-terminus and both arginine residues with deprotonated SB-HOBt. 66

Figure 2.8 Ion trap product ion spectra obtained from the nominal [M-H_2O]$^+$ ions derived from a) ion/ion reaction between doubly protonated YGRAR and deprotonated SB-HOBt followed by loss of HOBt and b) CID of singly protonated YGRAR. 67

Figure 2.9 Ion trap CID spectrum of the [M+H+sulfobenzoyl]+of M= 18O-YGRAR shows the presence of [M+H-H218O]+ (shaded region) (□ indicates a mass shift of 183 Da corresponding to the addition of Sulfobenzoyl). 68

Figure 2.10 Process leading to loss of carbodiimide following water loss from a protonated peptide with a C-terminal arginine. 69

Figure 2.11 a.) Ion-ion reaction between YRARG2+ (m/z 311) and Sulfobenzoyl HOBt-formation of the long-lived complex. b.) Shows the formation of [YRARG+ Sulfobenzoyl]+ after CID of the complex. 70

Figure 2.12 Ion trap CID spectrum of [YRARG+H+Sulfobenzoyl]+ shows the presence of [M+H-H2O]+ (shaded region) (□ indicates a mass shift of 183 Da corresponding to the addition of Sulfobenzoyl)..... 71

Figure 2.13 Comparison of ion trap CID product ion spectra derived from the $[M-H_2O]^+$ ions generated (a) via ion/ion reaction between deprotonated SB-HOBt and $[YRARG+2H]^{2+}$ and (b) CID of $[YRARG+H]^+$. 72

Figure 2.14 Comparison of ion trap CID results from $[M+6H-H_2O]^{6+}$ ions derived from ion/ion reaction (top) and ion trap CID of the $[M+6H]^{6+}$ion (bottom). 73

Figure 2.15 a) Post ion/ion reaction spectrum of [M+7H]7+/[SB-HOBt-H]- showing residual unreacted [M+7H]7+ and electrostatic complex generated by attachment of the reagent anion to the cation. b) Ion trap CID of the electrostatic complex without prior removal of 75

Figure 2.16 Ion trap CID spectrum of the [M+sulfobenzoyl]6+covalent adduct generated by the experiment of Figure S 2.5(b). (M=Ubiquitin) 76

Figure 2.17 Comparison of ion trap CID results from [M+6H-H2O]6+i/i rxn (top) and [M+6H-H2O]6+CID ion (bottom). (M = Ubiquitin) Water loss ions with major differences in relative abundances in the top versus bottom spectrum are labeled in blue font where water loss..... 77

Figure 2.18 Ubiquitin sequence showing products of CID of the [M-H2O]6+ from the ion/ion reaction and [M+6H-H2O]6+ formed from CID 78

Figure 3.1 Shows a MS spectrum with the isolation of the [monomer+4H] and $[dimer+8H]^{8+}$ of ubiquitin (inset Zoom in of the isotopic distribution confirming dimer formation)..... 87

Figure 3.2 Shows rf/DC isolation of the double deprotonated crosslinker Sulfo EGS..... 88

Figure 3.3 Shows the mutual storage of the $[D+9H]^{9+}$ and $[Sulfo\ EGS-2H]^{2-}$leading to formation of the electrostatic complex $[D+9H+Sulfo\ EGS]^{7+}$ 89

Figure 3.4 Shows SWIFT isolation of electrostatic complex $[D+9H+Sulfo\ EGS]^{7+}$ in q2 90

Figure 3.5 Shows the CID spectrum of electrostatic complex $[D+9H+Sulfo\ EGS]^{7+}$ resulting in dissociation of the protein complex (complementary pairs shaded in blue and green) and covalent modification (shaded in red) 91

Figure 3.6 Shows the CID spectrum of modified complex $[D+9H+Sulfo\ EGS-2Sulfo\ NHS]^{7+}$ resulting in fragment ions and complementary crosslinked monomer and peptide fragments..... 92

Figure 3.7 Shows the CID spectrum of electrostatic complex $[AT+11H+Sulfo\ EGS]^{9+}$ resulting in dissociation of the protein complex (complementary pairs shaded in yellow and orange) and loss of a Sulfo NHS moiety 93

Figure 3.8 Shows the CID spectrum of modified complex $[AT+11H+Sulfo\ EGS-2Sulfo\ NHS]^{9+}$ resulting neutral losses..... 94

Figure 4.1a.) a MS spectrum of β-Galactosidase tetrameric complex from a negative nanoESI source. b.) Shows incorporation of SWIFT isolation of a group of charge states. c.) shows SWIFT isolation of the 37- charge state of the β-galactosidase 109

Figure 4.2 Mass spectra of the charge state envelope of β galactosidase in positive mode(black) and negative mode(red)..... 110

Figure 4.3 The MS spectrum of myoglobin sprayed under denaturing conditions showing charge states between 23+ and 12+ * and m/z of 616 denotes loss of the heme group 111

Figure 4.4 Shows the isolation of the a.) 20+ charge state and b.)15+ charge state of apo-myoglobin 112

Figure 4.5 Shows the ion/ion reaction between a.) the 37- charge state of β-Galactosidase and [myo+15H]15+b.) the 37- charge state of β-Galactosidase and [myo+20H]20+c.) the entire charge state envelope of β-Galactosidase and [myo+15H]15+ 113

Figure 4.6 A mass spectrum of GroEL chaperonin sprayed in the negative mode showing charge states from 57- to 50- 114

Figure 4.7 Shows the a.) MS spectrum of carbonic anhydrase under denaturing conditions and the rF/DC isolation of the 20+ charge state and c.) the 30+ charge state. 115

Figure 4.8 Shows a MAMA-MIA reaction between the charge state envelope of GroEL and a.) [CA+20H]20+b.) [CA+30H]30+ 116

Figure 4.9 A overlay of mass spectra of GroEL chaperonin sprayed under negative mode obtained under low collisional energy upon injection (black) and high collisional energy (red)117

Figure 4.10 4.10 MS spectrum of a MAMA-MIA reaction between GroEL and [CA+30H]30+ after changing increasing collisional energy with ion transmission (red trace) compared to previous conditions (black trace). Inset shows a zoomed view of the first adduction..... 118

Figure 4.11 Shows the MS spectrum of ribosomal proteins under native conditions with a.)"gentle" injection and transfer conditions, b.) “harsh” injection and transfer conditions to drive off adducts, and c.) with 10 mM Mg2+ to maintain the intact 70S complex 119

Figure 4.12 Shows a MS spectrum taken optimal conditions with ion desolvation allowing for observation of various components and charge states 120

Figure 4.13 Shows the SWIFT isolation of the 30S ribosome. The insert shows a zoomed spectrum of the isolated distributions with multiple components. 121

Figure 4.14 Shows the MAMA MIA reaction between the isolated charge state envelope of 30S and 10+ charge state of ubiquitin denoted as [Ubi+10]10+showing 2 attachments with the second attachment separating the three components denoted as 800 kDa, (blue triangle) 85..... 122

Figure 4.15 Shows the SWIFT isolation of the unresolved 50S ribosome under gentle conditions. 123

Figure 4.16 Shows a MAMA MIA reaction between an isolated distribution of the 50# ribosome and [CA+20H]20+ showing features give mass estimates of 1,634 kDa (blue) and 1,808 kDa (orange) 124

Figure 5.1 A MS spectrum of CsI in the negative mode 131

Figure 5.2 A spectrum showing a proton transfer reaction between beta galactosidase and proton sponge 132

Figure 5.3 A spectrum showing the entire charge state charge inverted Beta Galactosidase after three attachments (shaded in red) of $[myoglobin+20H]^{20+}$ 133

Figure 5.4 A spectrum showing charge inverted GroEL after two (shaded in orange) and three attachments (shaded in red) of $[carbonic\ anhydrase+30H]^{30+}$ 134

Figure 5.5 Shows the MS spectrum of carbonic anhydrase with dimer peaks shaded blue 135

ABSTRACT

Mass spectrometry-based gas-phase ion/ion reactions have grown considerably in the last decade. Their applications range from structural elucidation, instrument calibration, and spectral deconvolution. One field that has been amenable to these methods is proteomic studies. Proteins and peptides have grown as candidates for biomarkers and vaccines. Proteins are vastly different with mass ranging from 1 kDa to well over 1 MDa and various types of post translational modifications. The structural heterogeneity that proteins can exhibit demonstrates the need for high resolution mass spectrometry methods. The combination of native mass spectrometry and soft ionization sources allow for preservation of structures seen in solution as analytes enter the gas phase. By developing methods that probe these structures, the information gathered can be related to the native structures in solution. Here I show, gas phase ion/ion reactions that can be utilized for location of salt bridge structures, gas-phase crosslinking of homo and heterodimer protein complexes, and mass determination of large (>800 kDa) protein complexes. These methods allow for greater control, faster data acquisition, and minimal sample preparation. These methods were developed on modified Sciex TripleTOF 5600 and 4000 QTRAP tandem mass spectrometers.

CHAPTER 1. INTRODUCTION TO GAS-PHASE ION/ION CHEMISTRY AND MASS SPECTROMETRY

Since its invention by J.J. Thomson and F.W Aston [1–3], mass spectrometry has grown to be one of the most versatile and robust analytical techniques available. Mass spectrometry has allowed for the analysis for a broad range of compounds and impacted a wide range of fields. In its simplest form, a mass spectrometry experiment consists of three segments: ionization of analyte, ion manipulation, and detection of analyte. These types of experiments are performed in different types of mass spectrometers across the world. Data is outputted as spectrum of peaks at different mass to charge (m/z) ratios. Here, experiments will be described that use mass spectrometry to understand the gas phase structures of proteins and peptides.

1.1 Electrospray

As the first part of a mass spectrometry experiment, the ionization of the analyte of interest. there are numerous techniques available. Some factors that influence the choice of ionization are compatibility with analyte, robustness, and information to be gained post-ionization. This work focuses on a variant of electrospray ionization (ESI) for numerous reasons that will be described below.

1.1.1 History

Prior to the "soft" ionization techniques available today, many ionization techniques were not amendable to ionization of proteins and peptides. Electron ionization (EI) was one of the first available ionization sources.[4–6] EI utilizes bombardment of the analyte by electrons to eject or capture an electron producing a radical cation or radical anion, respectively. Electrons are introduced into a sample by heating a filament and producing an electron beam. Once the electron (e^-) encounters the analyte (M), the reaction proceeds as shown for the formation of a radical cation ($M^{+\bullet}$). (Eq 1.1)

$$M + e^- \rightarrow M^{+\bullet} + 2e^- \quad (1.1)$$

EI exposes 70 eV kinetic energy electrons to the analyte which exceeds both the ionization energy and the thresholds of many bond dissociations such that fragmentation is likely to occur.

This type of ionization is most useful for the analysis of organic molecules because the fragmentation patterns are highly reproducible under typical conditions. This allows for compounds to be "fingerprinted" based on the fragmentation pattern observed. Typically, EI is most useful for molecules with a mass less than 600 Da as the fragmentation patterns are relatively easy to interpret. Larger ions tend to fragment more extensively producing secondary fragments and convoluting spectra. This also prevents measurement of the mass of the intact ion, as there is little to no $M^{+\bullet}$ ion remaining. Another limitation of EI is that it requires molecules to be in the gas phase prior to ionization. These reasons make EI unsuitable for peptide and protein analysis as these compounds commonly have masses ranging from hundreds of Daltons to complexes with mass well over a 1 MDa and are thermally labile with low volatility. This has led researchers to develop ways to ionize larger molecules and maintain intact ions.[7, 8] Although there were numerous other ionization techniques that arose after EI, the breakthrough experiments were performed by Malcom Dole. Dole's experiments used the first electrospray to nebulize polymer ions into the gas phase. In this process, Dole formed highly charged droplets containing the analyte and as the solvent evaporates, only gaseous analyte ions remain. These results were critical to John Fenn's experiments who is credited with development of electrospray for use in biological mass spectrometry.[9] Fenn's experiments with ESI and the parallel development of matrix assisted laser desorption ionization (MALDI) led to more ionization techniques typically coined "soft" ionization techniques.[10, 11] Soft ionization techniques have grown vastly since, with researchers combining aspects of multiple techniques with hopes to develop a universal ionization technique.[12] A universal technique is still a long way off, but it is necessary to understand the processes that drive ESI ionization and factors that can affect it.

1.1.2 Ionization Mechanism

To understand the types of ions one observes in a mass spectrum one must understand how ions entered the gas phase. Electrospray ionization has been well studied and can be separated into three stages; production of charged droplets containing the analyte of interest, removal of solvent due to evaporation, and production of gas phase ions from the droplet.[13, 14] **Figure 1.1** shows a schematic of a generic ESI source in positive mode producing cations via one or more processes described below.

1.1.3 Taylor Cone

In a generic electrospray set up, an electric field is established between a capillary holding a dilute solvent containing the analyte with a typical inner diameter of <100 μm and the orifice of the mass spectrometer. The forces of columbic attraction to the orifice and surface tension of the solvent cause the liquid at the end of the capillary to form an elliptical shape. Once the voltage is applied and surface tension is overcome, at the very tip of the "cone" droplets will be ejected. This phenomenon is called a Taylor cone after it's discoverer Sir Geoffrey Taylor.[15]

To produce a Taylor cone, the electric field (E_0) at the capillary tip must overcome the surface tension of the solvent containing the analyte. An electric field can be expressed by the equation

$$E_0 \approx \frac{4V_C}{[r_c / (\ln 8 / r_c + \ln x_0)]} \approx \frac{2V_C}{[r_c \ln \frac{4x_0}{r_c}]} \tag{1.2}$$

where V_C is the applied potential, r_c is the outer radius of the capillary and x_0 is the distance between the tip of the capillary and the orifice. The electric field needed to ionize a sample can be defined as

$$E_0 = [\frac{2T\cos\theta}{\varepsilon_0 x_0}]^{1/2} \tag{1.3}$$

Where T is the surface tension of the solvent, θ is the half angle of the Taylor cone, and ε_0 is the permittivity of the liquid. By combining equation 1.1 and equation 1.2 one can relate voltage applied (V_{on}) to produce an electrospray. This is shown in Equation 1.4.

$$V_{on} = [\frac{r_c T\cos\theta}{2\varepsilon_0}]^{1/2} \ln(\frac{4x_0}{r_c}) \tag{1.4}$$

The Taylor cone produced shown in **Figure 1.1** ejects charged droplets. As these droplets move through the atmosphere towards the orifice of the mass spectrometer. As these droplets move through air the solvent will evaporate and the charge will build up causing coulombic fission producing smaller droplets. This phenomenon is dictated as droplets approach the Raleigh limit which is described as

$$q = 8\pi(\varepsilon T R^3)^{1/2}$$

(1.5)

Where *q* is the charge of the droplet and R is the radius of the droplet. These droplets will undergo coulombic fission and produce smaller progeny droplets which will repeat this process until the analyte enters the gas phase.[16, 17]

Models

There are several models that are theorized to govern the process for ions entering the gas phase. The charge residue model and the chain ejection model are well received models that provide explanations for the types of ions witnessed after electrospray ionization.[18] The charge residue mechanism (CRM) theorizes that as droplets evaporate charges are deposited onto the nonvolatile analyte. It is proposed that proteins that are ionized under native conditions, maintain the native structure when undergo ionization. This model assumes there is one analyte per droplet and that the available charge is dictated by the Raleigh stability limit. The chain ejection model (CEM) is used to explain the ejection of unfolded polymer chains such as denatured proteins. In CEM, the proteins are elongated and as the solvent evaporates the analyte leaves droplet while withdrawing charges from the droplet. The combination of these two models called the combined charged residue field emission model, can be used to explain the differences of observed charge states between unfolded or denatured proteins and proteins with maintained native structures.[19] Another factor that can affect this process is the radius of the droplet formed. This has motivated? research into discovering ways to reduce droplet size by reducing the size of the electrospray source.

1.1.4 Nanospray

By reducing the radius of the capillary used in electrospray there are several benefits provided. The first improvement is a reduction voltage required to achieve the same electric field needed to induce a Taylor cone.[20, 21] This allows for lower voltages to be used to ionize analytes. There have also been studies that have shown a higher tolerance to nonvolatile salts that may contaminate samples.[22] For experiments described here dual nanoelectrospray (nESI) emitters are used consisting of borosilicate capillary tips with one emitter used to produce cations and the other to produce anions.[23, 24] Tips were pulled using a Flaming/Brown micropipette

puller (P-87, Sutter Instrument Co., Novato CA) to an outer diameter of ~10 µM. The emitters are pulsed sequentially using applied voltages of 12-24 kV. Protein concentrations were typically 10 µM in either 150-200 mM ammonium acetate for native conditions or 50:50 H_2O: Methanol (MeOH) with 1-5% acetic acid for denaturing conditions. Reagent concentrations typically were in the micro to sub millimolar range to have adequate number density for the reactions described below.

1.2 Mass Analyzers

Similar to ionization, instrumentation has grown significantly in the last three decades with many of these advances leading to improved mass analyzers. There are numerous developments in instrumentation that have led to improved analysis of proteins and protein complexes. Below are descriptions of developments that have relevant to the instruments used for many of the experiments detailed.

1.2.1 Quadrupoles

The most common mass analyzer is the quadrupole. Quadrupoles have the capabilities to trap, filter, and analyze ions making them some of the most versatile analyzers available. The experiments described here make use of a linear quadrupole ion trap (LIT).[25, 26]

Design

Quadrupoles consist of four parallel metal rods. These rods are typically cylindrical as an approximation to the ideal hyperbolic shape. There are other examples of ‘multi-pole” designs, such as hexapoles and octupoles, that are sometimes used as ion transmission devices. However, they do not offer as much flexibility for ion isolation and manipulation as do quadrupole LITs. Therefore, in the experiments discussed below a quadrupole design is used.[25–27]

Ion Trapping and Stability

Quadrupoles have the capability to store ions in theory for an infinite amount of time. However, ion molecule reactions and collisions with background gases will deplete ion population over time. Ion storage is possible by applying DC or RF potentials to electrodes placed at the ends

of the quadrupoles. Ions in a quadrupolar field have a defined motion that can be determined by the Mathieu equation.[28, 29] There are two types of potentials that can be applied to quadrupoles for experiments described below. RF potentials and DC potentials allow for stabile transmission of ions and ion isolation. For a given set of rods of inscribed radius, $r_{o,}$ only certain combinations of RF and DC potentials result in stable ion motion within the quadrupole array. It is convenient to relate the operating conditions of a quadrupole array in terms of the dimensionless quantities 'q' and 'a', which are proportional to the RF and DC amplitudes, respectively. The q value for an ion can be determined using

$$q = \frac{4eV}{mr_o^2\Omega^2} \tag{1.6}$$

where *m* is the mass of the ion, *V* is the RF potential applied, r_o is the radius of the trap, Ω is the radial frequency of the RF potential, and *e* is the elementary charge. The a-value can be derived using

$$a = \frac{8eU}{mr_o^2\Omega^2} \tag{1.7}$$

where *U* is the DC potential. The combinations of q- and a-values that lead to stability in both the x-and y-dimensions are summarized in the so-called Mathieu stability diagram shown in **Figure 1.2**. By manipulating q- and a- values it is possible to isolate ions of interest to perform tandem MS experiments also known as MS^n.[30, 31] In **Figure 1.2**, the colored region indicates the a- and q-values where ions are stable and overlap so ions are stable in both dimensions. There are additional regions of overlap but this region is the most used. Mass and q values are inversely related so as the q value increases the smaller the mass until the boundary of q = 0.908 where ions lose stability. The m/z-value where q = 0.908 is commonly referred to as the low mass cut-off (LMCO).

Ion Isolation

By neglecting to apply a DC potential, the a-values equate to zero allowing a wide range of m/z to be stable. This allows operators to take advantage of the narrowing shape of the stability region as a-values are increased. Increasing a-values reduce the mass range and limit which ions

are stable within the LIT. If an ion with a particular m/z has a q-value of 0.706, the a-value can be raised to 0.237. This would reduce the range of m/z values to a single m/z that would remain in the trap. This known as RF/DC isolation and is commonly employed in the experiments detailed below.

Mass Analysis and Detection

Ions are typically analyzed using a quadrupole by one of two methods: the first method takes advantage of the boundary of the q value at 0.908. By ramping the rf potential with no DC applied (a =0) ions are ejected linearly towards the detector. The second detection method which is utilized in Sciex instrument described below is known as mass selective axial ejection or MSAE.[32] This technique takes advantage of the fringe fields. These fringe fields are caused by the lenses used to trap ions in a linear ion trap these fields cause a cone of reflection. Ions are excited radially and once the overcome this cone they are ejected. This process is mass selective as ions come into resonance with the increasing rf potential. Ions are ejected from smallest m/z to largest towards an electron multiplier detector. For the experiments detailed below using a quadrupole as a mass analyzer, MSAE is utilized as the detection method.

1.2.2 Time of Flight

Another common mass analyzer is the Time of Flight (TOF) mass analyzer. It can be considered one of the simplest mass analyzers and offers a theoretically unlimited mass range.[33] This mass analyzer was first proposed by William Stephens in 1946.[34] TOF has undergone a number of important developments in recent decades that enable moderately high resolution and excellent mass measurement accuracy. As a result, these characteristics along with wide mass range have made TOF mass analyzers the workhorses of native mass spectrometry, which involves the generation of large protein complexes at relatively low charge[35]

Design

TOF mass spectrometers consist of three regions, the accelerator region the drift region and detector. Ions are accelerated to the detector region and separate based on mass as they move through the drift region towards the detector. The accelerator region provides ions with kinetic

energy and one of the requirements for high resolution is that the kinetic energy distribution be narrow. This ensures the ion population receive the same amount of kinetic energy as they move to the detector. As ions move through the drift region smaller ions will move with higher velocity than larger ions. This will cause for separation of ions and ions will arrive to the detector at different times. This allows for m/z to be determined via:

$$m/z = \frac{2eV}{D^2} \tag{1.8}$$

Where *V* is the acceleration potential and *D* is the length ions travel after acceleration. Detection occurs on the order of microseconds making TOF mass analyzers a fast analysis technique. TOF mass analyzers have improved resolution with the addition of reflectron lenses. These lenses change the trajectory of the ion path by adding a repulsive voltage and reflecting ions to a detector. This offers a correction for wide kinetic energy distributions that can arise from differences in ion positioning. This also increases the path length ions travel to the detector and allowing for more separation of mass to charge ratios. More recently developed TOF mass analyzers contain multiple reflectron components offering further increased resolution.[36]

1.2.3 Hybrid instruments

Pairing mass analyzers together has allowed for more complex experiments to be performed. Coupling multiple analyzers allows experiments to take advantage of the merits of one analyzer and while offering characteristics of another. This has been especially helpful for tandem mass spectrometry. For example, combining multiple quadrupoles to form a uniquely capable instrument to perform challenging experiments with high reproducibility.[37] TOF systems are also coupled to other mass analyzers including Multi TOF instruments and quadrupole TOF.[38–40] There are numerous other examples of pairings of mass analyzers. Here two instruments will be discussed as they will be utilized in some capacity for all the experiments below.

Sciex 4000 Triple Quadrupole

Triple quadrupoles (QqQ) are the most frequently used tandem mass analyzers.[25, 26, 41] Generally, these instruments are configured where the first quadrupole (Q1) acts as a mass filter to isolate a particular ion of interest. The second quadrupole (q2) acts a collision cell containing

an inert gas such argon or nitrogen. The gas molecules collide with the analyte to produce fragment ions. This process will be discussed in greater detail below. The third quadrupole (Q3) is typically a linear ion trap where tandem MS^n takes place followed by analysis

Figure 1.3 shows a diagram of the triple quadrupole which has been modified to perform ion/ion reactions. The ionization source consists of two nanospray emitters to sequentially generate cations and anions. The q2 collision cell acts as a reaction chamber by possessing the ability to store both anionic and cationic species simultaneously. This is accomplished by auxiliary RF potentials applied to the lenses denoted as IQ1 and IQ2 to allow for mutual ion polarity storage.[42]

Sciex 5600 TripleTOF

A hybrid instrument that takes advantage of the higher resolution and mass range of the TOF relative to a quadrupole mass filter is the quadrupole time of flight instrument (Q-TOF).[39] These instruments combine two quadrupoles of a triple quad instrument with a TOF mass analyzer. This instrument allows for MS^n analysis and higher resolution than a triple quadrupole experiment. A schematic of the instrument used for many of these experiments is shown in **Figure 1.4** It also has similar modifications as the Sciex 4000 instrument described above. The major difference is the use of a TOF mass analyzer (Sciex 5600) versus a quadrupole mass filter (Sciex 4000).[24]

1.3 Tandem MS

Tandem mass spectrometry (MS/MS or MS^n) is a technique that has been developed to further interrogate the ions introduced into a mass spectrometer. Since the discovery of metastable ions in 1947, scientists have expanded the boundaries of what can be determined from probing an ion.[43–45] The applications and scope of tandem mass spectrometry is a wide and expansive topic, the list below is not comprehensive. The most common activation technique used for MS/MS of proteins and peptides is collisional activation.[46, 47] There are multiple types of collisional activation (CAD/CID) that will be described below. Other techniques such as surface induced dissociation (SID)[48] and higher energy collisional dissociation (HCD)[49–51] are also frequently utilized in protein analysis but are discussed elsewhere. There are other activation techniques that include photodissociation such as ultraviolet photodissociation (UVPD) and infrared multiphoton dissociation (IRMPD) and electron-based electron transfer dissociation (ETD)

and electron capture dissociation (ECD).[52–54] Occasionally dissociation techniques will be combined to increase the structural information that would be obtained with a single dissociation technique alone.

1.3.1 Collisional Activation

1.3.2 Ion Trap CID

Ion trap collisional induced dissociation (IT-CID) takes advantage of an ion's secular frequency when stored.[45, 46] By applying a voltage at this frequency, ions of a particular m/z will come into resonance and move from the center of the trap. This motion will induce collisions with the bath gas. For the experiments described below, this gas is nitrogen. These collisions will deposit energy into the ion and this internal energy will be redistributed and cause bond dissociation. By increasing the amplitude of the applied voltage, other ions can experience off resonance excitation. This technique can also be used for isolation as ions can be ejected from the trap. The timescale for these dissociations is on the order of milliseconds in the linear traps described above.

Beam-type CID

Collisional induced dissociation can also occur during ion transmission in space. An example of this is beam-type collisional induced dissociation (BT-CID), which occurs by varying the rod offset voltage between two sets of quadrupoles.[55] This can increase the number of collisions between the analyte and the bath gas that take place in transit to the next quadrupole. This will deposit energy into the entire ion population producing fragment ions from all species in the trap. When combined with rf/DC isolation this technique allows a single ion to be probed after isolation for a MS/MS experiment. Typically, this causes fragmentation on the microsecond time scale and can result in higher energy pathways becoming available. This can cause fragmentation patterns to vary when comparing two activation techniques such as IT-CID and BT-CID.

Dipolar Direct Current CID

Another technique that uses collisions with the bath gas to induce fragmentation is dipolar direct current CID (DDC CID). DDC CID is a broadband activation technique that takes advantage

of a potential between the rods of an opposing pair of rods in a quadrupole mass analyzer.[56] Shown in **Figure 1.5** where one pair of rods are coupled and maintain a DC potential denoted as "Ref" indicating the reference voltage. The other pair of rods are set to opposite yet equal potentials from the reference voltage. This causes the entire ion population to be displaced from the center of the trap. The displacement leads to an increase in collisions with the bath gas, raising the temperature of the ions related to the difference in potential shown in Equation 1.8

$$\Delta T_k = \frac{m_g \Omega^2 r_o^2}{24k} \left(\frac{V_{DDC}}{V_{RF}}\right)^2 \tag{1.9}$$

Where m_g is the mass of the bath gas, Ω is the drive frequency, r_o is the radius of the ion trap, k is the Boltzmann constant. The raise in temperature is due to the displacement of the ions and the ensuing rF heating as ions move closer to the rods. This displacement can be estimated using equation 1.9

$$r_e = \frac{\Omega^2 r_o^3}{4e} m/_z \frac{V_{DDC}}{V_{RF}^2} \tag{1.10}$$

Which shows a limit related to higher mass to charge ratios. This can be shown by rearranging equation 1.9 the high mass limit can be determined shown in equation 1.10

$$m/_z\,(limit) = \frac{4e}{\Omega^2 r_o^2} \frac{V_{RF}^2}{V_{DDC}} \tag{1.11}$$

This activation technique can be performed with trapped ions and ions in transmission and is available on the Sciex TripleTOF in Q0 and q2 quadrupole mass analyzers.

1.3.3 Peptide Fragmentation

As the 20 amino acid residues combine to form peptides and proteins there are an immeasurable number of structures they can adopt. To probe these ions' structures, the activation techniques described above can be utilized to induce fragmentation.[57] This fragmentation occurs in a predictable fashion in part to many residues having different masses. This predictable nature allows for a nomenclature to be developed.[58] This gives scientists the ability to determine the

identity of fragment ions and ultimately the identity of the peptide or protein and convey those results universally. The nomenclature is shown in **Figure 1.6** with blue dashed lines representing fragments seen when using activation techniques denoted as a_n-, b_n-, and c_n- when the charged fragment contains the N terminus and x_n-, y_n-, and z_n- when the charged fragment contains the C terminus and *n* represents the residue number from intact terminus. The letter indicates the specific bond that has been broken. For example, if the amide bond is broken, the resulting fragments can be characterized as *b*- or *y*- ions. Under typical collisional activation conditions, peptides fragment and form b- and y ions while photoactivation and electron-based dissociation can result in *a*-, and *x*-, ions and *c*-, and *z*- ions respectfully. There is much work investigating improvements to fragmentation efficiency to increase peptide characterization with work investigating novel activation techniques, combining several dissociation methods, and increasing resolution to distinguish products. To this date, no activation technique is perfect for every analyte. Combining activation techniques and ion/ion reactions has shown promise as changing the ion type, charge, or covalently modification can result in more information than tandem mass spectrometry alone.[59]

1.4 Ion/ion Reactions

With electrospray providing the ability to produce multiply charged ions, gas-phase ion/ion reactions have allowed mass spectrometry a seemingly limitless method to manipulate ion and ion types to obtain new information from various analytes. After development on a 3-D ion trap, gas-phase ion/ion reactions were later performed on linear ion traps and hybrid instruments. Ion/ion reactions manipulate ion charge state or type by reacting oppositely charged species inside a mass spectrometer. There are numerous ion/ion reactions available to scientists such as proton transfer, electron transfer, complex formation, metal transfer, and covalent modifications This is not a trivial experiment, and it requires optimization of instrument parameters as well as solution conditions depending on the goal of the experiment. These reactions typically require some modification to instruments to generate and store oppositely charged ions. This has given rise to new methods that incorporate gas-phase ion/ion chemistry to obtain comparable results with faster throughput than solution-based derivatization and reduce spectral complexity.

1.4.1 Mutual storage of oppositely charged ions

The modifications necessary to perform ion/ion reactions are shown in **Figures 1.3** and **1.4** of both Sciex 4000 and TripleTOF respectfully.[24, 42] In a typical ion/ion reaction experiment, the analyte, for simplicity being indicated as a multiply charged cationic species, will enter the mass spectrometer, and undergo RF/DC isolation in Q1. Afterwards, the remaining ions are cooled and transferred into q2 where they are stored. Next, anions are generated and undergo a rf/DC isolation upon injection into Q1 and the reagent species is transferred to q2. The lenses on the ends of q2 have an auxiliary rf potential to store ions of both polarities. Mutually storing both ion polarities allows for reactions to occur. The thermodynamics of an ion/ion proton transfer reaction between a multiply charged cation and are dictated by the following equation:[60]

$$MH_n^{n+} + A^1 \rightarrow MH_{(n-1)}^{(n-1)+} + AH$$

(1.12)

Ion/ion reactions are especially useful in comparison to ion/molecule reactions due to the long-range interactions that are accessible to ion/ion reactions. These interactions are dictated by Equation 1.12

$$E = \frac{-z_1 z_2 e^2}{r}$$

(1.13)

Where E is the long-range interaction, z_1 and z_2 are the unit charges of the ions and r is the distance between the two ions. These long rang interactions are charge dependent. Ion/ion reactions are also expected to be exothermic due the differences between proton affinity of the anion compared to an ion/molecule reaction. This reaction is especially useful in congested spectra where multiply charged ions can overlap with another species and by reducing the charge of one species the m/z will change. This will remove the spectral overlap and assist in deconvoluting spectra. In cases where both cationic and anionic species are large and multiply charged there is a propensity of gas-phase ion/ion reactions to result in an electrostatic complex formed once ions reach a stable orbit. These reactions that lead to complex formation have general reactions shown in Equation 1.13

$$(M + nH)^{n+} + (Y\ mH)^{m-} \rightarrow (M + Y + (n-m)H)^{(n-m)+}$$

(1.14)

These complexes can be long lived and stable but when energy is deposited into this system via CID covalent reactions can be performed if necessary.

1.4.2 Gas-Phase Covalent Modification

Peptide and protein derivatization has become commonplace in proteomic analysis to assist with ionization efficiency, quantification, and characterization. These reactions are typically solution based and can take a long time compared to the timescale of a MS experiment. In some instances, ion/ion reactions have allowed these reactions to take place inside the mass spectrometer on the faster timescale.[61–64] There are some prerequisites for a covalent modification such as a stable orbit, reactants have to possess a polarizable "sticky" site (typically sulfonate or quaternary ammonium groups), and a reactive site for chemistry to occur. If these requirements are not met in most cases a competing reaction (e.g., proton transfer reaction) will occur as opposed to covalent modification. These gas phase covalent modifications have allowed derivatization to occur on the time scale of a typical mass spectrometry experiment.

1.4.3 Applications

The ability to form electrostatic complexes, perform gas-phase covalent modifications and proton transfers has led to new methods developed for proteomic analysis. Early work demonstrated the ability to modify peptides using 4-formyl-1,3-benzenedisulfonic acid (FBDSA) to modify unprotonated amine groups on synthetic peptide.[65] Sequential activation of this complex resulted in a Schiff base reaction occurring in the gas-phase which can give enhanced peptide fragmentation. Another common reagent used in gas phase ion/ion reactions are n-hydroxysuccinimide (NHS) esters and hydroxybenzotriazole esters (HOBt) typically containing a charge site (sulfo-, quaternary amine). These reagents have shown varying degrees of reactivity to mostly unprotonated amines and side chains of other residues in the past.[61, 62, 64] These reagents have been used to covalently modify peptides giving insight into charge site localization. When homo-bifunctional reagents were used, crosslinking reactions of peptides in the gas-phase were feasible. This allowed a reaction that is performed in solution to be performed in the gas phase with similar results.[66, 67] Proton transfer reactions have also been utilized to reduce the charge of proteins in to drive residue dependent cleavages.[68] Other reactions include metal

transfer for preferential cleavage of cyclic peptides which are difficult to obtain sequence information and many more.[69, 70]

1.5 Conclusions

Gas-phase ion/ion reactions have added a number of novel capabilities to biological mass spectrometry. They are now being incorporation in a variety of commercial instrument platforms. The groundwork that allows for these reactions is the development of ionization sources capable of soft ionization and formation of multiply charged ions. The development of highly capable instruments has also permitted the analysis of proteins and peptides. This works seeks to continue to incorporate ion/ion reactions into proteomic analysis by applying relevant reactions to overcome deficiencies described below.

1.6 References

1. F.R.S, J.J.T.M.A.: XLVII. On rays of positive electricity. Lond. Edinb. Dublin Philos. Mag. J. Sci. 13, 561–575 (1907). https://doi.org/10.1080/14786440709463633

2. Thomson, S.J.J.: XXVI. Rays of positive electricity. Lond. Edinb. Dublin Philos. Mag. J. Sci. 21, 225–249 (1911). https://doi.org/10.1080/14786440208637024

3.The Nobel Prize in Chemistry 1922, https://www.nobelprize.org/prizes/chemistry/1922/summary/

4. Märk, T.D., Dunn, G.H.: Electron Impact Ionization. Springer Science & Business Media (2013)

5. Some reflections on the early days of mass spectrometry at the university of minnesota. Int. J. Mass Spectrom. Ion Process. 100, 1–13 (1990). https://doi.org/10.1016/0168-1176(90)85063-8

6. Nier, A.O.: A Mass Spectrometer for Isotope and Gas Analysis. Rev. Sci. Instrum. 18, 398–411 (1947). https://doi.org/10.1063/1.1740961

7. Dole, M., Mack, L.L., Hines, R.L., Mobley, R.C., Ferguson, L.D., Alice, M.B.: Molecular Beams of Macroions. J. Chem. Phys. 49, 2240–2249 (1968). https://doi.org/10.1063/1.1670391

8. Dole, M., Hines, R.L., Mack, L.L., Mobley, R.C., Ferguson, L.D., Alice, M.B.: Gas Phase Macroions. Macromolecules. 1, 96–97 (1968). https://doi.org/10.1021/ma60001a017

9. Fenn, J.: Electrospray ionization mass spectrometry: How it all began. J. Biomol. Tech. JBT. 13, 101–118 (2002)

10. Fenn, J.B., Mann, M., Meng, C.K., Wong, S.F., Whitehouse, C.M.: Electrospray ionization for mass spectrometry of large biomolecules. Science. 246, 64–71 (1989). https://doi.org/10.1126/science.2675315

11.Hillenkamp, F., Karas, M., Beavis, R.C., Chait, B.T.: Matrix-Assisted Laser Desorption/Ionization Mass Spectrometry of Biopolymers. Anal. Chem. 63, 1193A-1203A (1991). https://doi.org/10.1021/ac00024a716

12. Awad, H., Khamis, M.M., El-Aneed, A.: Mass Spectrometry, Review of the Basics: Ionization. Appl. Spectrosc. Rev. 50, 158–175 (2015). https://doi.org/10.1080/05704928.2014.954046

13. Kebarle, P., Verkerk, U.H.: Electrospray: From ions in solution to ions in the gas phase, what we know now. Mass Spectrom. Rev. 28, 898–917 (2009). https://doi.org/10.1002/mas.20247

14. Cole, R.B., ebrary, I.: Electrospray and MALDI mass spectrometry [electronic resource]: fundamentals, instrumentation, practicalities, and biological applications. Hoboken, N.J.: Wiley (2010)

15. Disintegration of water drops in an electric field. Proc. R. Soc. Lond. Ser. Math. Phys. Sci. (1964). https://doi.org/10.1098/rspa.1964.0151

16. Rayleigh, Lord: XX. On the equilibrium of liquid conducting masses charged with electricity. (1882). https://doi.org/10.1080/14786448208628425

17. Taflin, D.C., Ward, T.L., Davis, E.J.: Electrified droplet fission and the Rayleigh limit. Langmuir. 5, 376–384 (1989). https://doi.org/10.1021/la00086a016

18. Konermann, L., Ahadi, E., Rodriguez, A.D., Vahidi, S.: Unraveling the Mechanism of Electrospray Ionization. Anal. Chem. 85, 2–9 (2013). https://doi.org/10.1021/ac302789c

19. Hogan, C.J., Carroll, J.A., Rohrs, H.W., Biswas, P., Gross, M.L.: A Combined Charged Residue-Field Emission Model of Macromolecular Electrospray Ionization. Anal. Chem. 81, 369–377 (2009). https://doi.org/10.1021/ac8016532

20. Yuill, E.M., Sa, N., Ray, S.J., Hieftje, G.M., Baker, L.A.: Electrospray Ionization from Nanopipette Emitters with Tip Diameters of Less than 100 nm. Anal. Chem. 85, 8498–8502 (2013). https://doi.org/10.1021/ac402214g

21. Xiang, P., Zhu, Y., Yang, Y., Zhao, Z., Williams, S.M., Moore, R.J., Kelly, R.T., Smith, R.D., Liu, S.: Picoflow Liquid Chromatography–Mass Spectrometry for Ultrasensitive Bottom-Up Proteomics Using 2-μm-i.d. Open Tubular Columns. Anal. Chem. 92, 4711–4715 (2020). https://doi.org/10.1021/acs.analchem.9b05639

22. Yuill, E.M., Baker, L.A.: Ion concentration in micro and nanoscale electrospray emitters. Anal. Bioanal. Chem. 410, 3639–3648 (2018). https://doi.org/10.1007/s00216-018-1043-5

23. Wells, J.M., Chrisman, P.A., McLuckey, S.A.: "Dueling" ESI: instrumentation to study ion/ion reactions of electrospray-generated cations and anions. J. Am. Soc. Mass Spectrom. 13, 614–622 (2002). https://doi.org/10.1016/S1044-0305(01)00364-6

24. Xia, Y., Chrisman, P.A., Erickson, D.E., Liu, J., Liang, X., Londry, F.A., Yang, M.J., McLuckey, S.A.: Implementation of Ion/Ion Reactions in a Quadrupole/Time-of-Flight Tandem Mass Spectrometer. Anal. Chem. 78, 4146–4154 (2006). https://doi.org/10.1021/ac0606296

25. March, R.E.: An Introduction to Quadrupole Ion Trap Mass Spectrometry. J. Mass Spectrom. 32, 351–369 (1997). https://doi.org/10.1002/(SICI)1096-9888(199704)32:4<351::AID-JMS512>3.0.CO;2-Y

26. Louris, J.N., Cooks, R. Graham., Syka, J.E.P., Kelley, P.E., Stafford, G.C., Todd, J.F.J.: Instrumentation, applications, and energy deposition in quadrupole ion-trap tandem mass spectrometry. Anal. Chem. 59, 1677–1685 (1987). https://doi.org/10.1021/ac00140a021

27. He, J., Yu, Q., Li, L., Hang, W., Huang, B.: Characteristics and comparison of different radiofrequency-only multipole cooling cells. Rapid Commun. Mass Spectrom. RCM. 22, 3327–3333 (2008). https://doi.org/10.1002/rcm.3734

28. McLachlan, N.W.: Theory and application of Mathieu functions. Clarendon Press, Oxford (1947)

29. Mathieu, É.: Mémoire sur le mouvement vibratoire d'une membrane de forme elliptique. J. Mathématiques Pures Appliquées. 13, 137–203 (1868)

30. McLafferty, F.W.: Tandem mass spectrometry (MS/MS): a promising new analytical technique for specific component determination in complex mixtures. Acc. Chem. Res. 13, 33–39 (1980). https://doi.org/10.1021/ar50146a001

31. McLafferty, F.W.: Tandem mass spectrometry. Science. 214, 280–287 (1981). https://doi.org/10.1126/science.7280693

32. Londry, F.A., Hager, J.W.: Mass selective axial ion ejection from a linear quadrupole ion trap. J. Am. Soc. Mass Spectrom. 14, 1130–1147 (2003). https://doi.org/10.1016/S1044-0305(03)00446-X

33. Wiley, W.C., McLaren, I.H.: Time-of-Flight Mass Spectrometer with Improved Resolution. Rev. Sci. Instrum. 26, 1150–1157 (1955). https://doi.org/10.1063/1.1715212

34. Wolff, M.M., Stephens, W.E.: A Pulsed Mass Spectrometer with Time Dispersion. Rev. Sci. Instrum. 24, 616–617 (1953). https://doi.org/10.1063/1.1770801

35. Mallis, C.S., Zheng, X., Qiu, X., McCabe, J.W., Shirzadeh, M., Lyu, J., Laganowsky, A., Russell, D.H.: Development of native MS capabilities on an extended mass range Q-TOF MS. Int. J. Mass Spectrom. 458, 116451 (2020). https://doi.org/10.1016/j.ijms.2020.116451

36. Mamyrin, B.A., Karataev, V.I., Shmikk, D.V., Zagulin, V.A.: Mass reflection: a new nonmagnetic time-of-flight high resolution mass- spectrometer. Zh Eksp Teor Fiz 64 No 1 82-89Jan 1973. (1973)

37. Yost, R.A., Enke, C.G.: Selected ion fragmentation with a tandem quadrupole mass spectrometer. J. Am. Chem. Soc. 100, 2274–2275 (1978). https://doi.org/10.1021/ja00475a072

38. Morris, H.R., Paxton, T., Dell, A., Langhorne, J., Berg, M., Bordoli, R.S., Hoyes, J., Bateman, R.H.: High Sensitivity Collisionally-activated Decomposition Tandem Mass Spectrometry on a Novel Quadrupole/Orthogonal-acceleration Time-of-flight Mass Spectrometer. Rapid Commun. Mass Spectrom. 10, 889–896 (1996). https://doi.org/10.1002/(SICI)1097-0231(19960610)10:8<889::AID-RCM615>3.0.CO;2-F

39. Glish, G.L., Goeringer, D.E.: A tandem quadrupole/time-of-flight instrument for mass spectrometry/mass spectrometry. Anal. Chem. 56, 2291–2295 (1984). https://doi.org/10.1021/ac00277a007

40. Cornish, T.J., Cotter, R.J.: Tandem time-of-flight mass spectrometer. Anal. Chem. 65, 1043–1047 (1993). https://doi.org/10.1021/ac00056a017

41. Dawson, P.H.: Quadrupole Mass Spectrometry and Its Applications. Elsevier (2013)

42. Xia, Y., Wu, J., McLuckey, S.A., Londry, F.A., Hager, J.W.: Mutual storage mode ion/ion reactions in a hybrid linear ion trap. J. Am. Soc. Mass Spectrom. 16, 71–81 (2005). https://doi.org/10.1016/j.jasms.2004.09.017

43. Cooks, R.G., Beynon, J.H.: Metastable ions and ion kinetic energy spectrometry: The development of a new research area. J. Chem. Educ. 51, 437 (1974). https://doi.org/10.1021/ed051p437

44. Levsen, K., Schwarz, H.: Collisional Activation Mass Spectrometry—A New Probe for Determining the Structure of Ions in the Gas Phase. Angew. Chem. Int. Ed. Engl. 15, 509–519 (1976). https://doi.org/10.1002/anie.197605091

45. McLuckey, S.A.: Principles of collisional activation in analytical mass spectrometry. J. Am. Soc. Mass Spectrom. 3, 599–614 (1992). https://doi.org/10.1016/1044-0305(92)85001-Z

46. Wells, J.M., McLuckey, S.A.: Collision-induced dissociation (CID) of peptides and proteins. Methods Enzymol. 402, 148–185 (2005). https://doi.org/10.1016/S0076-6879(05)02005-7

47. Popa, V., Trecroce, D.A., McAllister, R.G., Konermann, L.: Collision-Induced Dissociation of Electrosprayed Protein Complexes: An All-Atom Molecular Dynamics Model with Mobile Protons. J. Phys. Chem. B. 120, 5114–5124 (2016). https://doi.org/10.1021/acs.jpcb.6b03035

48. Dongré, A.R., Somogyi, Á., Wysocki, V.H.: Surface-induced Dissociation: An Effective Tool to Probe Structure, Energetics and Fragmentation Mechanisms of Protonated Peptides. J. Mass Spectrom. 31, 339–350 (1996). https://doi.org/10.1002/(SICI)1096-9888(199604)31:4<339::AID-JMS322>3.0.CO;2-L

49. Keilhauer, E.C., Geyer, P.E., Mann, M.: HCD Fragmentation of Glycated Peptides. J. Proteome Res. 15, 2881–2890 (2016). https://doi.org/10.1021/acs.jproteome.6b00464

50. Pejchinovski, M., Klein, J., Ramírez-Torres, A., Bitsika, V., Mermelekas, G., Vlahou, A., Mullen, W., Mischak, H., Jankowski, V.: Comparison of higher energy collisional dissociation and collision-induced dissociation MS/MS sequencing methods for identification of naturally occurring peptides in human urine. Proteomics Clin. Appl. 9, 531–542 (2015). https://doi.org/10.1002/prca.201400163

51. Nagaraj, N., D'Souza, R.C.J., Cox, J., Olsen, J.V., Mann, M.: Feasibility of Large-Scale Phosphoproteomics with Higher Energy Collisional Dissociation Fragmentation. J. Proteome Res. 9, 6786–6794 (2010). https://doi.org/10.1021/pr100637q

52. Julia, B.-M., Oliveira, E. de: Photodissociation Mass Spectrometry of Peptides and Proteins. In: Encyclopedia of Analytical Chemistry. pp. 1–22. American Cancer Society (2018)

53. Zhou, Y., Dong, J., Vachet, R.W.: Electron transfer dissociation of modified peptides and proteins. Curr. Pharm. Biotechnol. 12, 1558–1567 (2011). https://doi.org/10.2174/138920111798357230

54. van Agthoven, M.A., Chiron, L., Coutouly, M.-A., Delsuc, M.-A., Rolando, C.: Two-Dimensional ECD FT-ICR Mass Spectrometry of Peptides and Glycopeptides. Anal. Chem. 84, 5589–5595 (2012). https://doi.org/10.1021/ac3004874

55. Yu Xia, Xiaorong Liang, and, McLuckey*, S.A.: Ion Trap versus Low-Energy Beam-Type Collision-Induced Dissociation of Protonated Ubiquitin Ions, https://pubs.acs.org/doi/pdf/10.1021/ac051622b

56. Webb, I.K., Londry, F.A., McLuckey, S.A.: Implementation of dipolar direct current (DDC) collision-induced dissociation in storage and transmission modes on a quadrupole/time-of-flight tandem mass spectrometer. Rapid Commun. Mass Spectrom. 25, 2500–2510 (2011). https://doi.org/10.1002/rcm.5152

57. Brodbelt, J.S.: Ion Activation Methods for Peptides and Proteins. Anal. Chem. 88, 30–51 (2016). https://doi.org/10.1021/acs.analchem.5b04563

58. Proposal for a common nomenclature for sequence ions in mass spectra of peptides. - Abstract - Europe PMC, http://europepmc.org/abstract/med/6525415

59. Macias, L.A., Santos, I.C., Brodbelt, J.S.: Ion Activation Methods for Peptides and Proteins. Anal. Chem. 92, 227–251 (2020). https://doi.org/10.1021/acs.analchem.9b04859

60. Stephenson, J.L., McLuckey, S.A.: Ion/Ion Reactions in the Gas Phase: Proton Transfer Reactions Involving Multiply-Charged Proteins. J. Am. Chem. Soc. 118, 7390–7397 (1996). https://doi.org/10.1021/ja9611755

61. Bu, J., Peng, Z., Zhao, F., McLuckey, S.A.: Enhanced Reactivity in Nucleophilic Acyl Substitution Ion/Ion Reactions Using Triazole-Ester Reagents. J. Am. Soc. Mass Spectrom. 28, 1254–1261 (2017). https://doi.org/10.1007/s13361-017-1613-3

62. Peng, Z., McGee, W.M., Bu, J., Barefoot, N.Z., McLuckey, S.A.: Gas Phase Reactivity of Carboxylates with <Emphasis Type="Italic">N</Emphasis>-Hydroxysuccinimide Esters. J. Am. Soc. Mass Spectrom. 26, 174–180 (2015). https://doi.org/10.1007/s13361-014-1002-0

63. Peng, Z., Pilo, A.L., Luongo, C.A., McLuckey, S.A.: Gas-Phase Amidation of Carboxylic Acids with Woodward's Reagent K Ions. J. Am. Soc. Mass Spectrom. 26, 1686–1694 (2015). https://doi.org/10.1007/s13361-015-1209-8

64. Pitts-McCoy, A.M., Harrilal, C.P., McLuckey, S.A.: Gas-Phase Ion/Ion Chemistry as a Probe for the Presence of Carboxylate Groups in Polypeptide Cations. J. Am. Soc. Mass Spectrom. (2018). https://doi.org/10.1007/s13361-018-2079-7

65. Stutzman, J.R., Luongo, C.A., McLuckey, S.A.: Covalent and Non-covalent Binding in the Ion/Ion Charge Inversion of Peptide Cations with Benzene-disulfonic Acid Anions. J. Mass Spectrom. JMS. 47, 669–675 (2012). https://doi.org/10.1002/jms.2968

66. Webb, I.K., Mentinova, M., McGee, W.M., McLuckey, S.A.: Gas-Phase Intramolecular Protein Crosslinking via Ion/Ion Reactions: Ubiquitin and a Homobifunctional sulfo-NHS Ester. J. Am. Soc. Mass Spectrom. 24, 733–743 (2013). https://doi.org/10.1007/s13361-013-0590-4

67. Mentinova, M., McLuckey, S.A.: Intra- and Inter-Molecular Cross-Linking of Peptide Ions in the Gas Phase: Reagents and Conditions. J. Am. Soc. Mass Spectrom. 22, 912 (2011). https://doi.org/10.1007/s13361-011-0103-2

68. Foreman, D.J., Dziekonski, E.T., McLuckey, S.A.: Maximizing Selective Cleavages at Aspartic Acid and Proline Residues for the Identification of Intact Proteins. J. Am. Soc. Mass Spectrom. 30, 34–44 (2019). https://doi.org/10.1007/s13361-018-1965-3

69. Foreman, D.J., Lawler, J.T., Niedrauer, M.L., Hostetler, M.A., McLuckey, S.A.: Gold(I) Cationization Promotes Ring Opening in Lysine-Containing Cyclic Peptides. J. Am. Soc. Mass Spectrom. 30, 1914–1922 (2019). https://doi.org/10.1007/s13361-019-02247-x

70. Prentice, B.M., McLuckey, S.A.: Gas-phase ion/ion reactions of peptides and proteins: acid/base, redox, and covalent chemistries. Chem. Commun. 49, 947–965 (2013). https://doi.org/10.1039/C2CC36577D

71. Singh, P., Panchaud, A., Goodlett, D.R.: Chemical Cross-Linking and Mass Spectrometry As a Low-Resolution Protein Structure Determination Technique. Anal. Chem. 82, 2636–2642 (2010). https://doi.org/10.1021/ac1000724

72. O'Reilly, F.J., Rappsilber, J.: Cross-linking mass spectrometry: methods and applications in structural, molecular and systems biology. Nat. Struct. Mol. Biol. 25, 1000 (2018). https://doi.org/10.1038/s41594-018-0147-0

73. Iacobucci, C., Götze, M., Ihling, C.H., Piotrowski, C., Arlt, C., Schäfer, M., Hage, C., Schmidt, R., Sinz, A.: A cross-linking/mass spectrometry workflow based on MS-cleavable cross-linkers and the MeroX software for studying protein structures and protein–protein interactions. Nat. Protoc. 13, 2864–2889 (2018). https://doi.org/10.1038/s41596-018-0068-8

74. Yu, C., Huang, L.: Cross-Linking Mass Spectrometry: An Emerging Technology for Interactomics and Structural Biology. Anal. Chem. 90, 144–165 (2018). https://doi.org/10.1021/acs.analchem.7b04431

75. Chavez, J.D., Bruce, J.E.: Chemical cross-linking with mass spectrometry: a tool for systems structural biology. Curr. Opin. Chem. Biol. 48, 8–18 (2019). https://doi.org/10.1016/j.cbpa.2018.08.006

76. Webb, I.K., Mentinova, M., McGee, W.M., McLuckey, S.A.: Gas-Phase Intramolecular Protein Crosslinking via Ion/Ion Reactions: Ubiquitin and a Homobifunctional sulfo-NHS Ester. J. Am. Soc. Mass Spectrom. 24, 733–743 (2013). https://doi.org/10.1007/s13361-013-0590-4

77. Cheung See Kit, M., Carvalho, V.V., Vilseck, J.Z., Webb, I.K.: Gas-phase ion/ion chemistry for structurally sensitive probes of gaseous protein ion structure: Electrostatic and electrostatic to covalent cross-linking. Int. J. Mass Spectrom. 463, 116549 (2021). https://doi.org/10.1016/j.ijms.2021.116549

78. Fang, X., Xie, J., Chu, S., Jiang, Y., An, Y., Li, C., Gong, X., Zhai, R., Huang, Z., Qiu, C., Dai, X.: Quadrupole-linear ion trap tandem mass spectrometry system for clinical biomarker analysis. Engineering. (2021). https://doi.org/10.1016/j.eng.2020.10.021

79. Guan, S., Burlingame, A.L.: High Mass Selectivity for Top-down Proteomics by Application of SWIFT Technology. J. Am. Soc. Mass Spectrom. 21, 455–459 (2010). https://doi.org/10.1016/j.jasms.2009.11.011

80. Betancourt, S.K., Canez, C.R., Shields, S.W.J., Manthorpe, J.M., Smith, J.C., McLuckey, S.A.: Trimethylation Enhancement Using 13C-Diazomethane: Gas-Phase Charge Inversion of Modified Phospholipid Cations for Enhanced Structural Characterization. Anal. Chem. 89, 9452–9458 (2017). https://doi.org/10.1021/acs.analchem.7b02271

81. Shih, M., McLuckey, S.A.: Ion/ion charge inversion/attachment in conjunction with dipolar DC collisional activation as a selective screen for sulfo- and phosphopeptides. Int. J. Mass Spectrom. 444, 116181 (2019). https://doi.org/10.1016/j.ijms.2019.116181

82. Stutzman, J.R., McLuckey, S.A.: Ion/Ion Reactions of MALDI-Derived Peptide Ions: Increased Sequence Coverage via Covalent and Electrostatic Modification upon Charge Inversion. Anal. Chem. 84, 10679–10685 (2012). https://doi.org/10.1021/ac302374p

83. Randolph, C.E., Shenault, D.M., Blanksby, S.J., McLuckey, S.A.: Localization of Carbon–Carbon Double Bond and Cyclopropane Sites in Cardiolipins via Gas-Phase Charge Inversion Reactions. J. Am. Soc. Mass Spectrom. 32, 455–464 (2021). https://doi.org/10.1021/jasms.0c00348

84. Randolph, C.E., Shenault, D.M., Blanksby, S.J., McLuckey, S.A.: Structural Elucidation of Ether Glycerophospholipids Using Gas-Phase Ion/Ion Charge Inversion Chemistry. J. Am. Soc. Mass Spectrom. 31, 1093–1103 (2020). https://doi.org/10.1021/jasms.0c00025

85. Abdillahi, A.M., Lee, K.W., McLuckey, S.A.: Mass Analysis of Macro-molecular Analytes via Multiply-Charged Ion Attachment. Anal. Chem. 92, 16301–16306 (2020). https://doi.org/10.1021/acs.analchem.0c04335

86. Xia, Y., Chrisman, P.A., Erickson, D.E., Liu, J., Liang, X., Londry, F.A., Yang, M.J., McLuckey, S.A.: Implementation of Ion/Ion Reactions in a Quadrupole/Time-of-Flight Tandem Mass Spectrometer. Anal. Chem. 78, 4146–4154 (2006). https://doi.org/10.1021/ac0606296

87. Xia, Y., Liang, X., McLuckey, S.A.: Pulsed dual electrospray ionization for In/In reactions. J. Am. Soc. Mass Spectrom. 16, 1750–1756 (2005). https://doi.org/10.1016/j.jasms.2005.07.013

88. Hecht, E.S., Scigelova, M., Eliuk, S., Makarov, A.: Fundamentals and Advances of Orbitrap Mass Spectrometry. In: Encyclopedia of Analytical Chemistry. pp. 1–40. American Cancer Society (2019)

1.7 Figures

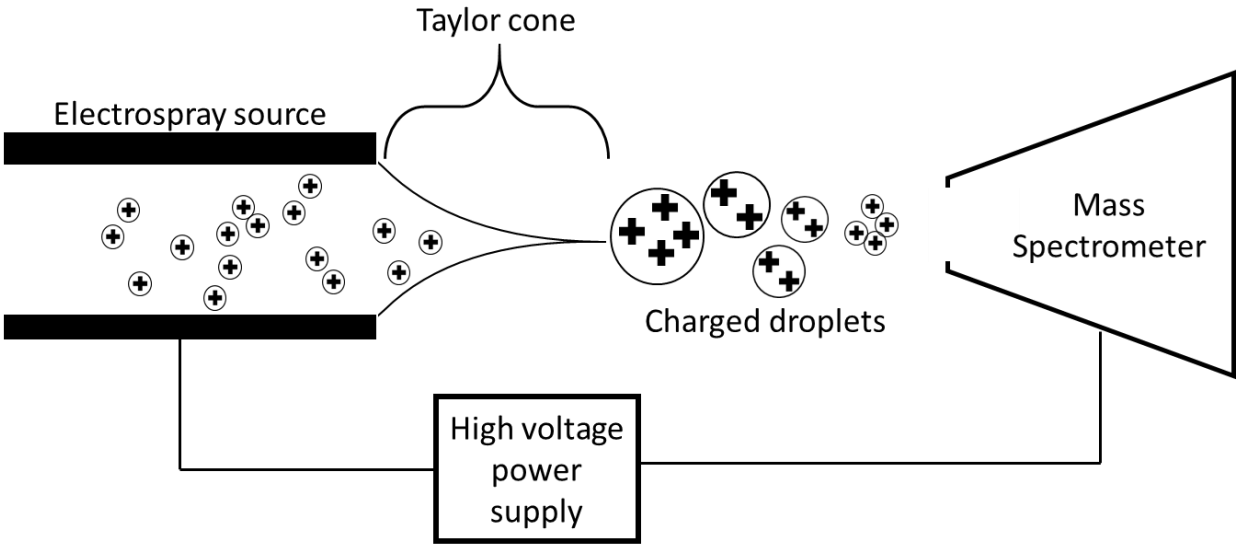

Figure 1.1. Generic electrospray ionization set up

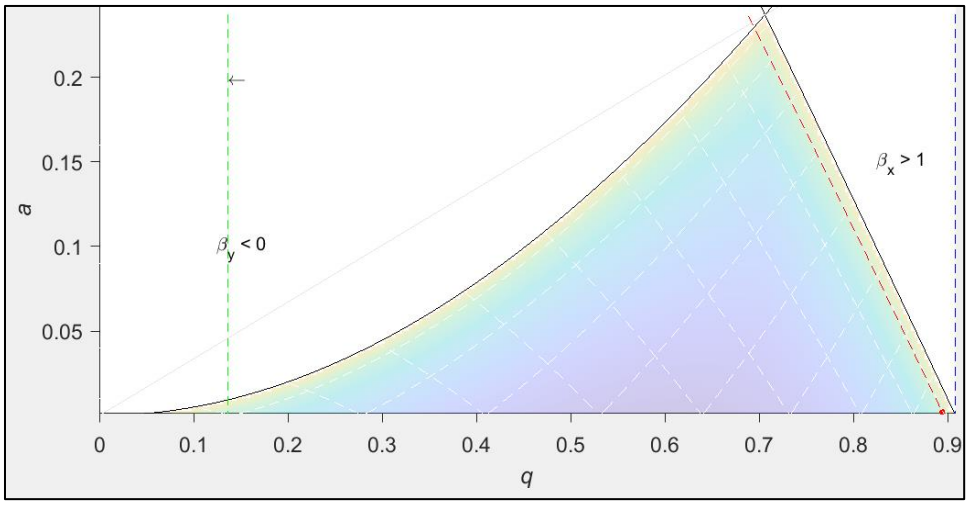

Figure 1.2 Mathieu stability diagram showing stability of ion in a quadrupolar field

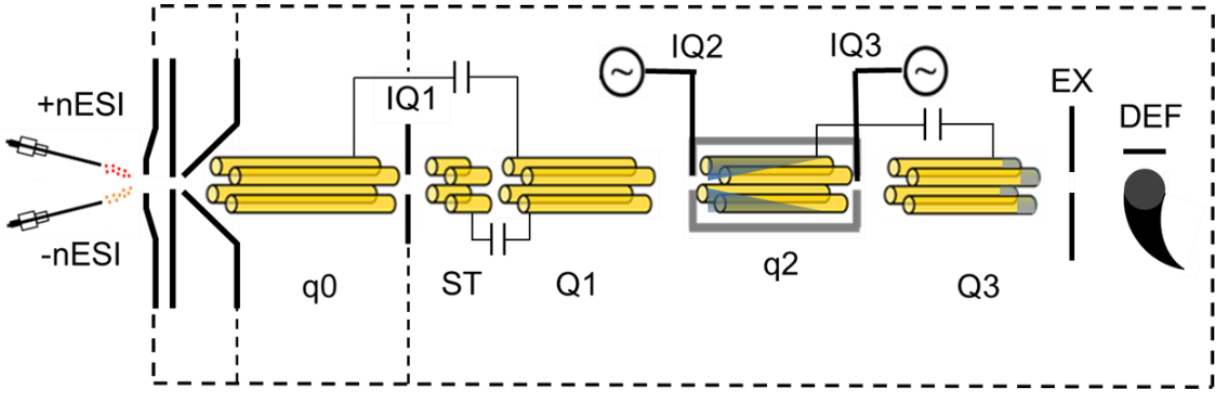

Figure 1.3 A schematic of a Sciex 4000 QTRAP modified for ion/ion reactions

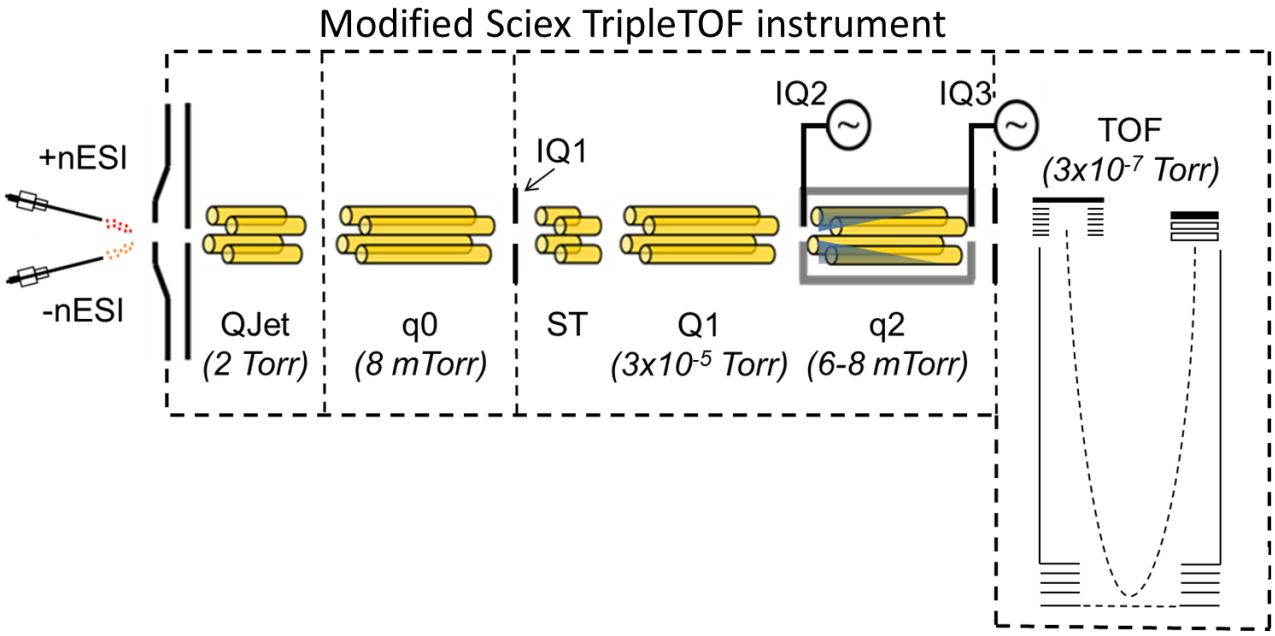

Figure 1.4 A schematic of a Sciex 5600 TripleTOF modified for ion/ion reactions

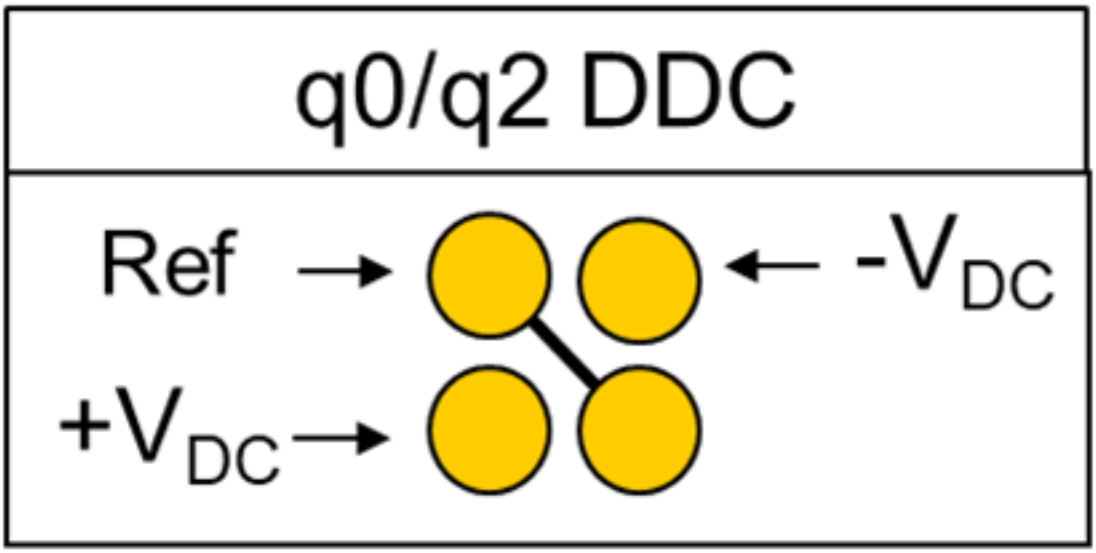

Figure 1.5 Schematic of the quadrupole mass analyzer along the x axis with DDC CID available on the Sciex 5600 TripleTOF in q0 and q2

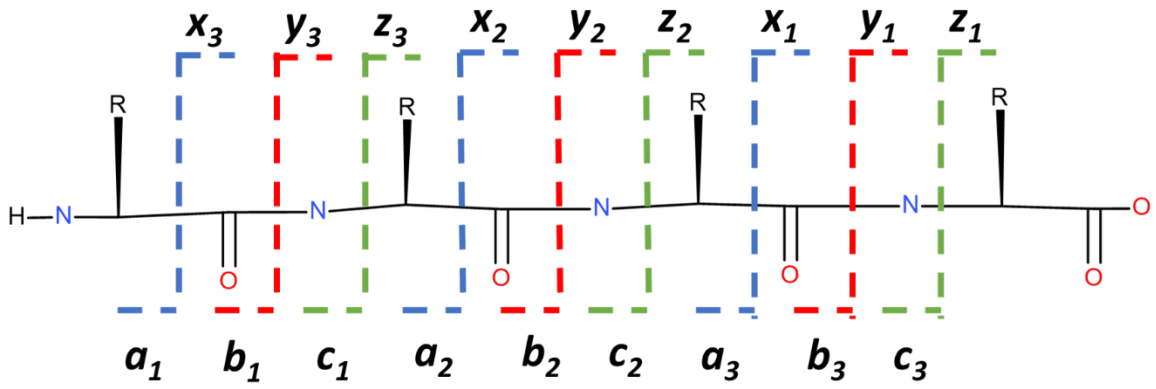

Figure 1.6 A schematic of the nomenclature system of protonated peptides and proteins when activated in mass spectrometry

CHAPTER 2. GAS-PHASE ION/ION CHEMISTRY AS A PROBE FOR THE PRESENCE OF CARBOXYLATE GROUPS IN POLYPEPTIDE CATIONS

The reactivity of 1-hydroxybenzoyl triazole (HOBt) esters with the carboxylate functionality present in peptides is demonstrated in the gas phase with a doubly deprotonated dianion. The reaction forms an anhydride linkage at the carboxylate site. Upon ion trap collisional-induced dissociation (CID) of the modified peptide, the resulting spectrum shows a nominal loss of the mass of the reagent and a water molecule. Analogous phenomenology was also noted for model peptide cations that likely contain zwitterionic/salt-bridged motifs in reactions with a negatively charged HOBt ester. Control experiments indicate that a carboxylate group is the likely reactive site, rather than other possible nucleophilic sites present in the peptide. These observations suggest that HOBt ester chemistry may be used as a chemical probe for the presence and location of carboxylate groups in net positively charged polypeptide ions. As an illustration, deprotonated sulfobenzoyl HOBt was reacted with the $[M+7H]^{7+}$ ion of ubiquitin. The ion was shown to react with the reagent and CID of the covalent reaction product yielded an abundant $[M+6H-H_2O]^{6+}$ ion. Comparison of the CID product ion spectrum of this ion with that of the water loss product generated from CID of the unmodified $[M+6H]^{6+}$ ion revealed the glutamic acid at residue 64 as a reactive site, suggesting that it is present in the deprotonated form.

2.1 Introduction

Strong electrostatic interactions such as zwitterionic pairing between oppositely charged functional groups offer stabilizing effects to the secondary and tertiary structures of peptides and proteins. Such pairings can be classified as salt bridges (+ − +) or zwitterions (+ −). Determining the existence and location(s) of such interactions in a polypeptide is relevant to its three-dimensional structural characterization. While amino acids in a zwitterionic state are known to exist in solution at neutral pH, their existence in the gas phase has previously been questioned [1]. However, there is growing experimental evidence that indicates that such charge separation is possible in the gas phase for systems as small as two amino acids [2, 3, 4]. Techniques used to elucidate the location and arrangement of salt bridges in the gas phase include computational

studies [5], ion mobility [6], ion spectroscopy [2], and interpretation of fragmentation via mass spectrometry [4, 7, 8]. Many of the experimental techniques rely upon some form of calculation to provide a precise prediction of zwitterionic structure.

Calculations have been used to characterize the tendency of salt bridge formation involving particular amino acid residues. For instance, it is predicted that zwitterionic states for non-basic residues such as glycine are not favorable in the gas phase [1]; however, both experimental and theoretical research has shown that zwitterionic structures can be favorable for more basic residues such as arginine [3,9, 10, 11]. Of the residues capable of comprising salt bridges in the gas-phase (arginine, lysine, aspartic acid, and glutamic acid), the arginine side chain is established as the primary positively charged component of zwitterionic conformations [12]. The aspartic acid and glutamic acid side chains and the C-terminus act as negatively charged components [12]. The influence that these residues have on the conformational landscape has been the subject of examination [13]. In the case of small polypeptides, comparisons between theoretical and experimental data can be made. Unfortunately, due to conformational complexity of larger systems, ab initio methods are too computationally expensive to be extended to proteins.

Ion mobility mass spectrometry (IM-MS) provides a direct probe of an ion's conformation via its drift time through a gas, which can be translated to a collision cross section (CCS). Research using this technique has demonstrated that the cross section of a protein is highly dependent on its charge state [14]. The dependence of CCS on protein charge state between has been attributed in part to conformational differences that arise from the loss of stabilizing electrostatic forces such as salt bridges and hydrogen bonds under the influence of the Coulombic field associated with multiple charging [15, 16]. Electrospray ionization (ESI), which tends to lead to multiple charging of polypeptides, is of particular utility for structural studies due to the possibility for the preservation of a least some elements of the native condensed-phase structure when ions are transferred to the gas-phase, provided the solution is not denaturing [17, 18, 19, 20]. IM-MS in conjunction with ESI has been particularly useful in the study of protein and peptide ion higher order structure. However, measurement of the CCS alone can neither provide detailed structural information nor information regarding chemical interactions within an ion.

The fragmentation patterns of proteins and peptides resulting from various activation techniques in tandem mass spectrometry have been reported to be sensitive to the presence of zwitterionic pairing [21, 22, 23]. For example, unique neutral losses have been attributed to

zwitterionic interactions in dipeptides [3, 8]. However, such losses have not proved to be conclusive for larger polypeptide ions as other mechanisms might also account for them. Recently, Bonner et al. have shown that photoexcitation of net positively charged ions that can contain anionic sites, specifically carboxylates, lead to fragmentation analogous to that observed with electron-based dissociation techniques [7]. This technique directly probes for the presence of zwitterionic sites, by photoactivation of the ion. Other light-based activation techniques such as infrared multiple photodissociation spectroscopy also show the ability to directly identify the presence of zwitterionic interactions by revealing unique vibrational signatures of the carboxylate functional group. These approaches that directly activate the carboxylate functionality appear to be useful for determining the presence of zwitterionic interactions.

In this work, we evaluated the possibility that functional-group selective ion/ion reactions might serve as chemical probes for the presence of carboxylate groups in polypeptide cations. Prior work has shown that N-hydroxysuccinimide (NHS) esters can serve as reagents for gas-phase covalent modification of nucleophilic functional groups such as primary amines [24], guanidine [25], and carboxylates [26]. In the reaction between NHS esters and carboxylates, a labile anhydride bond is formed at the carboxylate. Subsequent collisional activation results in the loss of the modification and, nominally, a molecule of water. This reaction does not occur with carboxylic acids (i.e., the protonated form of a carboxylate) as the nucleophilicity of the acidic form is much less than that of its conjugate base. Similar to NHS esters, 1-hydroxybenzotriazole (HOBt) esters undergo gas-phase reactions with amine groups but with increased reactivity, as HOBt is a better leaving group relative to NHS [27]. While HOBt esters have not yet been demonstrated to react with carboxylates in the gas phase, their increased reactivity with primary amines relative to NHS esters suggested to us that they would also be more reactive with carboxylates. We therefore sought to determine if HOBt esters might be reagents that could indicate the presence of carboxylate groups in polypeptide cations. If acidic side chains or the C-terminus were engaged in a zwitterionic interaction, the nucleophilicity of the site might be sufficient to displace HOBt and form an anhydride. Further interrogation of the modified polypeptide could then provide information regarding sites involved in the zwitterionic interaction.

2.2 Experimental

2.2.1 Materials

Reagent synthesis

The hydroxybenzotriazole ester of 4-trimethylammonium butyrate (TMAB-HOBt) was prepared from a modified method based on synthesis of [3-(2,5)-dioxopyrrolidin-1-yloxycarbonyl)-propyl] trimethyllammonium [28]. 1.3 mg of (3-carboxypropyl) trimethylammonium chloride, 0.9 mg of HOBt, and 1.7 mg of DCC were dissolved in 1 mL acetonitrile each. Ten microliters of aliquot of each were combined and diluted 100× in acetonitrile. Sulfobenzoyl HOBt was prepared as previously shown [27]. The group conjugated to HOBt for a particular reagent ion was chosen to attach to the analyte ion polarity of interest. Sulfonate is appropriate for reactions with cations whereas TMAB is appropriate for attachment to anions.

Peptide methyl esterification

Peptide methyl esterification was performed as described previously [29]. Two molars of hydrochloric acid in dry methanol were prepared by combining 40 µL of acetyl chloride and 250 µL of dry methanol. One milligram of YGRAR was dissolved in 100 µL of this solution and allowed to react for 2 h. The solution was lyophilized and reconstituted to make a peptide solution as described above

Carboxyl O^{18} Labeling

O18 labeling was performed according to a previously published procedure [30]. Briefly, 1 mg of peptide was dissolved in 200 µL H2 18O with 1% (v/v) trifluoroacetic acid. The solution was allowed to react at room temperature for approximately 3 days and lyophilized to dryness. The peptide was reconstituted in 50:50 (v/v) water/methanol and diluted to a final concentration of 100 µg/mL.

2.2.2 Mass Spectrometry

Experiments were performed using a QTRAP 4000 hybrid triple quadrupole/linear ion trap or a TripleTOF 5600 System (SCIEX, Concord, ON, Canada). Both instruments were previously modified to perform ion/ion reactions [31, 32]. Anions and cations were sequentially injected via alternatively pulsed nano-electrospray ionization (nESI). First, cations are injected, isolated in Q1, and transferred and stored in q2. Next, reagent ions are injected, isolated in Q1, and transferred to q2 [33]. The ions were mutually stored in the q2 reaction cell for 100–1000 ms [31, 34]. In the case of experiments performed on the QTRAP, reaction products formed in q2 were transferred to Q3 where they were subjected to MS^n using resonance excitation ion trap CID and analyzed by mass selective axial ejection (MSAE) [35, 36]. For experiments performed on the TripleTOF 5600, products were subjected to CID in q2. Fragment ions were back transferred to q1 for isolation, sequentially transferred to q2, and mass analyzed via orthogonal time-of-flight (TOF)

2.3 Results and Discussion

We begin by demonstrating the reactivity of HOBt esters with carboxylate groups using the same model peptide anion that was used to establish carboxylate reactivity with NHS esters. We then describe results based on the model peptide YGRAR to examine the reactivity of HOBt esters with carboxylate groups that might be engaged in zwitterionic structures in a polypeptide cation. We finish by describing results obtained with a small model protein (i.e., bovine ubiquitin) to provide evidence for the presence and location of a carboxylate in a multiply protonated polypeptide system.

2.3.1 HOBt-TMAB and Ac-AADAADAA-Ome

The doubly deprotonated peptide Ac-AADAADAA-Ome was reacted with the synthesized TMAB-HOBt reagent cation to demonstrate HOBt reactivity towards carboxylates in the gas phase. The peptide and reagent formed a long-lived electrostatic complex $[M\text{-}2H+TMAB\ HOBt]^-$ shown in **Figure 2.1a**. When the complex was subjected to CID, neutral HOBt (135 Da) was lost (**Figure 2.1b.),** analogous to the loss of NHS from reactions with the TMAB-NHS ester cation described previously [27]. The newly formed species [M-2H+TMAB] species was subjected to collisional

activation, which resulted in production of $[M\text{-}H\text{-}H_2O]^-$ shown in **Figure 2.1c**. The loss of HOBt indicates that a covalent reaction between the HOBt ester and the polypeptide anion takes place. (Note that quaternary ammonium cations react with carboxylates via alkyl cation transfer [37]. The absence of evidence for either proton or alkyl cation transfer indicates that the covalent reaction leading to loss of HOBt is, by far, the dominant process.) Fragmentation of the $[M\text{-}2H+TMAB]^-$ anion generated from loss of HOBt to yield the $[M\text{-}H_2O]^-$ product is fully consistent with the generation of an anhydride upon reaction with a carboxylate and the TMAB-HOBt ester, as illustrated in **Figure 2.2**.

2.3.2 Sulfobenzoyl HOBt and Ions Derived from YGRAR

The pentapeptide YGRAR was chosen as a model system because it has two arginine residues and a single carboxylic acid group (i.e., the C-terminus) that can engage in the formation of a salt bridge or zwitterion. In a cold-ion UV-IR spectroscopy study that will be described in detail elsewhere, the dominant conformer of singly protonated YGRAR has been shown to lack a carboxylic acid group by virtue of the absence of the signature O–H stretch (free/hydrogen bonded) in the hydride stretch region, the absence of a carboxylic acid C=O stretch in the amide I region, and the presence of the antisymmetric COO^- stretch in the amide II region [38]. This suggests that the C-terminus in this ion is deprotonated. The major conformer of doubly protonated YGRAR, on the other hand, showed the signature absorbances of carboxylic acid. We therefore focused our attention on the reaction of deprotonated sulfobenzoyl HOBt with doubly protonated YGRAR. Attachment of an anion to doubly protonated YGRAR results in a net singly charged ion population that can be comprised of a combination of structures with different charge partitioning, some of which can contain zwitterionic structures. The potential nucleophilic sites within a complex comprised of deprotonated sulfobenzoyl HOBt (SB-HOBt) and doubly protonated YGRAR that can react with the HOBt ester include unprotonated basic sites (i.e., the N-terminus or either of the guanidine groups) and a carboxylate group, if present. The ion/ ion product ion spectra for the reaction of deprotonated SBHOBt and all doubly protonated versions of YGRAR (i.e., unmodified, C-terminally ^{18}O-labeled, methyl esterified, and N-terminally acetylated) showed abundant complex formation (e.g., $[YGRAR+2H+SB\text{-}HOBt]^+$) as well as single proton

transfer to yield the $[M+H]^+$ ion (see **Figure 2.3** for the position/ion reaction spectra for the four forms of YGRAR mentioned above).

Figure 2.4 compares the CID spectra of the SBHOBt complexes generated with doubly protonated versions of YGRAR (**Figure 2.3a**), methyl-esterified YGRAR (YGRAR-OMe, **Figure 2.3b**), C-terminal ^{18}O-labeled YGRAR (indicated as ^{18}O-YGRAR with both C-terminal oxygen atoms exchanged for ^{18}O with isolation of this ion prior to ion/ion reaction shown in Figure 4, **Figure 2.3c**), and N-terminally acetylated YGRAR (ac-YGRAR, **Figure 2.3d**). All four complexes show loss of intact neutral SB-HOBt, which reflects complexes in the activated population that underwent proton transfer, as opposed to covalent reaction. In the cases of YGRAR, ^{18}O-YGRAR, and YGRAR-OMe, however, there is also an abundant product generated by loss of HOBt, which reflects covalent bond formation in the complex. In the case of ac-YGRAR, on the other hand, no evidence for loss of HOBt is apparent. In ac-YGRAR, there are two nominal basic sites (i.e., the two arginine side-chains).

In the doubly protonated species, both arginines are expected to be ionized. The sulfonate group of SB-HOBt is expected to form a strong electrostatic interaction with one of these sites. In order for the complex to have a net positive charge, an excess proton must be present on the other arginine and the C-terminus must also be protonated. Hence, there are no available nucleophilic sites to react with the HOBt ester (i.e., the C-terminus and one arginine are protonated and the other arginine is involved with the electrostatic interaction with the sulfonate group). Hence, no nucleophilic displacement of HOBt can occur to give rise to a covalent reaction. Unmodified YGRAR has three nominal basic sites (i.e., the N-terminus and the two guanidine side chains of the arginine **Figure 2.5**. Reaction between the carboxylate group in a doubly deprotonated Ac-AADAADAA-Ome with deprotonation at both the aspartic acid side chains with a positively charged TMAB-HOBt) and one acidic site (i.e., the C-terminus). Upon attachment of a negatively charged sulfobenzoyl reagent to a doubly charged YGRAR, there are nine ways to partition charge among the acidic and basic sites to result in a singly charged ion. Three conformers involve the protonation of all of the basic sites, with one being associated with the sulfonate group of the reagent and the C-terminus being deprotonated. The six remaining conformers do not involve zwitterion formation (i.e., the C-terminus is neutral, see **Figure 2.5**). (The same situation prevails for the O^{18}-labeled peptide.) In the case of the methyl-esterified peptide, only the six non-zwitterionic combinations are possible. In all of the non-zwitterionic systems, one unprotonated

basic site (i.e., unprotonated N-terminus or an unprotonated arginine residue) is available to react with the ester. In the case of the zwitterionic systems, the only nominal nucleophile available to react is the deprotonated C-terminus.

Figure 2.6 compares the ion trap CID spectra of the covalently modified ions derived from YGRAR (**Figure 2.6a**) and YGRAR-OMe (**Figure 2.6b**). The two spectra are similar in that the major product ions are consistent with covalently modified b_3 and b_4 ions (the indicates an increase in mass of 183 Da) which suggests covalent modification at either the N-terminus or the central arginine in the peptide. Given the lower proton affinity of the N-terminus relative to the guanidine side chain of arginine, it is likely that the main reactive site is the N-terminus. Furthermore, acylation of arginine leads to a dominant loss of 35 Da via a concerted loss of ammonia and water [39] when the covalent adduct lacks an alpha-hydrogen, as is the case here. There is a relatively small signal indicating the loss of 35 Da in the spectra of **Figure 2.6a**. There is also a mechanism for the loss of adduct plus 42 Da from peptides with acylated arginines [37], which is not observed in these peptides. Hence, relatively little reactivity associated with the arginine residues is apparent in either spectrum of **Figure 2.8**. A significant difference between the two spectra is the appearance of a product associated with the loss of 202 Da, corresponding to $[M+H-H_2O]^+$, for YGRAR but not for YGRAR-OMe. The analogous experiment performed with modified O^{18}-YGRAR (**Figure 2.7**) showed a loss of 204 Da, which indicates that one of the oxygen atoms associated with the neutral loss arises from the C-terminus. The reaction between SB-HOBt and the carboxylate group of the C-terminus is shown schematically in **Figure 2.10**. The data of Figure 3 are consistent with unique reactivity for YGRAR relative to YGRAR-OMe with SB-HOBt. However, water loss from a peptide ion is hardly unusual and is generally less likely from a methyl-esterified peptide in any case. For this reason, we compared the CID spectrum of the nominal $[M+H-H_2O]^+$ ion generated via the ion/ion reaction process associated with **Figure 2.11a** (designated $[M+H-H_2O]^+$ i/i rxn) with that of the $[M+H-H_2O]^+$ ion generated from water loss upon CID of singly protonated unmodified YGRAR (see **Figure 2.11b**) (designated $[M+H-H_2O]^+$ CID)

Interestingly, the $[M+H-H_2O]^+$ i/i rxn species fragments almost exclusively via the loss of 43 Da under ion trap CID conditions, whereas the $[M+H-H_2O]^+$ CID ion shows somewhat more diverse fragmentation with the dominant process leading to loss of 42 Da. The latter neutral loss species corresponds to carbodiimide (i.e., HN=C=NH). The loss of this species has previously been proposed to arise following water loss from peptide ions with a C-terminal arginine [40].

Figure 2.12 reproduces the mechanism proposed for loss of carbodiimide following water loss from a peptide ion with arginine at the C-terminus. The loss of 43 Da from the $[M-H_2O]^+$ ion derived from the ion/ion reaction process corresponds to the loss of isocyanic acid (HN=C=O). A prominent loss of isocyanic acid has been reported to occur from peptide ions that have undergone citrullation [41]. In this case, we propose that this loss results from a rearrangement process involving a C-terminal arginine and the anhydride linkage at the C-terminus arising from the ion/ion reaction, as summarized in **Figure 2.13**.

2.3.3 Sulfobenzoyl HOBt and YRARG

The processes of **Figures 2.12** and **2.13** are expected to be most likely when an arginine residue is present at the C-terminus and the oxygen of the water loss comes from the C-terminus. Experiments analogous to those described above for YGRAR were carried out for YRARG to reduce the likelihood for either NH=C=NH or HN=C=O loss. Doubly protonated YRARG was subjected to ion/ion reaction with deprotonated SBHOBt resulting in proton transfer and in the formation of an electrostatic complex, $[YRARG+2H+sulfobenzoyl\ HOBt]^+$, (see **Figure 2.14(a)**). This complex was subjected to CID forming the modified peptide $[YRARG+2H+sulfobenzoyl]^+$ (see **Figure 2.14(b)**). CID of $[YRARG+2H+sulfobenzoyl]^+$ complex generated a nominal $[M+H-H_2O]^+$ product along with many others, most of which are consistent with a reaction at the N-terminus. The formation of the $[M+H-H_2O]^+$ product suggests that at least some of the precursor ion population was composed of a zwitterion and that the carboxylate group reacted with SB-HOBt to generate an anhydride linkage at the C-terminus. **Figure 2.15** compares the CID spectrum of the $[M+H-H_2O]^+$ ion derived from the ion/ion reaction process (designated $[M+H-H_2O]^+$ i/i rxn) (**Figure 2.15a**) with that of the water loss product derived from CID of the $[M+H]^+$ ion (designated $[M+H-H_2O]^+$ CID) (**Figure 2.15b**). In this case, essentially no loss of 43 Da is observed from the ion/ion reaction product, in contrast with the analogous ion derived from YGRAR described above. The spectrum includes an abundant b3 ion and an abundant b_4-42 ion, the latter of which is likely to arise from deguanidination of the residue 4 arginine to generate an ornithine side chain followed by cleavage C-terminal to the ornithine residue [42].

This spectrum is quite distinct from that of the $[M+H-H_2O]^+$ CID ion. While many of the product ions are held in common, the relative abundances are dramatically different, which

indicates that these isomeric ions are of different structure or are comprised of mixtures of structures with different composition. We note that different mechanisms for the generation of $[M+H-H_2O]^+$ ions could, in principle, lead to a common structure or mixture of structures. However, at least in the cases of YGRAR and YRARG, the different mechanisms for nominal water loss from the precursor peptide do not lead to the same structure of set of structures.

2.3.4 Sulfobenzoyl HOBt and Ubiquitin $[M+7H]^{7+}$

The preceding results indicate that an ion/ion reaction can be sensitive to the presence of a carboxylate group in a net positively charged polypeptide ion.

For the small model systems, however, the attachment of a sulfonate group to the cation could play a major role in determining the charge distribution within the ion/ion electrostatic complex. As the polypeptide ion increases in size and charge, the perturbation associated with attachment of the reagent anion is expected to decrease in relative importance. We therefore examined SB-HOBt chemistry with multiply protonated ubiquitin ions and summarize here the results derived from **Figure 2.16**. Process leading to loss of carbodiimide following water loss from a protonated peptide with a C-terminal arginine Scheme 2.4. Process leading to the formation of the $[M-H_2O]^+$ ion from the ion/ion covalent reaction followed by loss of isocyanic acid examination of the [M+7H]7+ ion.

The reaction of singly deprotonated SB-HOBt with the ubiquitin $[M+7H]^{7+}$ ion resulted in the attachment of the reagent anion to the protein ion as the dominant process (**Figure 2.17(a)**) and CID of the electrostatic complex predominantly gave rise to HOBt loss to give $[M+7H+sulfobenzoyl]^{6+}$ with a minor degree of proton transfer to give $[M+6H]^{6+}$ (Figure S 2.6(b)). Ion trap CID of the covalently modified protein (i.e., the $[M+7H+sulfobenzoyl]^{6+}$ ion) yielded a variety of b- and y-type ions with and without the covalent adduct, as expected for modifications at neutral basic sites (**Figure 2.17(b)**).

However, the base product ion peak corresponded to $[M+6H-H_2O]^{6+}$ with very little formation of $[M+6H]^{6+}$. **Figure 2.18** provides a full butterfly^ plot of the ion trap CID product ion spectra of the $[M+6H-H_2O]^{6+}$ ion derived from the ion/ion reaction process (positive abundance axis designated $[M+6H-H_2O]^{6+}$ i/i rxn) and the $[M+6H-H_2O]^{6+}$ ion derived from ion trap CID (negative abundance axis designated $[M+6H-H_2O]^{6+}$ CID). While both ion populations are

comprised of a mixture of structures, there are many similarities in the spectra and a few notable differences. The identities and relative abundances of most of the product ions in the two spectra are very similar. The differences between the two spectra are highlighted in **Figure 2.19**, which displays a subset of the data displayed in **Figure 2.18**. By examining complementary ion pairs, it is possible to narrow down the origins of the sites of water loss. For example, in the case of the [M+6H-H2O]6+ CID the complementary ion pair from cleavage of the D39-Q40 amide linkage is in the form of y_{37}-H_2O/b_{39}, as opposed to y_{37}/b_{39}-H_2O. For the complementary pair from D58-Y59 amide bond cleavage, on the other hand, the dominant combination is y_{18}/b_{58}-H_2O rather than y_{18}-H_2O/b_{58}. This places the origin of the water loss to be largely arising from the region spanned by residues Q40-D58 (see **Figure 2.20**). Comparable abundances of b_{52} and b_{52}-H_2O ions are observed, which is consistent with water loss taking place from more than one site but largely within the residue Q40-D58 span. The results for the $[M + 6H\text{-}H_2O]^{6+}$ i/i rxn is fully consistent with little water loss up to residue 40. However, comparable contributions from y_{18}/ b_{58}-H_2O and y_{18}-H_2O/b_{58} indicate that there is a water loss site beyond residue D58 in many of the ions derived from ion/ion reaction. Of particular note is the presence of y_{12} ions (with very little y_{12}-H_2O) in both plots and a y_{13}-H_2O ion in the ion/ion reaction product data that is absent in the data from CID of the water loss peak derived directly from the $[M+6H]^{6+}$ precursor. These results suggest that some of the ions lost a water molecule from residue 64, a glutamic acid. The findings described above for the model systems taken collectively with the comparison of **Figure 2.19** lead us to hypothesize that the glutamic acid of residue 64 is reactive with SB-HOBt, at least for some of the structures in the precursor ion population. For the reactive structure(s), the glutamic acid at position 64 is thus likely to exist with a negative charge possessing sufficient nucleophilicity to lead to covalent reaction. We note that there may be other carboxylates within the ion that are not accessible to the reactive site of the reagent due to the restricted number and locations of reagent attachment sites.

2.4 Conclusions

The carboxylate group has been shown to react with triazole esters in the gas phase, in analogy with N-hydroxysuccinimide esters, via the reaction of the TMAB-HOBt cation with dianions of Ac-AADAADAA-Ome. A labile anhydride linkage is formed between the carboxylate

and the triazole ester. When a triazole ester is linked to a readily ionized group, it can be used as a reagent to covalently modify a carboxylate containing ion of opposite charge. In this work, we explored the possibility that a triazole ester ion might react with a cation that contains a carboxylate group. Such a scenario nominally prevails in zwitterionic/salt-bridged polypeptide cations. The nucleophilicity of a carboxylate group engaged in an interaction with one or more cations, however, may be significantly lower than that of a carboxylate in a net negative ion. Nevertheless, we demonstrate here that there is some reactivity using the dications of a series of modified and unmodified ions derived from the peptide YGRAR and deprotonated SB-HOBt. Upon CID of a peptide cation that is covalently modified at a carboxylate group, the anhydride linkage cleaves to generate a nominal $[M+nH-H^2O]n+$ ion. The structure or mixture of structures that comprise this ion population may very well differ from the structure or mixture of water loss structures generated via CID of the corresponding $[M+nH]^{n+}$ ion because the mechanisms of formation differ. The CID spectrum of $[M+nH-H_2O]^{n+}$ peak can be used to localize the site(s) of modification. The reaction of deprotonated SB-HOBt with the $[M+7H]^{7+}$ ion of ubiquitin and subsequent CID of the $[M+6H-H2O]^{6+}$ i/i rxn ion led to the conclusion of carboxylate location at the glutamic acid at residue 64. The results indicate the potential for triazole esters as chemical probes that can be used to complement other approaches for the study of gas-phase zwitterion/salt bridge structures.

2.5 References

1. Ding, Y., Krogh-Jespersen, K.: The glycine zwitterion does not exist in the gas phase: results from a detailed ab initio electronic structure study. Chem. Phys. Lett. 199, 261–266 (1992)

2. Prell, J.S., O'Brien, J.T., Steill, J.D., Oomens, J., Williams, E.R.: Structures of protonated dipeptides: the role of arginine in stabilizing salt bridges. J. Am. Chem. Soc. 131, 11442–11449 (2009)

3. Mertens, L.A., Marzluff, E.M.: Gas phase hydrogen/deuterium exchange of arginine and arginine dipeptides complexed with alkali metals. J. Phys. Chem. A. 115, 9180–9187 (2011)

4. Hiserodt, R.D., Brown, S.M., Swijter, D.F.H., Hawkins, N., Mussinan, C.J.: A study of b1+H2O and b1-ions in the product ion spectra of dipeptides containing N-terminal basic amino acid residues. J. Am. Soc. Mass Spectrom. 18, 1414–1422 (2007)

5. Popa, V., Trecroce, D.A., McAllister, R.G., Konermann, L.: Collisioninduced dissociation of electrosprayed protein complexes: an all-atom molecular dynamics model with mobile protons. J. Phys. Chem. B. 120, 5114–5124 (2016)

6. Jenner, M., Ellis, J., Huang, W.-C., Lloyd Raven, E., Roberts, G.C.K., Oldham, N.J.: Detection of a protein conformational equilibrium by electrospray ionisation-ion mobility-mass spectrometry. Angew. Chem. Int. Ed. 50, 8291–8294 (2011)

7. Bonner, J., Lyon, Y.A., Nellessen, C., Julian, R.R.: Photoelectron transfer dissociation reveals surprising favorability of zwitterionic states in large gaseous peptides and proteins. J. Am. Chem. Soc. 139, 10286–10293 (2017)

8. Kjeldsen, F., Silivra, O.A., Zubarev, R.A.: Zwitterionic states in gasphase polypeptide ions revealed by 157-nm ultra-violet photodissociation. Chem. Eur. J. 12, 7920–7928 (2006)

9. Jockusch, R.A., Price, W.D., Williams, E.R.: Structure of cationized arginine (Arg·M+, M = H, Li, Na, K, Rb, and Cs) in the gas phase: further evidence for zwitterionic arginine. J. Phys. Chem. A. 103, 9266–9274 (1999)

10. Price, W.D., Jockusch, R.A., Williams, E.R.: Is arginine a zwitterion in the gas phase? J. Am. Chem. Soc. 119, 11988–11989 (1997)

11. Ling, S., Yu, W., Huang, Z., Lin, Z., Harañczyk, M., Gutowski, M.: Gaseous arginine conformers and their unique intramolecular interactions. J. Phys. Chem. A. 110, 12282–12291 (2006)

12. Marchese, R., Grandori, R., Carloni, P., Raugei, S.: On the Zwitterionic nature of gas-phase peptides and protein ions. PLoS Comput. Biol. 6, e1000775 (2010)

13. Jaeqx, S., Oomens, J., Rijs, A.M.: Gas-phase salt bridge interactions between glutamic acid and arginine. Phys. Chem. Chem. Phys. 15, 16341–16352 (2013)

14. Scarff, C.A., Thalassinos, K., Hilton, G.R., Scrivens, J.H.: Travelling wave ion mobility mass spectrometry studies of protein structure: biological significance and comparison with X-ray crystallography and nuclear magnetic resonance spectroscopy measurements. Rapid Commun. Mass Spectrom. 22, 3297–3304 (2008)

15. Covey, T., Douglas, D.J.: Collision cross sections for protein ions. J. Am. Soc. Mass Spectrom. 4, 616–623 (1993)

16. Clemmer, D.E., Hudgins, R.R., Jarrold, M.F.: Naked protein conformations: cytochrome c in the gas phase. J. Am. Chem. Soc. 117, 10141–10142 (1995)

17. Wyttenbach, T., Bowers, M.T.: Structural stability from solution to the gas phase: native solution structure of ubiquitin survives analysis in a solvent-free ion mobility–mass spectrometry environment. J. Phys. Chem. B. 115, 12266–12275 (2011)

18. Bush, M.F., Hall, Z., Giles, K., Hoyes, J., Robinson, C.V., Ruotolo, B.T.: Collision cross sections of proteins and their complexes: a calibration framework and database for gas-phase structural biology. Anal. Chem.82, 9557–9565 (2010)

19. Silveira, J.A., Fort, K.L., Kim, D., Servage, K.A., Pierson, N.A.,Clemmer, D.E., Russell, D.H.: From solution to the gas phase: stepwisedehydration and kinetic trapping of substance P reveals the origin ofpeptide conformations. J. Am. Chem. Soc. 135, 19147–19153 (2013)

20. Pagel, K., Natan, E., Hall, Z., Fersht, A.R., Robinson, C.V.: Intrinsically disordered p53 and its complexes populate compact conformations in the gas phase. Angew. Chem. Int. Ed. 52, 361–365 (2013)

21. Skinner, O.S., McLafferty, F.W., Breuker, K.: How ubiquitin unfolds after transfer into the gas phase. J. Am. Soc. Mass Spectrom. 23, 1011–1014 (2012)

22. Zhang, Z., Browne, S.J., Vachet, R.W.: Exploring salt bridge structures of gas-phase protein ions using multiple stages of electron transfer and collision induced dissociation. J. Am. Soc. Mass Spectrom. 25, 604–613 (2014)

23. Zhang, Z., Vachet, R.W.: Gas-phase protein salt bridge stabilities from collisional activation and electron transfer dissociation. Int. J. Mass Spectrom. 420, 51–56 (2017)

24. Mentinova, M., McLuckey, S.A.: Covalent modification of gaseous peptide ions with N-hydroxysuccinimide ester reagent ions. J. Am. Chem. Soc. 132, 18248–18257 (2010)

25. McGee, W.M., Mentinova, M., McLuckey, S.A.: Gas-phase conjugation to arginine residues in polypeptide ions via N-hydroxysuccinimide esterbased reagent ions. J. Am. Chem. Soc. 134, 11412–11414 (2012)

26. Peng, Z., McGee, W.M., Bu, J., Barefoot, N.Z., McLuckey, S.A.: Gas phase reactivity of carboxylates with N-hydroxysuccinimide esters. J. Am. Soc. Mass Spectrom. 26, 174–180 (2015)

27. Bu, J., Peng, Z., Zhao, F., McLuckey, S.A.: Enhanced reactivity in nucleophilic acyl substitution ion/ion reactions using triazole-ester reagents. J. Am. Soc. Mass Spectrom. 28, 1254–1261 (2017)

28. Mirzaei, H., Regnier, F.: Enhancing electrospray ionization efficiency of peptides by derivatization. Anal. Chem. 78, 4175–4183 (2006)

29. Peng, Z., Pilo, A.L., Luongo, C.A., McLuckey, S.A.: Gas-phase amidation of carboxylic acids with Woodward's reagent K ions. J. Am. Soc. Mass Spectrom. 26, 1686–1694 (2015)

30. Niles, R., Witkowska, H.E., Allen, S., Hall, S.C., Fisher, S.J., Hardt, M.: Acid-catalyzed Oxygen-18 labeling of peptides. Anal. Chem. 81, 2804–2809 (2009)

31. Hager, J.W.: A new linear ion trap mass spectrometer. Rapid Commun.Mass Spectrom. 16, 512–526 (2002)

32. Xia, Y., Chrisman, P.A., Erickson, D.E., Liu, J., Liang, X., Londry, F.A., Yang, M.J., McLuckey, S.A.: Implementation of ion/ion reactions in a quadrupole/time-of-flight tandem mass spectrometer. Anal. Chem. 78, 4146–4154 (2006)

33. Xia, Y., Liang, X., McLuckey, S.A.: Pulsed dual electrospray ionization for In/In reactions. J. Am. Soc. Mass Spectrom. 16, 1750–1756 (2005)

34. Xia, Y., Wu, J., McLuckey, S.A., Londry, F.A., Hager, J.W.: Mutual storage mode ion/ion reactions in a hybrid linear ion trap. J. Am. Soc. Mass Spectrom. 16, 71–81 (2005)

35. Louris, J.N., Cooks, R.G., Syka, J.E.P., Kelley, P.E., Stafford, G.C., Todd, J.F.J.: Instrumentation, applications, and energy deposition in quadrupole ion-trap tandem mass-spectrometry. Anal. Chem. 59, 1677– 1685 (1987)

36. Londry, F.A., Hager, J.W.: Mass selective axial ion ejection from a linear quadrupole ion trap. J. Am. Soc. Mass Spectrom. 14, 1130–1147 (2003)

37. Gilbert, J.D., Prentice, B.M., McLuckey, S.A.: Ion/ion reactions with Bonium^ reagents: an approach for the gas-phase transfer of organic cations to multiply-charged anions. J. Am. Soc. Mass Spectrom. 29, 818–825 (2015)

38. Harrilal, Christopher. Investigating electronic and structural changes imposed by Zwitterionic pairing in model peptides systems using IR-UV double resonance spectroscopy. 66th ASMS Conference on Mass Spectrometry and Allied Topics, American Society for Mass Spectrometry. San Diego Convention Center, CA (2018)

39. McGee, W.M., McLuckey, S.A.: Gas phase dissociation behavior of acylarginine peptides. Int. J. Mass Spectrom. 354-355, 181–187 (2013)

40. Deery, M.J., Summerfield, S.G., Buzy, A., Jennings, K.R.: A mechanism for the loss of 60 u from peptides containing an arginine residue at the Cterminus. J. Am. Soc. Mass Spectrom. 8, 253–261 (2009)

41. Hao, G., Wang, D., Gu, J., Shen, Q., Gross, S.S., Wang, Y.: Neutral loss of isocyanic acid in peptide CID spectra: a novel diagnostic marker for mass spectrometric identification of protein citrullination. J. Am. Soc. Mass Spectrom. 20, 723–727 (2009)

42. McGee, W.M., McLuckey, S.A.: The ornithine effect in peptide cation dissociation. J. Mass Spectrom. 48, 856–861 (2013)

2.6 Figures

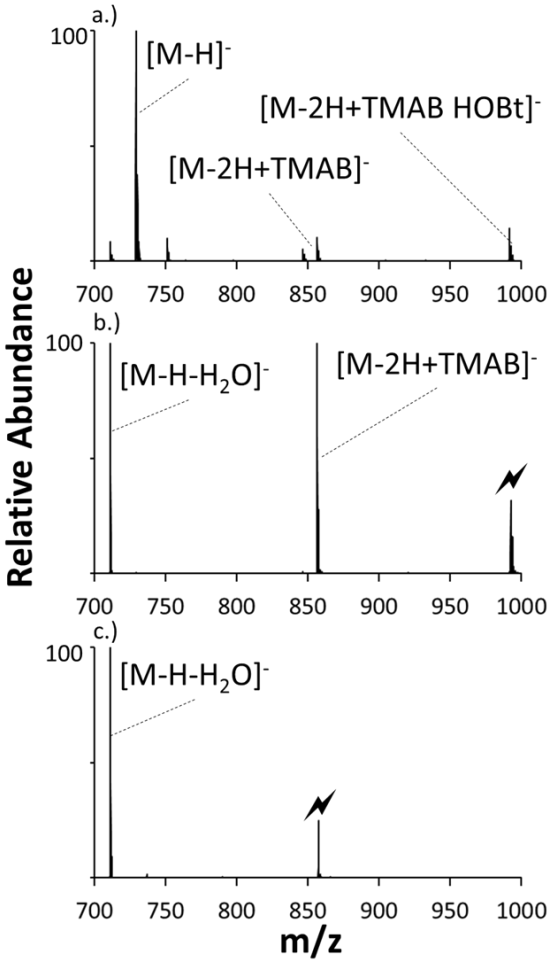

Figure 2.1 Product ion spectra derived from (a) Ion-ion reaction between [Ac-ADAADAA-Ome-2H]$^-$ and [TMAB-HOBt]$^+$ (b) CID of complex [M-2H+(TMAB-HOBt)]$^-$ (c)CID of [M-2H+TMAB]$^-$ Formation of the [M-H-H_2O]$^-$ (indicated by the blue outline).

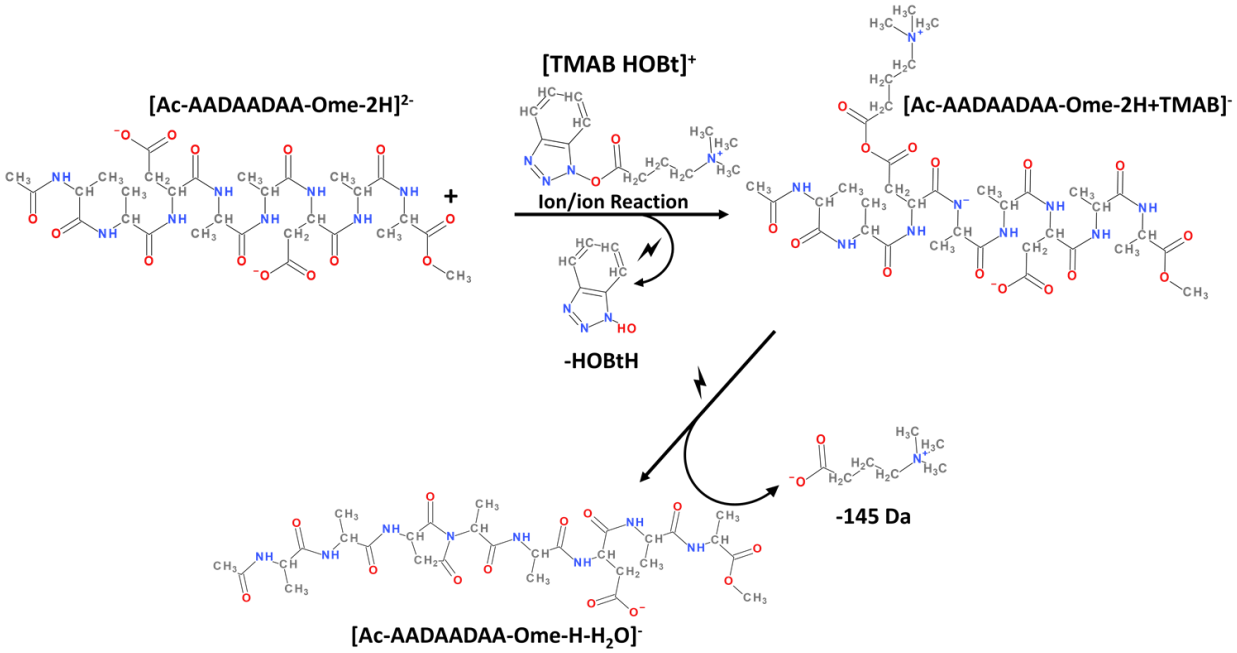

Figure 2.2 Reaction between the carboxylate group in a doubly-deprotonated Ac-AADAADAA-Ome with deprotonation at both the aspartic acid side chains with a positively charged TMAB HOBt

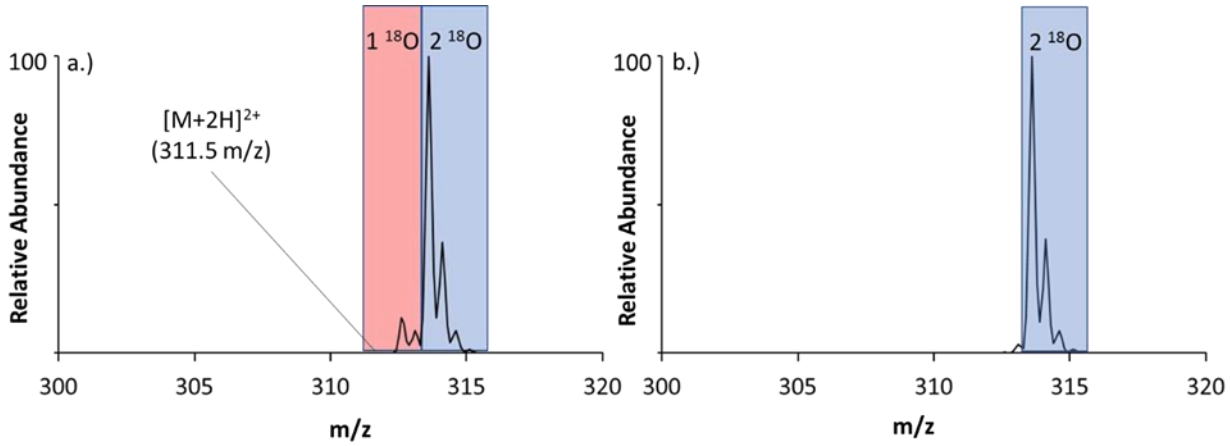

Figure 2.3 Distribution of 18O heavy labeled [YGRAR+2H]2+ b) isolation of mass corresponding to the exchange of 2 heavy oxygens

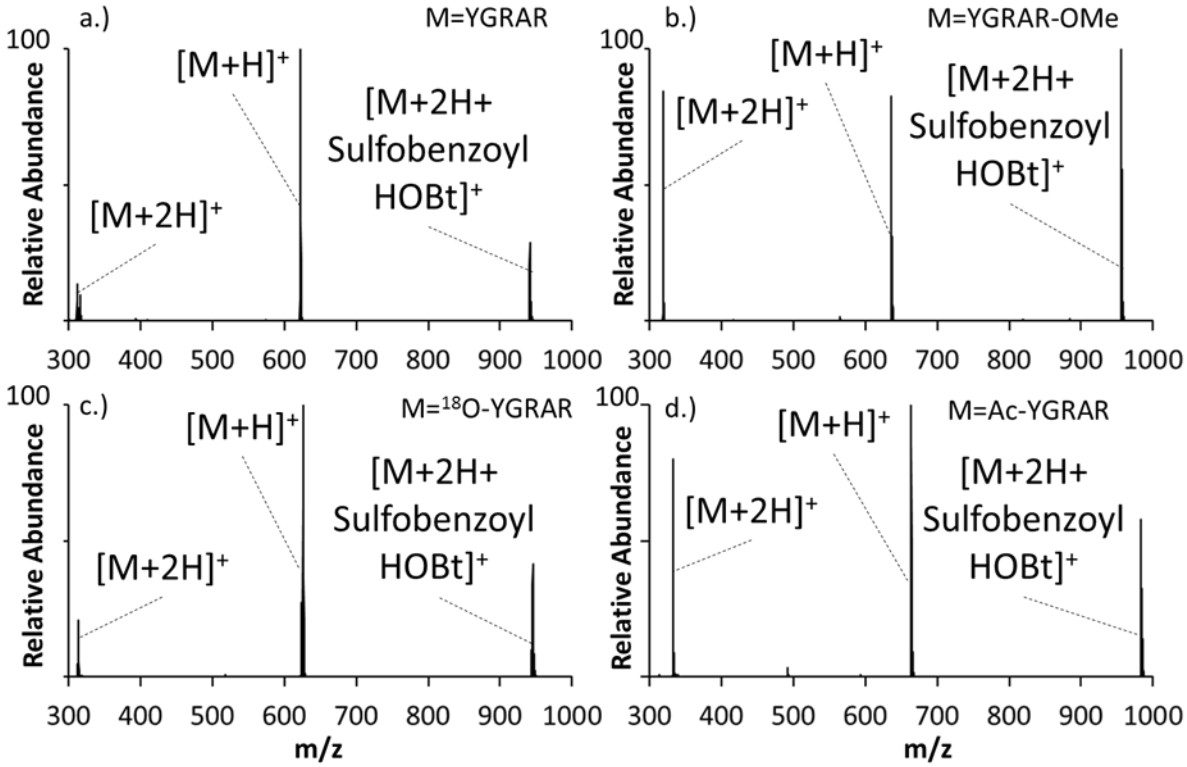

Figure 2.4a.) Ion-ion reaction spectrum showing formation of a) [YGRAR+2H+Sulfobenzoyl HOBt]+ b.) [YGRAR-OMe+2H+Sulfobenzoyl HOBt]+ c.) [O18-YGRAR+2H+Sulfobenzoyl HOBt]+ and d.) [ac-YGRAR+2H+Sulfobenzoyl HOBt]+.

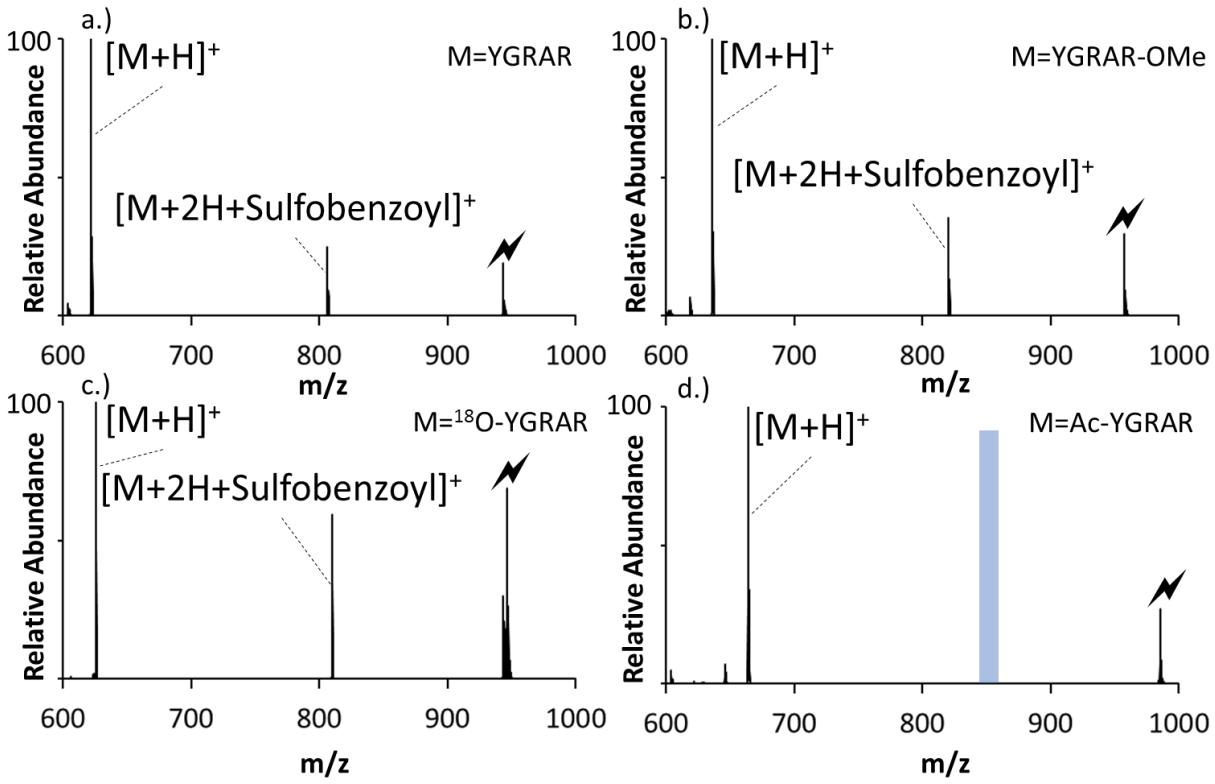

Figure 2.5 Ion trap CID of the complexes $[M+2H+SB\text{-}HOBt]^+$ generated via ion/ion reactions between deprotonated SB-HOBt and doubly protonated (a) YGRAR, (b) YGRAR-OMe, (c) O^{18}-YGRAR, and (d) ac-YGRAR. (Shaded regions indicate where $[M+2H+Sulfobenzoyl]^+$ would be formed.) ↯ indicates parent ion

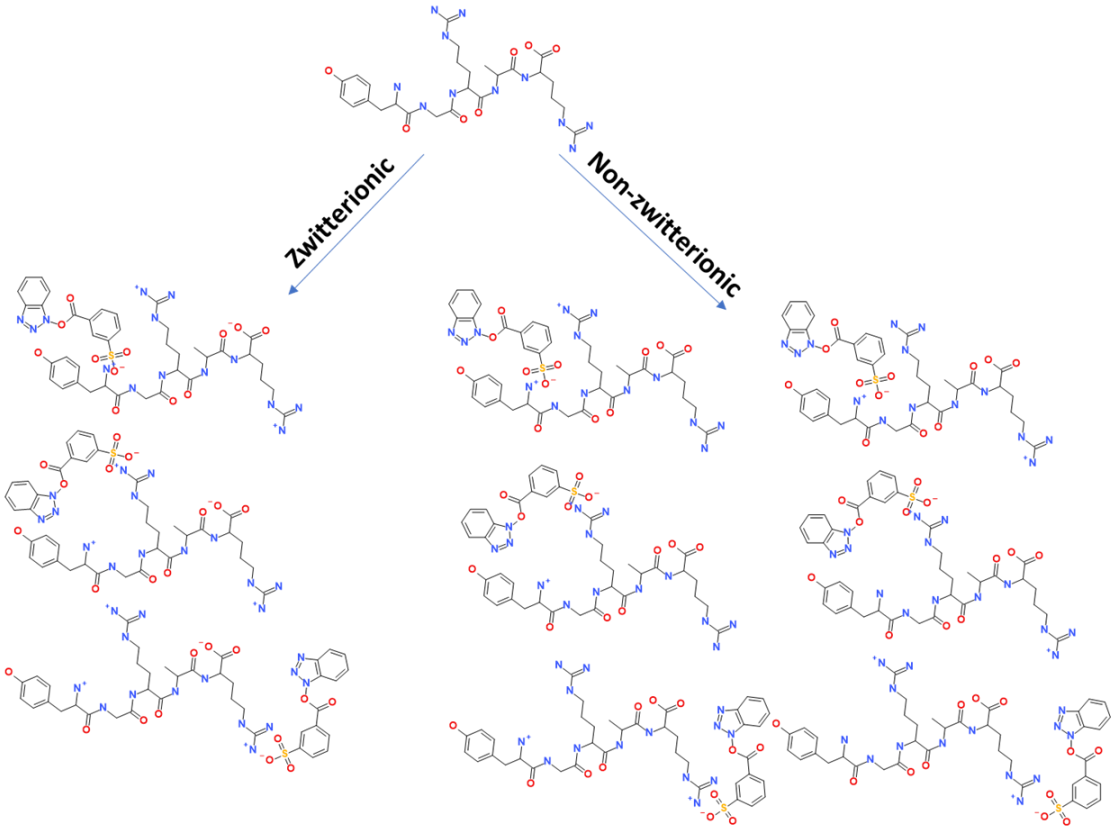

Figure 2.6 Different charge site isomers of [M+2H+Sulfobenzoyl HOBt]+

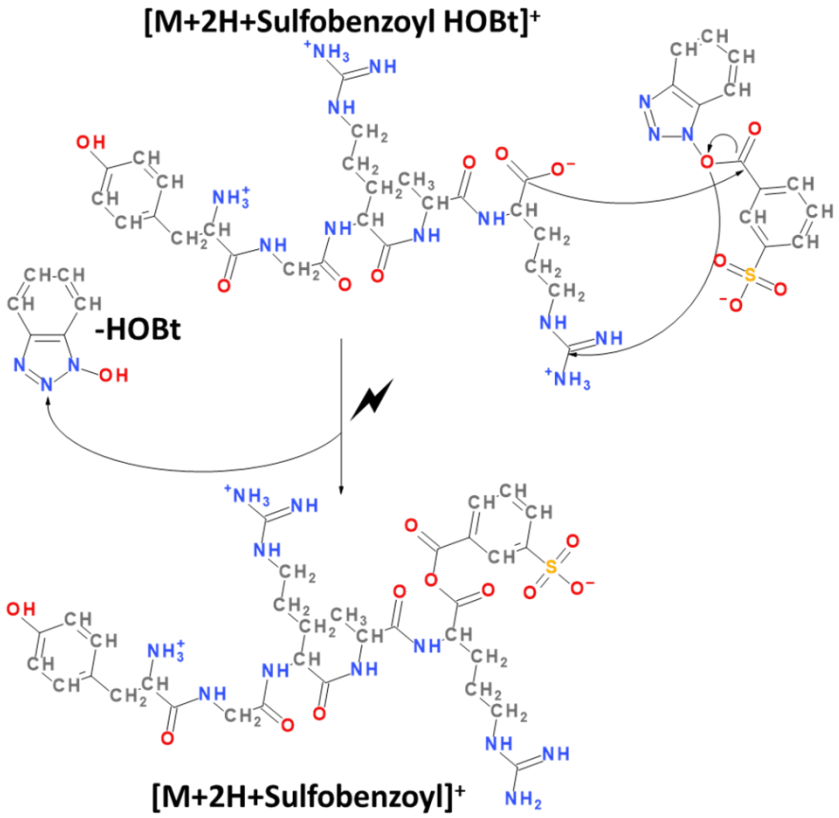

Figure 2.7 Reaction between the carboxylate group in a doubly-charged YGRAR with protonation at the N-terminus and both arginine residues with deprotonated SB-HOBt.

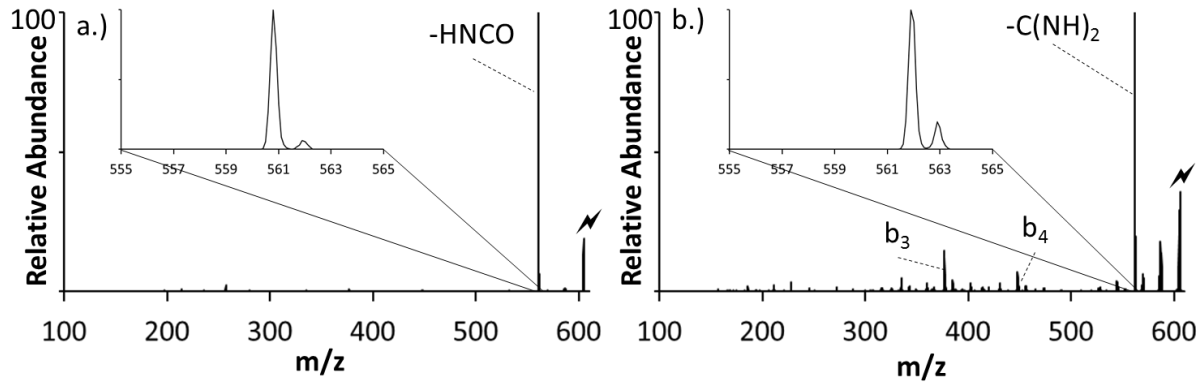

Figure 2.8 Ion trap product ion spectra obtained from the nominal $[M-H_2O]^+$ ions derived from a) ion/ion reaction between doubly protonated YGRAR and deprotonated SB-HOBt followed by loss of HOBt and b) CID of singly protonated YGRAR.

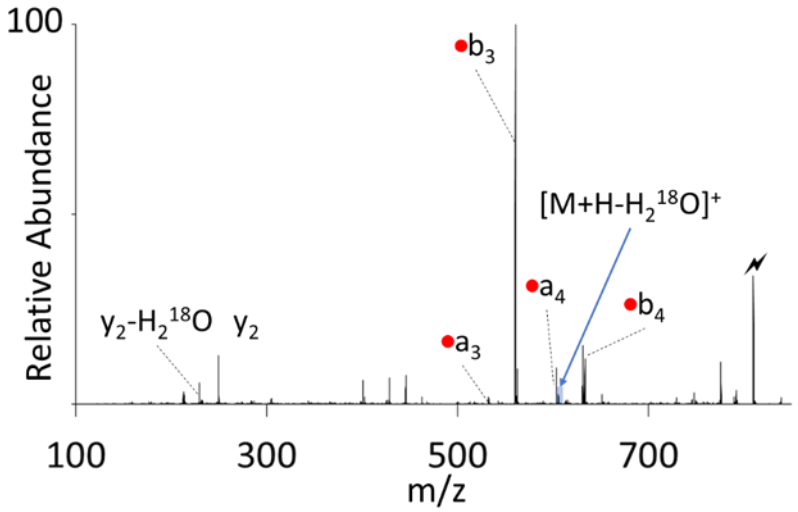

Figure 2.9 Ion trap CID spectrum of the [M+H+sulfobenzoyl]+of M= 18O-YGRAR shows the presence of [M+H-H218O]+ (shaded region) (indicates a mass shift of 183 Da corresponding to the addition of Sulfobenzoyl).

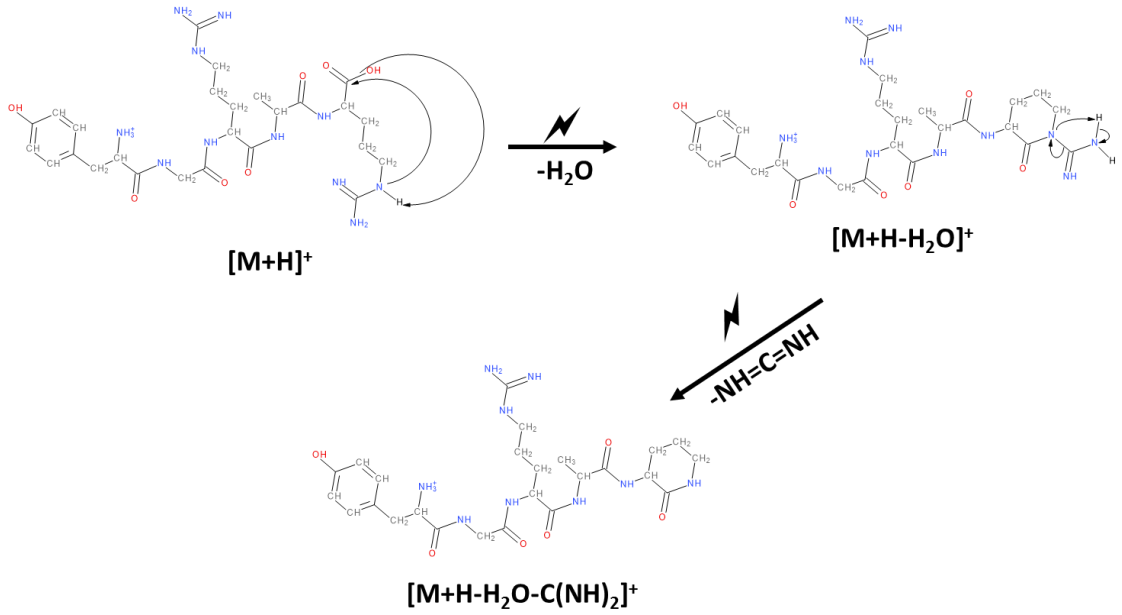

Figure 2.10 Process leading to loss of carbodiimide following water loss from a protonated peptide with a C-terminal arginine.

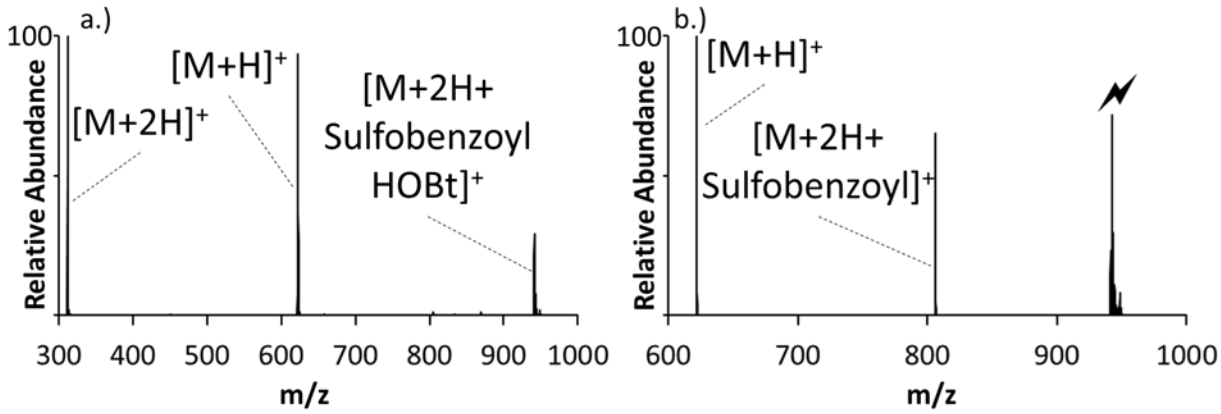

Figure 2.11 a.) Ion-ion reaction between YRARG2+ (m/z 311) and Sulfobenzoyl HOBt- formation of the long-lived complex. b.) Shows the formation of [YRARG+ Sulfobenzoyl]+ after CID of the complex.

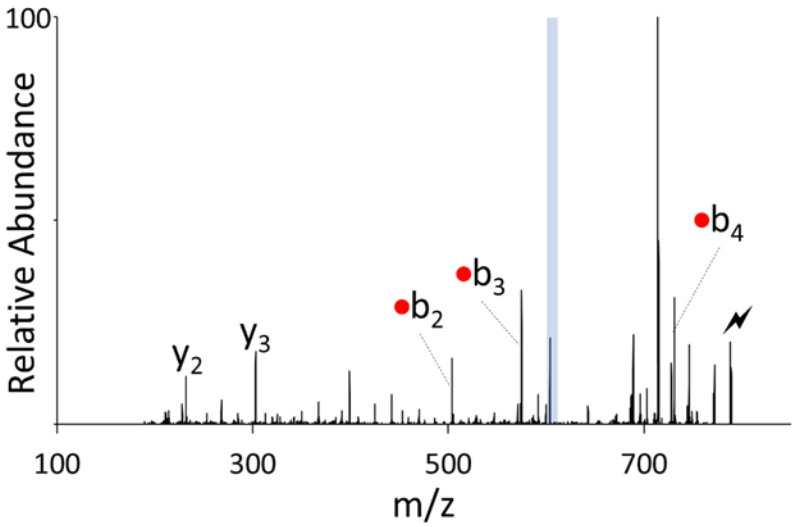

Figure 2.12 Ion trap CID spectrum of [YRARG+H+Sulfobenzoyl]+ shows the presence of [M+H-H2O]+ (shaded region) (indicates a mass shift of 183 Da corresponding to the addition of Sulfobenzoyl).

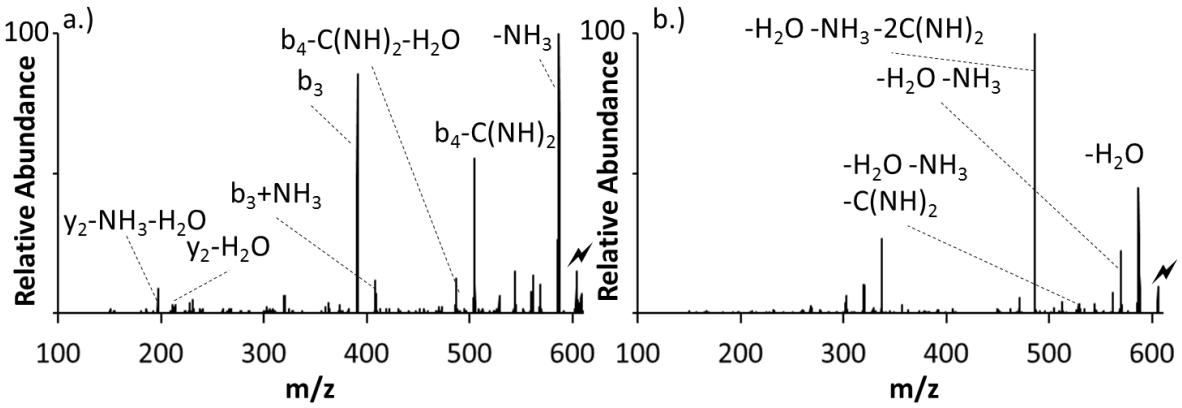

Figure 2.13 Comparison of ion trap CID product ion spectra derived from the $[M\text{-}H_2O]^+$ ions generated (a) via ion/ion reaction between deprotonated SB-HOBt and $[YRARG+2H]^{2+}$ and (b) CID of $[YRARG+H]^+$.

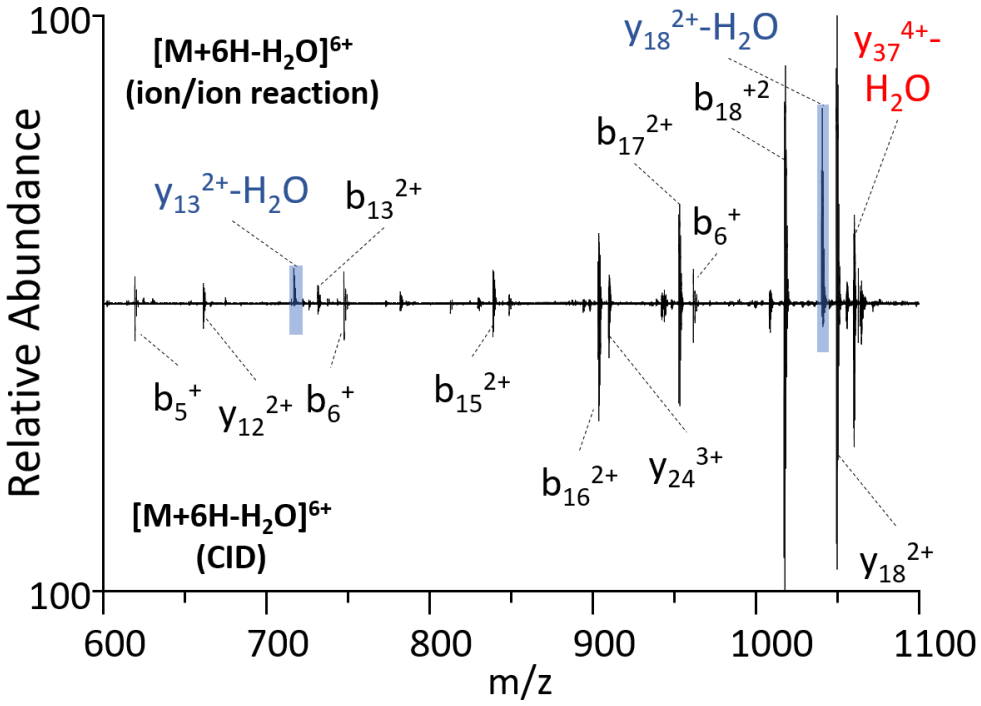

Figure 2.14 Comparison of ion trap CID results from $[M+6H-H_2O]^{6+}$ ions derived from ion/ion reaction (top) and ion trap CID of the $[M+6H]^{6+}$ion (bottom).

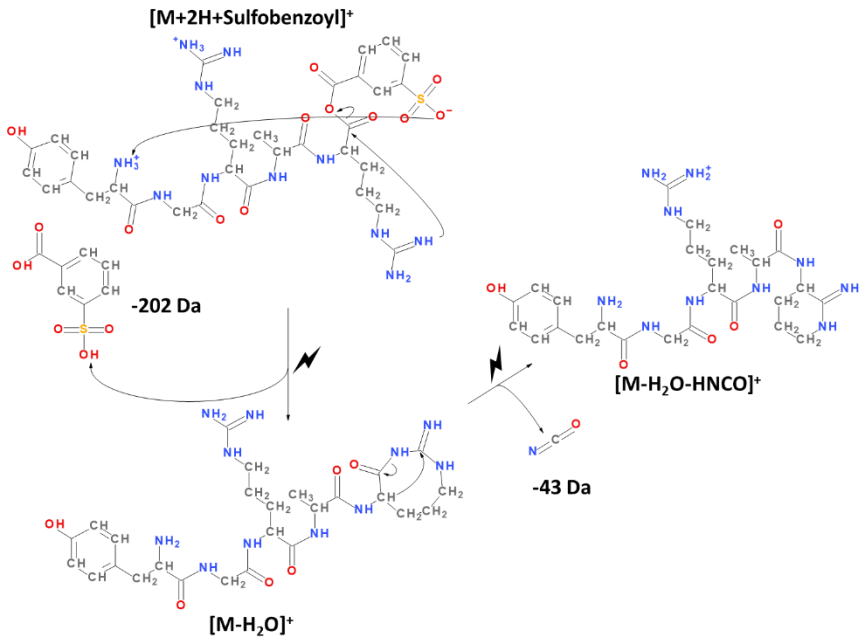

Scheme 2.1 Process leading to the formation of the $[M-H_2O]^+$ ion from the ion/ion covalent reaction followed by loss of isocyanic acid.

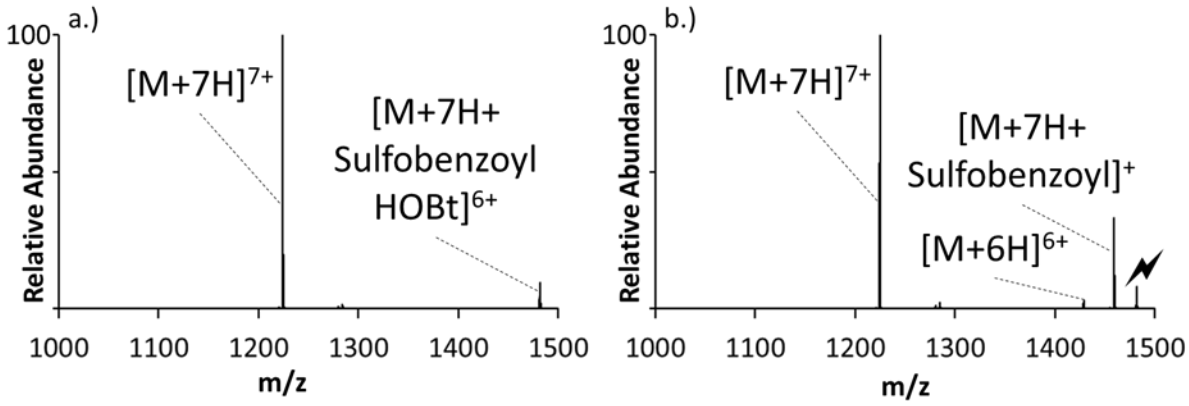

Figure 2.15 a) Post ion/ion reaction spectrum of [M+7H]7+/[SB-HOBt-H]- showing residual unreacted [M+7H]7+ and electrostatic complex generated by attachment of the reagent anion to the cation. b) Ion trap CID of the electrostatic complex without prior removal of

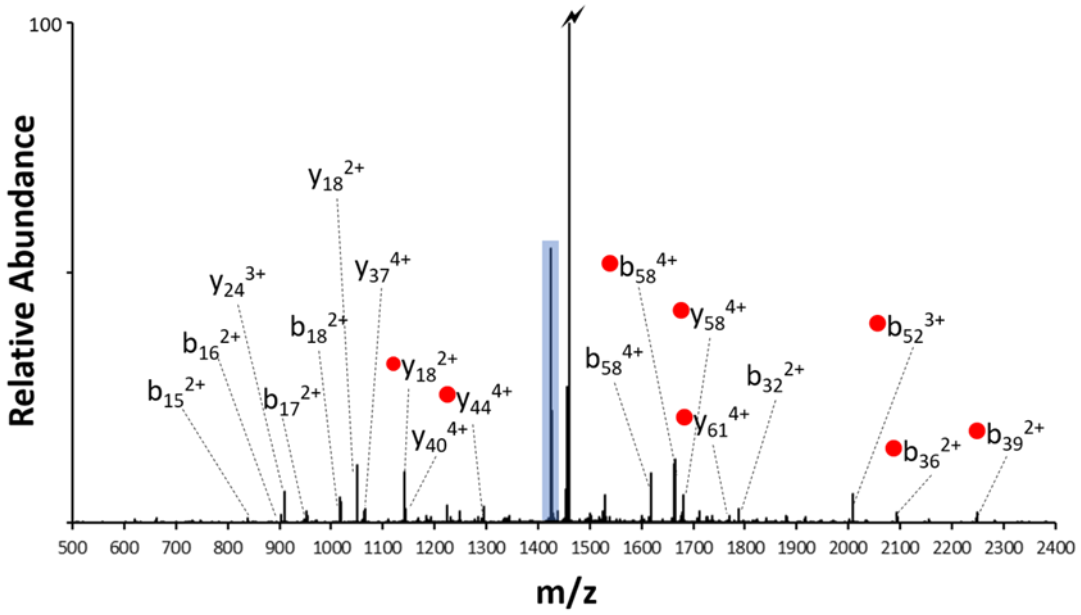

Figure 2.16 Ion trap CID spectrum of the [M+sulfobenzoyl]6+covalent adduct generated by the experiment of Figure S 2.5(b). (M=Ubiquitin)

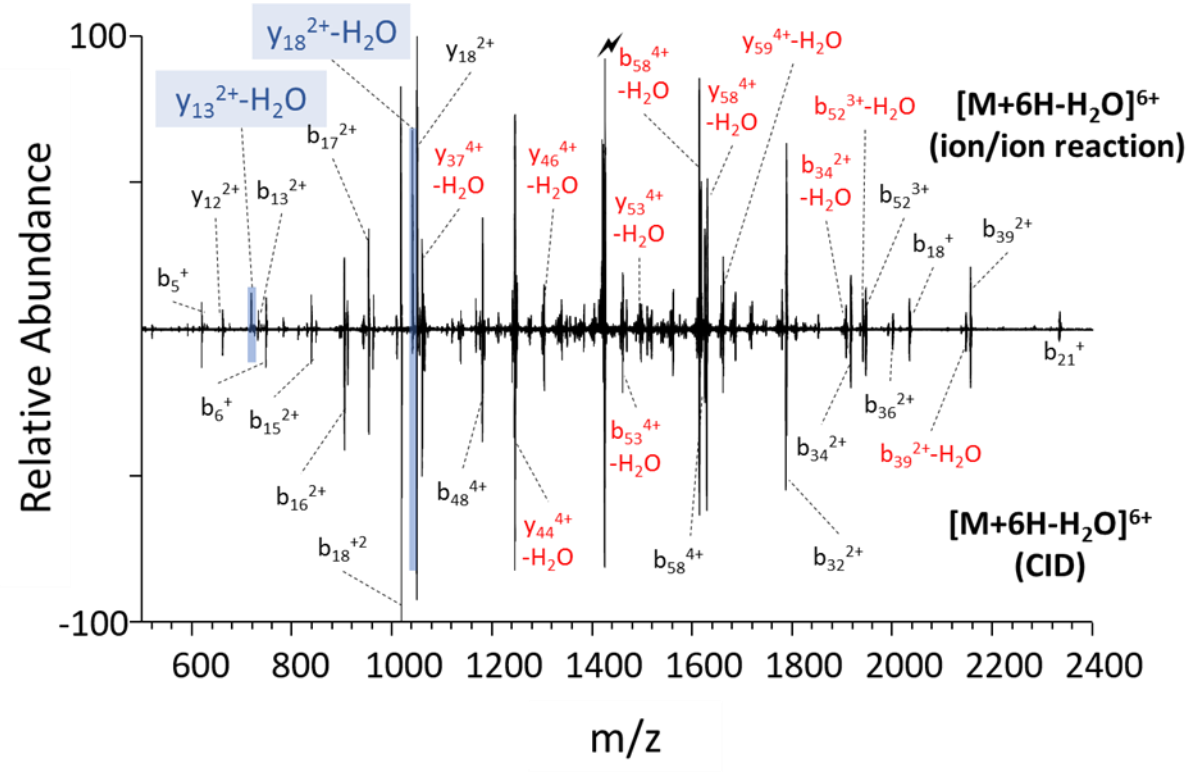

Figure 2.17 Comparison of ion trap CID results from [M+6H-H2O]6+i/i rxn (top) and [M+6H-H2O]6+CID ion (bottom). (M = Ubiquitin) Water loss ions with major differences in relative abundances in the top versus bottom spectrum are labeled in blue font where water loss

Figure 2.18 Ubiquitin sequence showing products of CID of the [M-H2O]6+ from the ion/ion reaction and [M+6H-H2O]6+ formed from CID

CHAPTER 3. GAS PHASE CROSS-LINKING OF PROTEIN COMPLEXES VIA ION/ION REACTIONS

Crosslinking mass spectrometry (XL-MS) has grown as method to gain insight to the three-dimensional structure of proteins and protein complexes. This method uses reagents to covalently modify side chains of amino acid residues and, provided two residues are within a reagent's length, link two residues to one another. This allows for determination of which residues are within proximity to each other and, when combined with other techniques, can offer spatial structural information. Typically, these reactions are performed in solution and previously a method has been developed to reproduce similar results in the gas phase, albeit with a monomer protein system. The merits to performing this reaction in the gas phase are higher degree of control and throughput and reduced ambiguity. Here a method is shown to perform this reaction in the gas phase with dimer protein complexes.

3.1 Introduction

Crosslinking mass spectrometry (XL-MS) has grown to be a well-established method to probe the structure of proteins and protein complexes.[1–4] This tool is especially powerful when other methods such as x-ray crystallography or cryogenic electron microscopy are incompatible with the protein system of interest. XL-MS has allowed researchers to pinpoint the distance between two residues by covalently binding the side chains of two residues. This is performed in solution and gives insight into the three-dimensional structure of the analyte as reactions can only occur within the length constraint of the crosslinker.[5]

Some of the struggles with crosslinking mass spectrometry arise from the optimization of solution conditions. A crosslinking experiment requires incubation of a protein or several proteins when investigating protein networks. This can lead to multiple types of crosslinks to occur such as type 0 (dead end) or type 1 (intra-linked) crosslinked peptides.74] Many crosslinking reagents used in these studies use facile reactions between NHS esters and nucleophilic sites. Previous experiments with NHS esters have shown gas phase reactivity to unprotonated lysine and arginine side chains but no reactivity to protonated residues. These reagents can be subjected to negative electrospray and form doubly and singly deprotonated anions. Previously, the utility of gas-phase

crosslinking has been shown to allow for higher amounts of user control and to obtain comparable data to crosslinking reactions performed in solution.[6–8] This method utilized gas-phase ion/ion reactions to mass select charge states of protein cations and mutual store these ions with anionic crosslinkers. This resulted in the oppositely charged ions to form a long-lived electrostatic complex. Collisional activation of this complex resulted in covalent modification of the analyte provided there was an unprotonated reactive site. Subsequent activation of the crosslinked analyte resulted in a mixture of fragment ions and crosslinked fragment ions.

These previous experiments were monomer protein units or peptides but there are many protein-protein interactions and protein complexes formed. These interactions and complexes dictate many biological functions within a system so understand the structures of protein complexes are pertinent to understanding their function. This demonstrates a necessity to determine the feasibility of performing these reactions on protein complexes. Here we show, gas phase crosslinking of protein complexes using homobifunctional NHS crosslinker Sulfo-EGS to crosslink homo- and hetero- dimer protein complexes.

3.2 Experimental

3.2.1 Materials

Ubiquitin

Ubiquitin from bovine erythrocytes were purchased from Sigma-Aldrich (St. Louis, MO, USA). Solutions were made in in 50:50 (vol:vol) methanol:water at a concentration of 100 µM to allow for dimer formation.

Trypsin and Aprotinin

Trypsin and Aprotinin were purchased from Sigma-Aldrich (St. Louis, MO, USA). Solutions were made in 150 mM ammonium acetate at concentrations of 10 µM.

Reagents

The crosslinker ethylene glycol bis(sulfosuccinimidyl succinate) (sulfo-EGS) was purchased from Thermo Fisher Scientific Inc. (Rockford, IL, USA). Sulfo-EGS was dissolved in

50:50 (vol:vol) methanol:water at 5 mM. ammonium acetate was purchased from Sigma-Aldrich (St. Louis, MO). Methanol, and acetic acid were obtained from Fisher Scientific (Fairmont, NJ).

3.2.2 Mass Spectrometry

Experiments were performed using a TripleTOF 5600 System (SCIEX, Concord, ON, Canada). This instrument was previously modified to perform ion/ion reactions [9]. Anions and cations were sequentially injected via alternatively pulsed nano-electrospray ionization (nESI). First, cationic protein complexes are injected, isolated in Q1, and transferred and stored in q2. Next, anionic crosslinker ions are injected, isolated in Q1, and transferred to q2[10]. The ions were mutually stored in the q2 reaction cell for 10–1000 ms to allow for ample complex formation. The electrostatic complex was isolated stored waveform inverse Fourier transform (SWIFT) isolation.[11, 12] This isolation method using a custom waveform applied to the rods in q2 to applies a voltage to frequencies of unwanted ions to eject them from q2. Once isolated ions were subjected to resonance excitation (ion trap CID) to covalently modify the protein complex. Once the complex was modified, a second custom waveform was applied to perform tandem MS to determine the modification site. Fragment ions from activation of the complex mass analyzed via orthogonal time-of-flight (TOF) and data analysis was performed manually.

3.3 Results and Discussion

3.3.1 Ubiquitin

It has been shown that nonspecific dimers can form simply by increasing the concentration of analyte. This is demonstrated is **Figure 3.1** which shows an isolated $[M+4H]^{4+}$ with residual peaks of $[M+3H]^{3+}$ and $[M+5H]^{5+}$. The presence of these residual charge states are due to presence of dimer, which overlaps with the 4+ charge state of the monomer, undergoing activation. Evidence for the presence of dimer (D) is shown in the inset which shows a zoomed image of the $[M+4H]^{4+}$. In the inset, the shaded regions show isotopic spacing corresponding to $[D+8H]^{8+}$. The activation from the rF/DC isolation in q1 is sufficient to disrupt the noncovalent interactions maintaining the complex. This activation reduced the signal of the dimer therefore the $[D+9H]^{9+}$ was isolated because there was not spectral overlap at that m/z and it allowed a wider isolation reducing collisional activation. Unfortunately, residual charge states were still present but lower

abundance. (not shown) The reaction was allowed to proceed due to subsequent isolation steps removing unwanted species.

The $[D+9H]^{9+}$ was stored in q2 and the crosslinker Sulfo-EGS was injected . The doubly deprotonated crosslinker denoted as $[Sulfo\ EGS-2H]^{2-}$ isolated in q1 shown **Figure 3.2**, and mutually stored in q2 with the protein complex. This resulting spectrum is shown **Figure 3.3** where multiple attachments of the reagent can be observed (labeled in red). This workflow calls for isolation of the single attachment of the reagent ion and this was accomplished using SWIFT isolation. SWIFT isolation requires a supplemental AC waveform to be applied using a waveform generator. Custom waveforms were prepared using MS Devices (additional software provided by Sciex). Once applied unwanted species were ejected from the trap with only the electrostatic complex $[D+9H+Sulfo\ EGS]^{7+}$ shown in **Figure 3.4.** This shows the utility of SWIFT as rf/DC isolation of the noncovalent protein complex resulted in dissociation of the complex. While using SWIFT isolation in q2, the electrostatic complex can be isolated with no evidence of residual heating. After isolation, $[D+9H+Sulfo\ EGS]^{7+}$ was subjected to CID to covalently modify the protein complex. Upon collisional activation the complex does undergo dissociation and multiple products are observed shown in **Figure 3.5**. The complex forms two separate populations corresponding to each of the monomers with some peaks electrostatically bound to the reagent, covalently modified, or monomer without Sulfo EGS. Each of the products possess a complementary ion pair with pairs shaded blue or green. Although these products reduced the overall signal, there was a small portion of the electrostatic complex the underwent covalent modification and maintained the protein complex (shaded red). This product is assumed to be the result of two neutral losses of the Sulfo NHS moiety similar to previous studies.[67, 76] This neutral loss occurs when a nucleophilic reaction occurred driven by collisional activation and the Sulfo NHS acts as a leaving group. Once again isolation was performed, using a second waveform generator with a custom waveform to isolate the covalently modified protein complex. Once isolated (not shown) the modified protein complex was subjected to ion trap CID to fragment the complex. This spectrum is shown in **Figure 3.6** where *b*- and *y*- fragment ions are observed as well as complementary fragment ions possessing the mass of the crosslinking reagent and an intact monomer of ubiquitin. This demonstrates that although much of the signal is lost due dissociation of the complex, the sensitivity of this method allows for enough to perform this reaction in the gas-phase.

3.3.2 Trypsin & Aprotinin

This reaction was applied to trypsin (T), a proteolytic digestive enzyme, and aprotinin, a trypsin inhibitor. These two proteins when in solution form a noncovalent complex with aprotinin (A) inhibiting tryptic digestion. This heterodimer complex (AT) was subjected to the method above beginning with isolation of the $[AT+11H]^{11+}$. Afterwards the complex was mutually stored with $[Sulfo\ EGS+2H]^{2-}$ and the electrostatic complex was formed and isolated using SWIFT isolation. (not shown) After isolation the electrostatic complex $[AT+11H+Sulfo\ EGS]^{9+}$ was subjected to ion-trap CID. Upon CID the complex dissociates in similar fashion to the ubiquitin dimer complex however there are a few notable differences. Shown in **Figure 3.7** the CID spectrum of the electrostatic complex results in two charge state populations for each species. The aprotinin and trypsin both show some peaks electrostatically bound to the reagent, covalently modified, or monomer without Sulfo EGS like ubiquitin. The presence of an additional charge state for each of the components of the complex suggest that there is variation in the charge partition of the complex. This complex also required a second CID step to form the covalent product as there is only a single neutral loss as opposed to two as seen in the case of ubiquitin. Nonetheless after an additional step of CID there was a second neutral loss corresponding to loss of the Sulfo EGS moiety inferring covalent modification. CID of the modified protein complex was less informative as there was mostly only small neutral loss resulting in a mostly unfragmented complex shown in **Figure 3.8**. This spectrum shows the lack of fragment and complementary fragments observed compared to ubiquitin. It is likely the disulfide bonds present in both trypsin (six) and aprotinin (three) are preventing extensive fragmentation as CID does not fragment these bonds. In this case, crosslinking in the gas phase would not be applicable without reduction of the disulfide that maintains protein structure. This seems to be a limitation of this method when applied to complexes that require disulfide linkages however more experiments are needed to confirm.

3.4 Conclusions

In conclusion, gas-phase crosslinking reaction can be applied to protein complexes however, care must be taken to preserve the complexes. These noncovalent interactions can be fragile, and instrument parameters must be optimized for each system. SWIFT isolation has shown promise to circumvent the complex loss due to collisional heating from rF/DC isolation. When applying this

method to more complex systems like the heterodimer trypsin and aprotinin additional challenges like disulfide bridging which prevents fragmentation. Future work should investigate a heterodimer system that has no or very few disulfide bonds. A heterodimer to attempt this method on is barnase and barstar which is an enzyme and an inhibitor system with masses of ~12 kDa and 10 kDa, respectively. [13] Also the implementation of an additional activation technique that can cause fragmentation in the presence of disulfide bonds.

3.5 References

1. Singh, P., Panchaud, A., Goodlett, D.R.: Chemical Cross-Linking and Mass Spectrometry As a Low-Resolution Protein Structure Determination Technique. Anal. Chem. 82, 2636–2642 (2010). https://doi.org/10.1021/ac1000724

2. O'Reilly, F.J., Rappsilber, J.: Cross-linking mass spectrometry: methods and applications in structural, molecular and systems biology. Nat. Struct. Mol. Biol. 25, 1000 (2018). https://doi.org/10.1038/s41594-018-0147-0

3. Iacobucci, C., Götze, M., Ihling, C.H., Piotrowski, C., Arlt, C., Schäfer, M., Hage, C., Schmidt, R., Sinz, A.: A cross-linking/mass spectrometry workflow based on MS-cleavable cross-linkers and the MeroX software for studying protein structures and protein–protein interactions. Nat. Protoc. 13, 2864–2889 (2018). https://doi.org/10.1038/s41596-018-0068-8

4. Yu, C., Huang, L.: Cross-Linking Mass Spectrometry: An Emerging Technology for Interactomics and Structural Biology. Anal. Chem. 90, 144–165 (2018). https://doi.org/10.1021/acs.analchem.7b04431

5. Chavez, J.D., Bruce, J.E.: Chemical cross-linking with mass spectrometry: a tool for systems structural biology. Curr. Opin. Chem. Biol. 48, 8–18 (2019). https://doi.org/10.1016/j.cbpa.2018.08.006

6. Webb, I.K., Mentinova, M., McGee, W.M., McLuckey, S.A.: Gas-Phase Intramolecular Protein Crosslinking via Ion/Ion Reactions: Ubiquitin and a Homobifunctional sulfo-NHS Ester. J. Am. Soc. Mass Spectrom. 24, 733–743 (2013). https://doi.org/10.1007/s13361-013-0590-4

7. Mentinova, M., McLuckey, S.A.: Intra- and Inter-Molecular Cross-Linking of Peptide Ions in the Gas Phase: Reagents and Conditions. J. Am. Soc. Mass Spectrom. 22, 912 (2011). https://doi.org/10.1007/s13361-011-0103-2

8. Cheung See Kit, M., Carvalho, V.V., Vilseck, J.Z., Webb, I.K.: Gas-phase ion/ion chemistry for structurally sensitive probes of gaseous protein ion structure: Electrostatic and electrostatic to covalent cross-linking. Int. J. Mass Spectrom. 463, 116549 (2021). https://doi.org/10.1016/j.ijms.2021.116549

9. Xia, Y., Chrisman, P.A., Erickson, D.E., Liu, J., Liang, X., Londry, F.A., Yang, M.J., McLuckey, S.A.: Implementation of Ion/Ion Reactions in a Quadrupole/Time-of-Flight Tandem Mass Spectrometer. Anal. Chem. 78, 4146–4154 (2006). https://doi.org/10.1021/ac0606296

10. Xia, Y., Wu, J., McLuckey, S.A., Londry, F.A., Hager, J.W.: Mutual storage mode ion/ion reactions in a hybrid linear ion trap. J. Am. Soc. Mass Spectrom. 16, 71–81 (2005). https://doi.org/10.1016/j.jasms.2004.09.017

11. Fang, X., Xie, J., Chu, S., Jiang, Y., An, Y., Li, C., Gong, X., Zhai, R., Huang, Z., Qiu, C., Dai, X.: Quadrupole-linear ion trap tandem mass spectrometry system for clinical biomarker analysis. Engineering. (2021). https://doi.org/10.1016/j.eng.2020.10.021

12. Guan, S., Burlingame, A.L.: High Mass Selectivity for Top-down Proteomics by Application of SWIFT Technology. J. Am. Soc. Mass Spectrom. 21, 455–459 (2010). https://doi.org/10.1016/j.jasms.2009.11.011

14. Pan, H.: A non-covalent dimer formed in electrospray ionisation mass spectrometry behaving as a precursor for fragmentations. Rapid Commun. Mass Spectrom. 22, 3555–3560 (2008). https://doi.org/10.1002/rcm.3767

13. Barnase and barstar: two small proteins to fold and fit together. Trends Biochem. Sci. 14, 450–454 (1989). https://doi.org/10.1016/0968-0004(89)90104-7

3.6 Figures

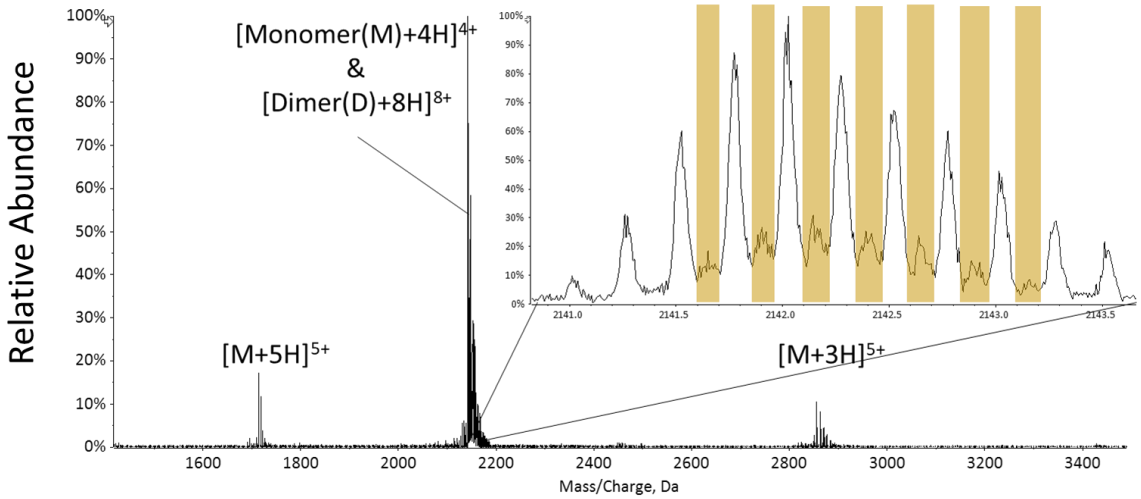

Figure 3.1 Shows a MS spectrum with the isolation of the [monomer+4H] and [dimer+8H]$^{8+}$ of ubiquitin (inset Zoom in of the isotopic distribution confirming dimer formation)

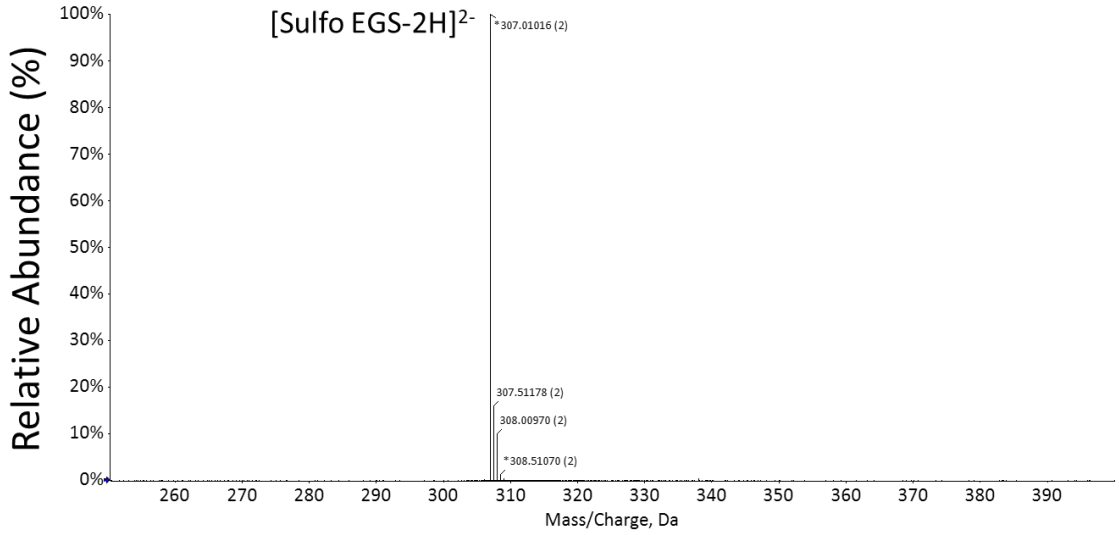

Figure 3.2 Shows rf/DC isolation of the double deprotonated crosslinker Sulfo EGS

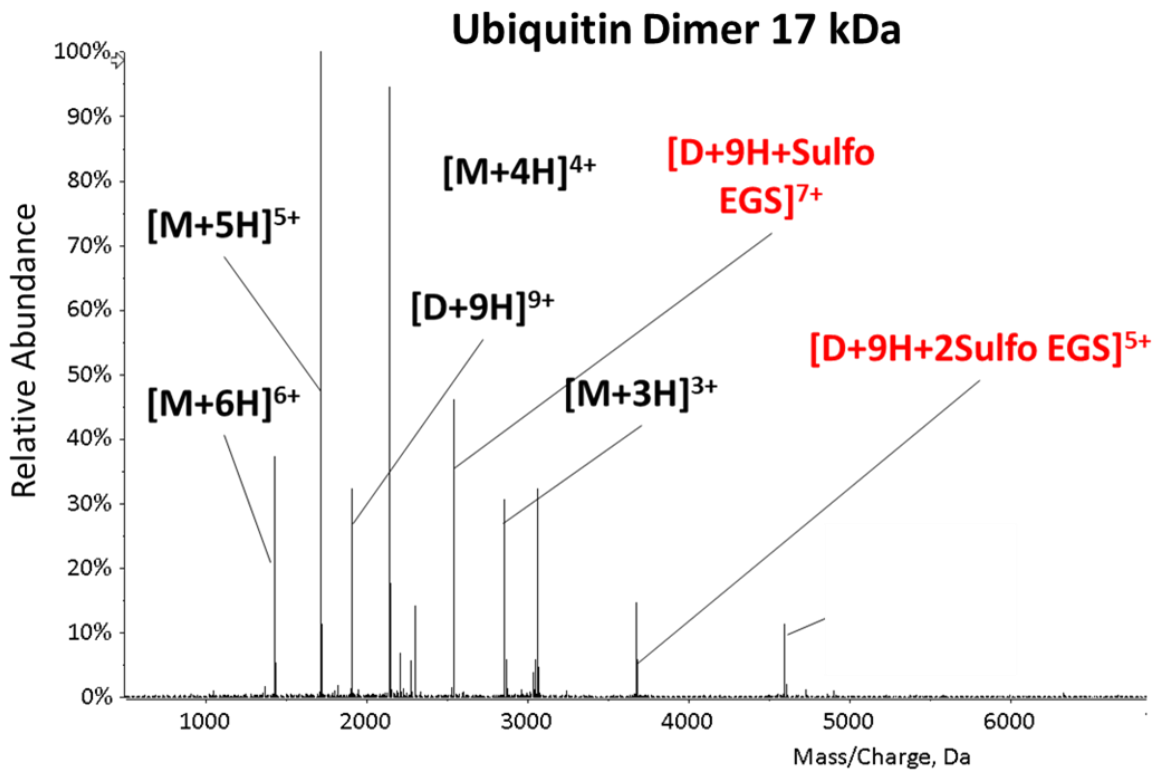

Figure 3.3 Shows the mutual storage of the $[D+9H]^{9+}$ and $[Sulfo\ EGS-2H]^{2-}$ leading to formation of the electrostatic complex $[D+9H+Sulfo\ EGS]^{7+}$

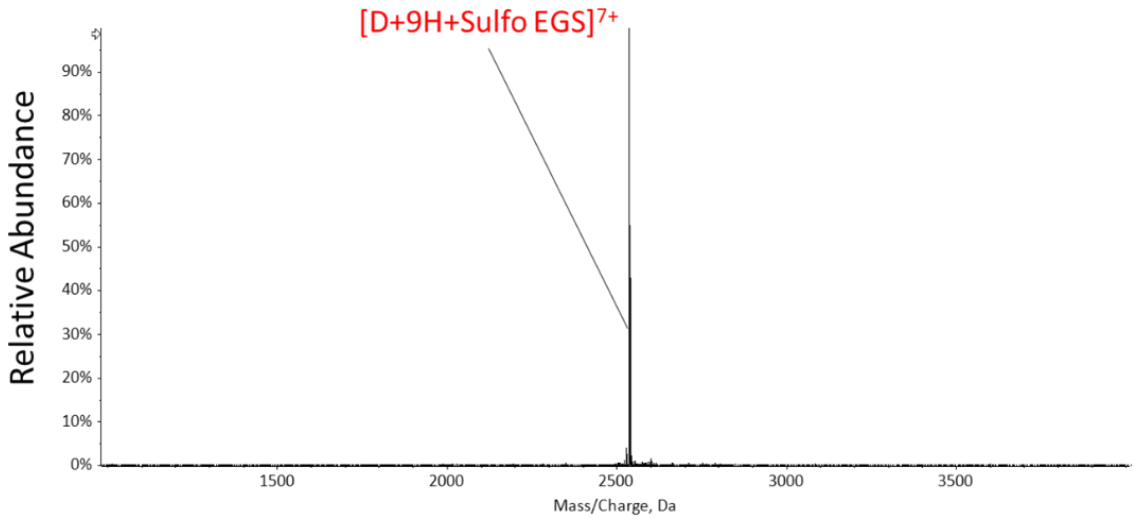

Figure 3.4 Shows SWIFT isolation of electrostatic complex $[D+9H+Sulfo\ EGS]^{7+}$ in q2

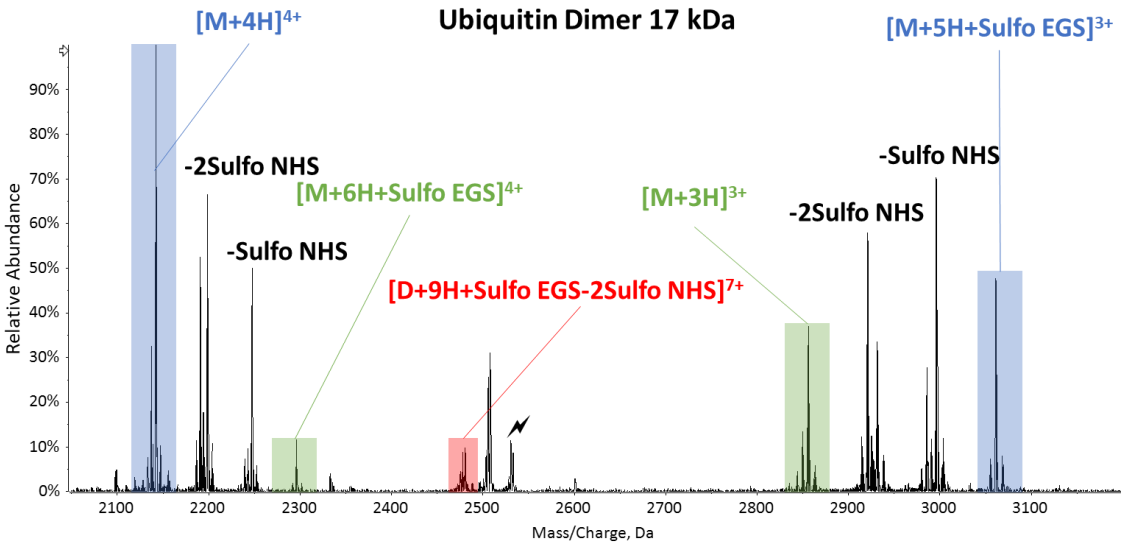

Figure 3.5 Shows the CID spectrum of electrostatic complex $[D+9H+Sulfo\ EGS]^{7+}$ resulting in dissociation of the protein complex (complementary pairs shaded in blue and green) and covalent modification (shaded in red)

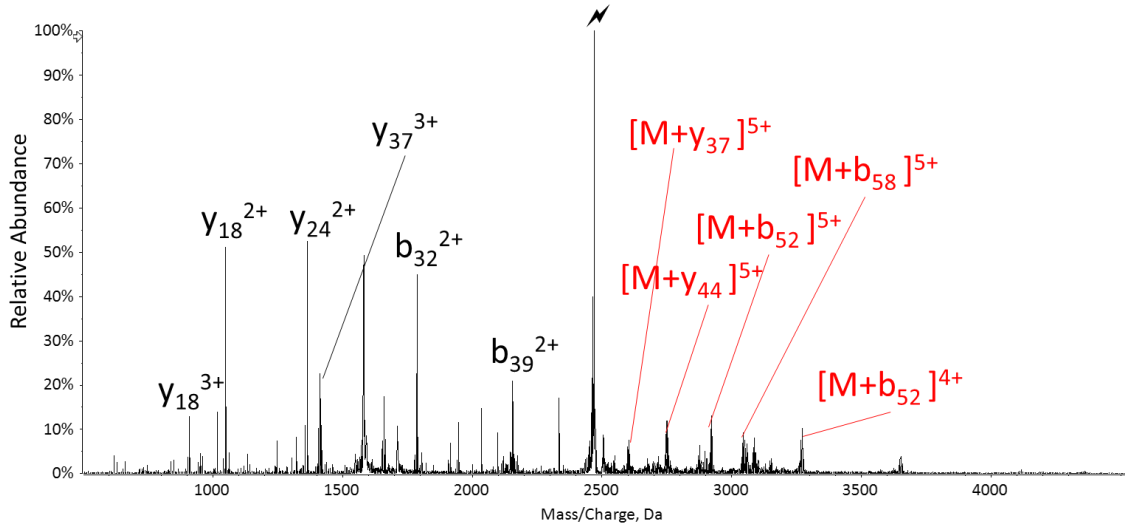

Figure 3.6 Shows the CID spectrum of modified complex $[D+9H+Sulfo\ EGS\text{-}2Sulfo\ NHS]^{7+}$ resulting in fragment ions and complementary crosslinked monomer and peptide fragments

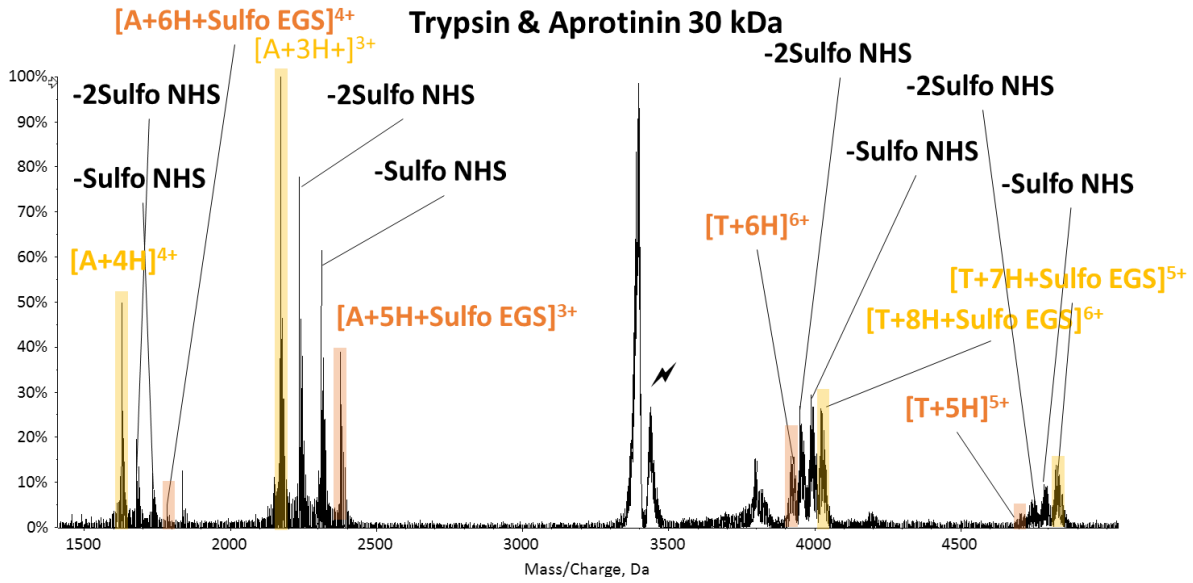

Figure 3.7 Shows the CID spectrum of electrostatic complex $[AT+11H+Sulfo\ EGS]^{9+}$ resulting in dissociation of the protein complex (complementary pairs shaded in yellow and orange) and loss of a Sulfo NHS moiety

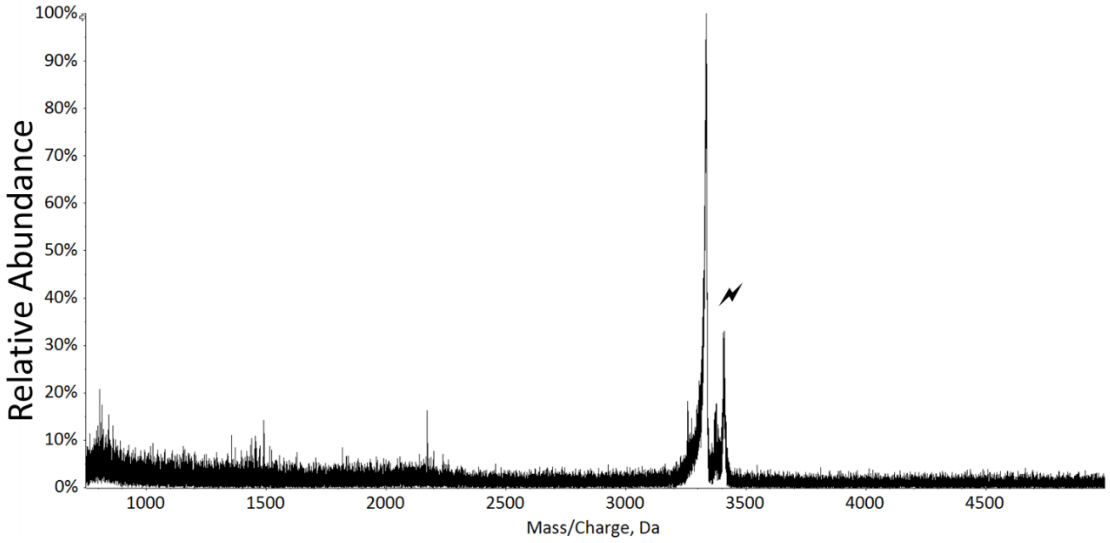

Figure 3.8 Shows the CID spectrum of modified complex $[AT+11H+Sulfo\ EGS\text{-}2Sulfo\ NHS]^{9+}$ resulting neutral losses

CHAPTER 4. DEVELOPMENT OF NEGATIVE MASS ANALYSIS OF MACROMOLECULAR ANALYTES VIA MULTIPLY CHARGED ION ATTACHMENT (N-MAMA-MIA) FOR MASS DETERMINATION OF PROTEIN COMPLEXES

Advances in so-called 'native' mass spectrometry, whereby nano-electrospray ionization (nESI) is applied to solutions as close to physiological conditions as possible, continue to increase the sizes of biological complexes that can be subjected to mass spectrometry. However, many challenges are associated with generating accurate mass information from ions derived from biological complexes. Among these is the inherent heterogeneity of large protein complexes due to post-translational modifications to components in the complex, wide isotopic distributions, extensive salt adduction, and incomplete desolvation. The resulting mass spectra often have poorly resolved charge state envelopes with relatively few charge states, thereby complicating the assignment of charge and, as a result, mass. This is an issue that is present for both positively and negatively charged complexes. Recently, we have described a technique using ion/ion reactions to obtain mass information from high mass positively charged ions by adduction of multiply charged anions. Here we demonstrate a similar approach for the mass measurement of negatively-charged native protein complexes using positively charged ion attachment. This method incorporates SWIFT isolation and demonstrates the utility of gas phase ion/ion reactions for macromolecular mass analysis of anionic protein complexes through attachment of multiply-charged protein cations.

4.1 Introduction

As native mass spectrometry pushes the envelope to analyze larger and more complex protein systems, there is a need for further technology development to allow for the measurement of highly heterogeneous systems. It has been shown that as proteins enter the gas-phase, depending on solution conditions, higher-order structures of the native complex are preserved at some level. [1, 2] While native MS has proven to be a useful tool in structural biology, spectral overlap remains a significant challenge in the analysis of complexes that approach or exceed MDa masses. A native MS experiment begins with nano-ESI of a solution containing the complex of interest. As ESI generally produces a distribution of multiply-charged ions, mass measurement requires the

assignment of charge so that mass can be determined. Charge state assignment in native MS generally relies on generating a series of mass-to-charge measurements in which adjacent charge states differ by known intervals of mass and charge. (In the vast majority of cases, charge differs by +/- 1 unit charge while the mass is often assumed to differ by that of a proton.) Spectral overlap is caused by the reduction of spacing between adjacent charge states. This is typically caused by non-covalent adductions and/or the heterogeneity of proteins due to post-translational modifications. These factors can cause mass spectra to become highly convoluted and form large unresolved signals making accurate mass and charge assignment difficult or impossible. Even the highest resolving mass analyzers cannot resolve closely spaced charge states for highly heterogeneous systems.[3] An added complexity for the high resolution Orbitrap and FT-ICR analyzers is the fact that resolution decreases as $(m/z)^{-½}$ and $(m/z)^{-1}$, respectively. A characteristic of native MS is that nESI typically generates ions of high m/z (e.g., often extending to a few tens of thousands). Hybrid quadrupole time-of-flight (QTOF) mass spectrometers are often used in native mass spectrometry because TOF has a very wide mass range and the resolution is roughly independent of mass-to-charge ratio. However, the charge state overlap and charge state assignment is challenging for any form of mass analysis as the size and heterogeneity of the complex increases. To address some of the limitations to charge state determination, ion/ion reactions have been developed.[4–6]Typically, proton transfer reactions (PTR) are the simplest way to reduce spectral overlap. Unfortunately, for MDa sized heterogeneous complexes the m/z spacings between charge states that differ by +/- 1 are too small to resolve when the mass distribution (i.e., heterogeneity) is wide. These reactions spread the signal across a wide m/z range resulting in a poorly resolved peak or "blob" shifting to higher m/z but remaining unresolved. To address the limited spacings between adjacent charge states in native MS, we developed an approach that gives large spacings between adjacent charge states by attaching a multiply-charged ion of known mass and charge to a high mass complex.[7] We have named the approach Mass Analysis of Macro-molecular Analytes via Multiply-charged Ion Attachment (MAMA-MIA). This method generates MDa protein complexes via native nESI and reacts them with multiply charged reagent ion of the opposite polarity. The reagent ions attach non-covalently to the protein complex and reduce the charge by a known Δz while increasing the mass by a known Δm. These changes are predictable based on the mass and charge of the reagent and upon attachment allows one to

determine the mass of the complex [7]. In the case of a negatively charged analyte complex, the *m/z* value for a given charge state is given by:

$$\boldsymbol{m/z_1 = \frac{M-nx}{n}} \tag{4.1}$$

where M is the mass of the neutral molecule, n is the charge state, and x is the average mass of the cation that is removed from the complex (which is usually a proton from deprotonation of an acidic site). The m/z value of the product generated by the attachment of a single reagent of mass = Δm and charge = Δz is given by:

$$\boldsymbol{m/z_2 = \frac{M-nx+\Delta m}{n-\Delta z}} \tag{4.2}$$

The magnitude of the charge on the initial analyte ion, n, is given by:

$$\boldsymbol{n = \frac{\Delta z(m/z_2)+\Delta m}{(m/z_2-m/z_1)}} \tag{4.3}$$

The same relationship applies for any two adjacent attachment products such that M, the mass of the original complex represented by peak apex, can be determined from any of the attachment products via:

$$\boldsymbol{M = \left(m/z_{(N+1)}\right)(n - N\Delta z) + nx - N\Delta m} \tag{4.4}$$

where N is the number of attached reagent anions.

The first step in this method involves the accumulation protein complex ions and isolation of a small population of the charge state envelope. This slice of the unresolved peak is reacted with a single charge state of the reagent ions. Multiple attachments of the reagent ion can occur, depending upon the number of admitted reagent cations and the length of the mutual storage time. Multiple attachments provide advantages for mass determination as the error in charge

determination is reduced when charge states are spread over a wide m/z range. Using the set of equations listed above and knowing the charge and mass of the reagent one can determine the mass of the complex.[8, 9] Previously, this method has been applied to cationic ribosomal protein complexes ranging in mass from 0.8-2.4 MDa using negatively charged myoglobin reagents for mass determination.[7]

The emphasis of this work is to develop reagent cations that can be used for the mass determination of negatively charged bio-complexes. Protein anions generated by negative mode electrospray have been studied extensively in the past and there some notable differences between negatively and positively sprayed protein complexes.[2] One difference is that the average charge state of negatively sprayed native protein under native MS conditions is lower than that of its positively sprayed counterparts.[2] This has been hypothesized to result from differences between the charge carrier emission process available to negatively sprayed proteins relative to their positively sprayed counterparts.[2] There have also been studies to determine if the structures of negatively charged proteins differ from those of positively charged proteins [10]. These studies have shown that there is very little difference between the collisional cross sections of cation and anions generated from the same complexes. Interestingly, collision induced unfolding (CIU) has shown there are differences in how anionic and cationic species unfold.[10]This is speculated to be due to lower charge states resulting in lower Coulombic repulsion. In certain instances, negatively sprayed proteins maintain oligomeric structures better than positively charged counterparts.[11]These instances can be facilitated by various detergents and other additives that maintain structures or reduce charge. These studies show there is merit in investigating negatively charged protein complexes and developing methods that can elucidate mass information as spectral complexity is still a concern for high mass structures. In this work, we describe several cationic reagents for use with anionic protein complexes and apply the MAMA MIA method to a negatively sprayed protein complex that exhibits poor spectral quality to reduce spectral complexity and obtain mass information.

4.2 Experimental

4.2.1 Materials

Sample preparation for native mass spectrometry of bio-complexes.

Beta galactosidase was purchased from Sigma Aldrich. The lyophilized solid was reconstituted in a 150 mM ammonium acetate (Sigma Aldrich) buffer to create a stock solution at a concentration of 10 µM (calculated by using the mass of the tetramer). The sample underwent adduct removal, via centrifugation, a minimum of four times with the same buffer adjusted to pH 7 using a 10 kilodalton (kDa) molecular weight cutoff (MWCO) Amicon Ultra 0.5 mL filter (Millipore Sigma). The recovered sample (17 µL) was diluted with the same buffer to achieve the same original concentration from the stock solution. GroEL (Sigma Aldrich) lyophilized powder preparation was described before in detail [8] *E. coli* 70S ribosome solution was purchased from New England Biolabs. The original sample, with an initial concentration of 13 µM, was constituted in a buffer containing 10 mM magnesium acetate, which is necessary for the 70S ribosome to be intact in the condensed phase. The sample preparation for the working solutions was described in detail previously [12] and modified accordingly. Briefly, the sample was buffer exchanged 8 times with 150 mM ammonium acetate and 0.5 mM, 10 mM magnesium acetate (Sigma Aldrich) with the same filter mentioned above.

Reagent preparation

Myoglobin, ubiquitin, and carbonic anhydrase were purchased from Sigma Aldrich. The lyophilized solid was reconstituted in 50:50 H_2O: Methanol with 1-5% glacial acetic acid at 10 µM concentration. Denaturing conditions were used to ensure higher charge state formation.

4.2.2 Mass spectrometry

All experiments were performed on a TripleTOF 5600 hybrid QqTOF mass spectrometer (SCIEX, Concord, ON, Canada) which was previously modified for ion/ion reactions [13]. Alternatively-pulsed nano-electrospray ionization (nESI) allows for sequential injection of multiply deprotonated protein complexes and multiply protonated reagent proteins [14]. Deprotonated analyte protein complexes were sprayed under native conditions and isolated in q2, using stored waveform inverse Fourier transform (SWIFT) isolation. Custom waveforms were

built and downloaded to waveform generators using MS Devices software (SCIEX). Reagent proteins were isolated in Q1 using rf/DC apex isolation. The reagent proteins were sprayed under denatured conditions and were transferred to q2 for mutual storage with analyte protein complexes. The reagent ion number density was varied by altering the voltage and injection time to optimize these reactions. The ions were stored for 5-50 milliseconds in q2 for gas phase ion/ion reactions.[15] Mass analysis was performed using time-of-flight (TOF).

4.2.3 Simulation

Predicted mass spectra of ion/ion reaction products were calculated and plotted using a R Shiny app developed in our lab (https://mcluckey-apps.shinyapps.io/iirxnspeccalc/). The analyte mass distribution is a normal distribution defined by a user defined mean and standard deviation. The user inputs a range of charge states for the analyte, and the relative intensities of the charge states are calculated from a user defined mean and standard deviation. The reagent ion can similarly be defined with a mass and charge distribution; however, for the experiments in this publication, the reagent ion is limited to one charge state. Additionally, the reagent ion has a number distribution which describes the extent of proton transfer or ion attachment. (Note that proton transfer is the same as ion attachment where the mass of the "attaching" reagent is −1 Da and the charge is −1.) The number distribution is also a normal distribution with a user defined mean and standard deviation. All possible masses and charges determined from the different number of reagent ions added to the analyte ion are calculated, and their ratios give the m/z values of the reaction products. The relative intensities of reaction products are given by multiplying the corresponding relative intensities from the charge distributions and the reagent ion number distribution. The widths of the product peaks are calculated by multiplying the variances (standard deviation squared) of the analyte and reagent ions that correspond to a particular reaction product and dividing it by the corresponding charge of that reaction product. The resulting product peaks are plotted individually and their intensities are summed to give the total predicted spectrum.

Results and Discussion

4.2.4 β-Galactosidase

β-Galactosidase is a commonly studied protein that forms a homo-tetrameric complex with a mass of ~465.4 kDa. This complex facilitates the enzymatic digestion of lactose in biological systems. In **Figure 4.1a** shows the MS spectrum of an anionic β-Galactosidase complex from a native solution. The spectrum shows the tetrameric complex with charge states from 42- to 35-. **Figure 4.1b** shows incorporation of a SWIFT isolation step to mass select only a subset of the charge state envelope. Previously, isolation of these ions was performed using high resonance ejection amplitudes and varying the RF voltages to eject undesired ions from q2. This can cause instability as the frequency is inversely proportional to m/z so higher m/z values are more subject to off-resonance excitation. Therefore, applying a high resonance ejection amplitude for isolation can be difficult to optimize to prevent unwanted fragmentation. This is overcome by incorporating SWIFT isolation in q2. This method allows for high resolution isolation to be reproducible without changing rf voltages as evident in **Figure 4.1c** which shows a single charge state of β-galactosidase.

A single charge state or a distribution of charge states, as reflected in the panels of **Figure 4.1**, can be subjected to the MAMA MIA experiment. As previously shown, multiply charged anions formed electrostatic complexes when introduced to native cationic protein complexes ions residing in the trap.[7] Analogous behavior is noted when using native anionic protein complexes and cationic reagents. However, the magnitudes of the charge states involved in the two different polarity combinations, i.e., positive native complex/negative reagent versus negative native complex/positive reagent, can As mentioned above, protein ions are generally formed at lower absolute charge states in the negative mode than in the positive mode.[2] In the case of native protein complexes, an example is shown in **Figure 4.2**, which compares positive and negative mode nESI mass spectra of β-Galactosidase. The negatively charged ions have charge states from 43^--37^- while the positively charged ions have charge states of 48^+-43^+. It is also generally the case that it is possible to produce more highly charged reagent ions under denaturing conditions in the positive mode compared to negative mode.[16] The MS spectrum of the reagent apo-myoglobin (evident by the loss of heme denoted by an asterisk) is shown in **Figure 4.3.** The isolation of the 15+ charge state and 20+ charge state is shown in **Figure 4.4a** and **Figure 4.4b,** respectively. The net effect of these differences is that it is generally easier to achieve greater

changes in m/z upon each reagent ion attachment with the negative native complex/positive reagent combination. An example of a negative native complex/positive reagent ion attachment experiment is shown in **Figure 4.5a,** where the single 37- charge state of β-Galactosidase is reacted with 15+ charge state of apo-myoglobin (myo). There are two attachments visible in this spectrum corresponding, in each case, to a charge reduction of 15 charges and an increase in mass equivalent to myoglobin (~17 kDa). In **Figure 4.5b** the 37^- charge state is reacted with the $[myo+20H]^{20+}$ ion, which shows only a single attachment as the next attachment would be a charge inverted complex. (Charge inversion upon attachment of multiply-charged cations is discussed further in Chapter 5.) In both cases, there are low abundance signals one charge state above and below the dominant charge-attachment product. These additional charge states likely arise from incomplete ejection of the charge states adjacent to those of the reagent or analyte. **Figure 4.5c** shows an ion/ion reaction between the entire charge state envelope of β-Galactosidase reacted with $[myo+15H]^{15+}$ under similar reaction conditions used for the experiment of **Figure 4.5a**. Increasing number of charge states, and therefore the total negative charge, of the analyte results in a lower relative contribution from the addition of two reagent cations. The increase in total negative charge can be compensated for by adding more reagent cations (data not shown). These data of **Figure 4.5** demonstrate the utility of performing MAMA-MIA ion/ion reactions in the negative analyte mode.

4.2.5 GroEL Chaperonin

GroEL is a tetradecamer chaperon protein complex that assist in folding of other polypeptides when a biological system is under stress. The monomer mass is ~57 kDa, when assembled the nominal mass of the complex is ~802 kDa.[17–19] When GroEL is sprayed under native conditions in the negative mode, the spectrum shows a charge state envelope with charge states from 57^--50^- shown in **Figure 4.6**. The mass determined from this charge state distribution is approximately 807 kDa. The discrepancy from the mass shown here and masses reported elsewhere is likely due to residual neutral species being maintained through the desolvation process.[17–20] To obtain more highly charged ion attachment the reagent was altered to carbonic anhydrase. The MS spectrum of carbonic anhydrase denoted as (CA) is shown in **Figure 4.7a** with the isolation of the 20+ charge state (**Figure 4.7b**) and the 30+ charge state (**Figure 4.7c**) A MAMA-MIA reaction was performed by isolating the distribution of GroEL and reacting it with the 20+ charge state of carbonic anhydrase denoted as $[CA+20H]^{20+}$. There are two attachments

observed reducing the overall charge of the complex by 20 charges and increasing the mass by ~29 kDa with each attachment (shaded) shown in **Figure 4.8a**. This mass is further confirmed as the experiment was repeated with a 30+ charge state of carbonic anhydrase. This is shown in **Figure 4.8b** where only a single attachment is visible in this mass range. The mass calculated from the MAMA-MIA reaction confirms a mass value of 807 kDa. To obtain a mass value closer to literature values reported from positive native MS, instrument parameters were optimized to induce increased desolvation with higher collisional energy during ion transmission. The most drastic effects were seen in increasing the potential between the lens prior to the q2 reaction chamber and the DC rod offset applied to q2. This increase in collisional energy prior to the ion/ion reaction led to reduction of mass shown in **Figure 4.9**. This figure shows an overlay of the MS spectrum corresponding to increased collisional energy to obtain the 802 kDa mass and previous experiments corresponding to the 807 kDa measurement. This distribution was subjected to a MAMA-MIA reaction between $[CA+30H]^{30+}$. Shown in **Figure 4.10** (red trace) the MAMA-MIA reaction again confirms the reduced mass with the calculated mass is determined to be ~802 kDa. This result highlights the fact that the MAMA-MIA reaction reflects the mass of the complex, including any residual adducts, and does not impart high enough energy to remove adducts even at higher charge states. This demonstrates the importance of the optimization of desolvation and adduct removal prior to the MAMA MIA reaction to obtain accurate mass values (unless you are interested in a system with minimal activation, which will be shifted to higher mass and likely will show poorer resolution). It also validates the utility to maintain these noncovalent interactions in the gas phase to determine masses of noncovalent interactions that remain after the transition into the gas-phase. The MAMA-MIA reaction allows for the masses to be measured in both cases.

4.2.6 Ribosome 30S/50S

The *E. Coli* ribosome is an inherently heterogeneous complex comprised of two subunits (30S, 50S) that form the intact ribosome complex (70S). In total, the 70S complex contains three large nucleic acid strands and roughly sixty proteins.[21] Some of the protein components are very weakly associated with the complex and are often missing. In native MS studies, ions of the 30S, 50S and 70S complexes are all observed when high concentrations of Mg^{2+} ions are present.[12] At low concentrations, the 70S complex is usually absent. Both 30S and 50S components when analyzed in the positive mode using MAMA MIA showed multiple mass

components related to the presence or absence of smaller proteins within the complex.[7] The MS spectrum of this analyte often exhibited poor desolvation shown in **Figure 4.11a** only with high collisional energy upon injection offering improved resolution. It is only under these conditions in the negative mode are charge states clearly visible and a mass can be determined. This is demonstrated in **Figure 4.11b** which shows a MS spectrum where injections were tuned for increased collisional energy. The collisional energy is sufficient to resolve the charge states of the 30S (~800 kDa) however it also leads to loss of the 50S complex. These conditions often result in reduced signal therefore requiring increased averaging and longer analysis. A MS spectrum obtained under gentler conditions with increased Mg^{2+} is shown in **Figure 4.11c**. Under these conditions the proteins are heavily adducted with the heterogeneity preventing mass assignment however the intact 70S is observed. It is important to note the intact 70S ribosome was only visible with the 10mM magnesium (Mg^{2+}) acetate concentration. The lower showed no evidence of intact 70S ribosome complex. **Figure 4.11** This spectrum shows a more typical analysis optimized for higher signal intensity than rather than resolution.

Under optimal conditions, it is possible to tune instrumental parameters to obtain a higher resolution MS spectrum shown in **Figure 4.12** where the 50S is observed with resolved charge states at low Mg^{2+} concentration. SWIFT isolation of a population of the 30S ribosome is shown in **Figure 4.13.** The insert shows at least three components. **Figure 4.14** shows A MAMA MIA reaction between the isolated population of 30S ribosome and a 10+ ubiquitin reagent denoted as $[ubi+10H]^{10+}$. The insert shows adequate separation of the components with masses determined to be 800.8±1 kDa, (blue triangle) 858±2 kDa, (orange diamond) and 767±3 kDa (red circle). The masses correspond to combinations of proteins that typically interact with this complex described previously.[7] These masses are slightly smaller than the masses measured in the positive mode. This is likely due the increased collisional energy driving off more neutral species. This demonstrates the subtle mass differences that can be seen reiterating the importance of negative mode analysis.

When sprayed under negative conditions the 50S subunit exhibited poorer desolvation compared to the 30S subunit. This is likely due to the combination of higher mass and increased heterogeneity. Upon isolation of a slice of the charge state distribution centered around 25000 m/z. Shown in **Figure 4.15**. there are very few discernible features in this isolated peak. This isolated slice was subjected to mutual storage with $[CA+20H]^{20+}$shown in **Figure 4.16**. In this spectrum

two attachments are observed however an accurate mass measurement cannot be determined due to poor spectral quality. A rough estimate of 1,634±14 kDa (shown in blue) and 1,804±1 kDa (shown in orange) based on the tops of discernible peaks in the precursor and attachment peaks. can be determined using m/z values corresponding to the top of each distribution. These masses are significantly larger than reported in literature likely due to heavy adduction. This does demonstrate the capability of the MAMA MIA reaction obtain a mass measurement from a blob with an unknown mass and charge. More work is needed to optimize instrument parameters for increased desolvation and solution preparation to remove contaminants and potential adducts to obtain accurate mass.

4.3 Conclusion

In conclusion, we demonstrate that MAMA-MIA can be applied to negatively charged protein complexes to overcome charge state overlap and obtain mass information. As stated previously, with each attachment the spectral overlap is reduced which decreases the ambiguity in mass and charge assignment. There are two noticeable benefits with performing these reactions in the negative mode. First negative complexes have been shown to have lower average charge than positive counterparts. Secondly, using positive cations provides access to higher charged reagent ions compared to negative protein ions. This allows larger spacing between the m/z of precursor and sequential attachments. The addition of SWIFT isolation allows MAMA-MIA reactions to be performed on mass selected analytes at higher m/z values. Here we show evidence of two stable populations of GroEL that exist, corresponding to both the 807 and 802 kDa masses. The biological significance of this larger population was not explored as that was outside the scope of this work. We postulate that while each individual system is different, GroEL under native conditions requires collisional activation in the negative mode to drive off neutral species. In the case of the ribosomal protein 30S, this species is able to survive the high collisional energy to drive off adducts giving rise to smaller mass measurements compared to those in positive mode.[7] The measurement of these components show the ability of the MAMA MIA reaction to tackle heterogeneity and spectral overlap. In the case of the 50S, where signal intensity was prioritized over resolution, a rough mass measurement was obtained. This demonstrates the utility of MAMA MIA to potentially screen unresolved blobs when instrument optimization has been exhausted.

4.4 References

1. Lorenzen, K., Duijn, E. van: Native Mass Spectrometry as a Tool in Structural Biology. In: Current Protocols in Protein Science. John Wiley & Sons, Inc. (2001)

2. Allen, S.J., Schwartz, A.M., Bush, M.F.: Effects of Polarity on the Structures and Charge States of Native-Like Proteins and Protein Complexes in the Gas Phase. Anal. Chem. 85, 12055–12061 (2013). https://doi.org/10.1021/ac403139d

3. Leney, A.C., Heck, A.J.R.: Native Mass Spectrometry: What is in the Name? J. Am. Soc. Mass Spectrom. 28, 5–13 (2017). https://doi.org/10.1007/s13361-016-1545-3

4. Stephenson, J.L., McLuckey, S.A.: Reactions of poly(ethylene glycol) cations with iodide and perfluorocarbon anions. J. Am. Soc. Mass Spectrom. 9, 957–965 (1998). https://doi.org/10.1021/jasms.8b01223

5. Prentice, B.M., McLuckey, S.A.: Gas-phase ion/ion reactions of peptides and proteins: acid/base, redox, and covalent chemistries. Chem. Commun. 49, 947–965 (2013). https://doi.org/10.1039/C2CC36577D

6. McLuckey, S.A., Huang, T.-Y.: Ion/Ion Reactions: New Chemistry for Analytical MS. Anal. Chem. 81, 8669–8676 (2009). https://doi.org/10.1021/ac9014935

7. Abdillahi, A.M., Lee, K.W., McLuckey, S.A.: Mass Analysis of Macro-molecular Analytes via Multiply-Charged Ion Attachment. Anal. Chem. 92, 16301–16306 (2020). https://doi.org/10.1021/acs.analchem.0c04335

8. Fenn, J.B., Mann, M., Meng, C.K., Wong, S.F., Whitehouse, C.M.: Electrospray ionization for mass spectrometry of large biomolecules. Science. 246, 64–71 (1989). https://doi.org/10.1126/science.2675315

9. Covey, T.R., Bonner, R.F., Shushan, B.I., Henion, J.: The determination of protein, oligonucleotide, and peptide molecular weights by ion-spray mass spectrometry. Rapid Commun. Mass Spectrom. RCM. 2, 249–256 (1988). https://doi.org/10.1002/rcm.1290021111

10. Hong, S., Bush, M.F.: Collision-Induced Unfolding Is Sensitive to the Polarity of Proteins and Protein Complexes. J. Am. Soc. Mass Spectrom. 30, 2430–2437 (2019). https://doi.org/10.1007/s13361-019-02326-z

11. Liko, I., Hopper, J.T.S., Allison, T.M., Benesch, J.L.P., Robinson, C.V.: Negative Ions Enhance Survival of Membrane Protein Complexes. J. Am. Soc. Mass Spectrom. 27, 1099–1104 (2016). https://doi.org/10.1007/s13361-016-1381-5

12. van de Waterbeemd, M., Fort, K.L., Boll, D., Reinhardt-Szyba, M., Routh, A., Makarov, A., Heck, A.J.R.: High-fidelity mass analysis unveils heterogeneity in intact ribosomal particles. Nat. Methods. 14, 283–286 (2017). https://doi.org/10.1038/nmeth.4147

13. Xia, Y., Chrisman, P.A., Erickson, D.E., Liu, J., Liang, X., Londry, F.A., Yang, M.J., McLuckey, S.A.: Implementation of Ion/Ion Reactions in a Quadrupole/Time-of-Flight Tandem Mass Spectrometer. Anal. Chem. 78, 4146–4154 (2006). https://doi.org/10.1021/ac0606296

14. Wells, J.M., Chrisman, P.A., McLuckey, S.A.: "Dueling" ESI: instrumentation to study ion/ion reactions of electrospray-generated cations and anions. J. Am. Soc. Mass Spectrom. 13, 614–622 (2002). https://doi.org/10.1016/S1044-0305(01)00364-6

15. Xia, Y., Wu, J., McLuckey, S.A., Londry, F.A., Hager, J.W.: Mutual storage mode ion/ion reactions in a hybrid linear ion trap. J. Am. Soc. Mass Spectrom. 16, 71–81 (2005). https://doi.org/10.1016/j.jasms.2004.09.017

16. Konermann, L., Douglas, D.J.: Unfolding of proteins monitored by electrospray ionization mass spectrometry: a comparison of positive and negative ion modes. J. Am. Soc. Mass Spectrom. 9, 1248–1254 (1998). https://doi.org/10.1016/S1044-0305(98)00103-2

17. Zahn, R., Buckle, A.M., Perrett, S., Johnson, C.M., Corrales, F.J., Golbik, R., Fersht, A.R.: Chaperone activity and structure of monomeric polypeptide binding domains of GroEL. Proc. Natl. Acad. Sci. 93, 15024–15029 (1996). https://doi.org/10.1073/pnas.93.26.15024

18. van Duijn, E., Simmons, D.A., van den Heuvel, R.H.H., Bakkes, P.J., van Heerikhuizen, H., Heeren, R.M.A., Robinson, C.V., van der Vies, S.M., Heck, A.J.R.: Tandem Mass Spectrometry of Intact GroEL−Substrate Complexes Reveals Substrate-Specific Conformational Changes in the trans Ring. J. Am. Chem. Soc. 128, 4694–4702 (2006). https://doi.org/10.1021/ja056756l

19. Zhou, M., Jones, C.M., Wysocki, V.H.: Dissecting the Large Noncovalent Protein Complex GroEL with Surface-Induced Dissociation and Ion Mobility–Mass Spectrometry. Anal. Chem. 85, 8262–8267 (2013). https://doi.org/10.1021/ac401497c

20. van Duijn, E., Bakkes, P.J., Heeren, R.M.A., van den Heuvel, R.H.H., van Heerikhuizen, H., van der Vies, S.M., Heck, A.J.R.: Monitoring macromolecular complexes involved in the chaperonin-assisted protein folding cycle by mass spectrometry. Nat. Methods. 2, 371–376 (2005). https://doi.org/10.1038/nmeth753

21. Wilson, D.N., Nierhaus, K.H.: Ribosomal Proteins in the Spotlight. Crit. Rev. Biochem. Mol. Biol. 40, 243–267 (2005). https://doi.org/10.1080/10409230500256523

4.5 Figures

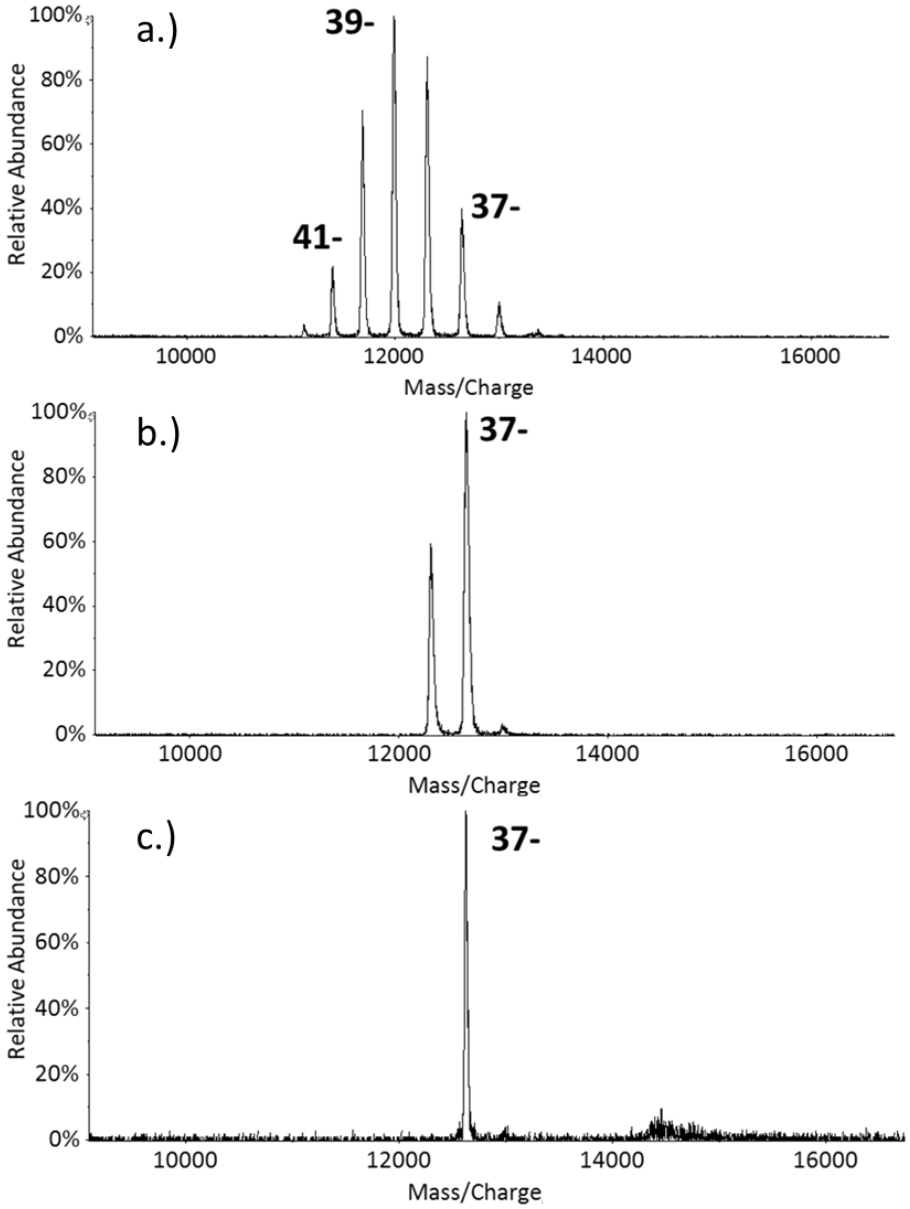

Figure 4.1a.) a MS spectrum of β-Galactosidase tetrameric complex from a negative nanoESI source. b.) Shows incorporation of SWIFT isolation of a group of charge states. c.) shows SWIFT isolation of the 37- charge state of the β-galactosidase

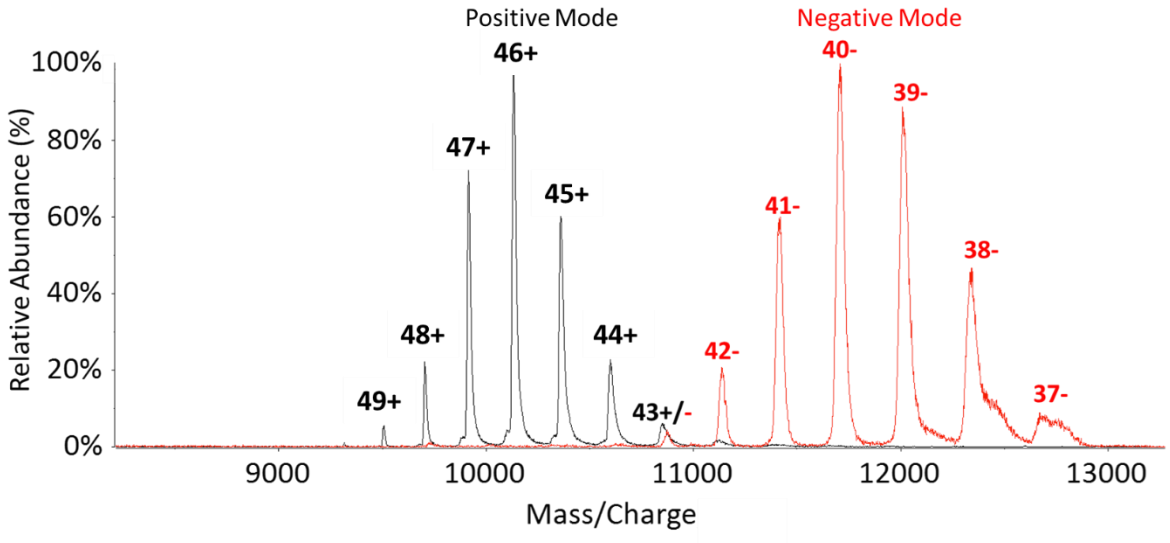

Figure 4.2 Mass spectra of the charge state envelope of β galactosidase in positive mode(black) and negative mode(red)

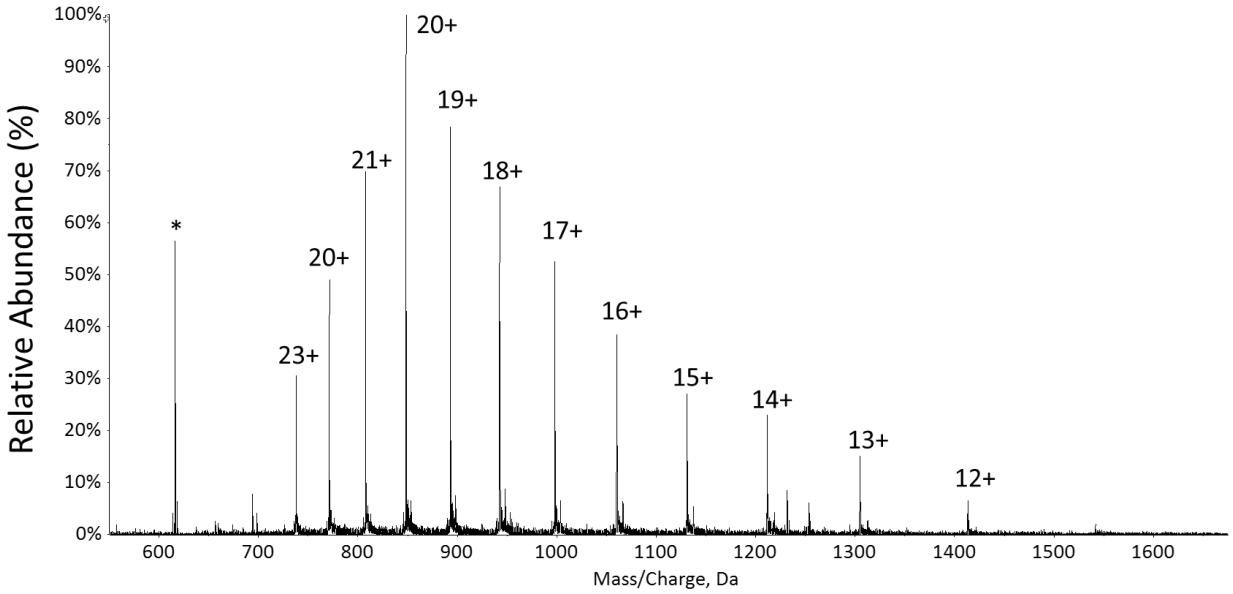

Figure 4.3 The MS spectrum of myoglobin sprayed under denaturing conditions showing charge states between 23+ and 12+ * and m/z of 616 denotes loss of the heme group

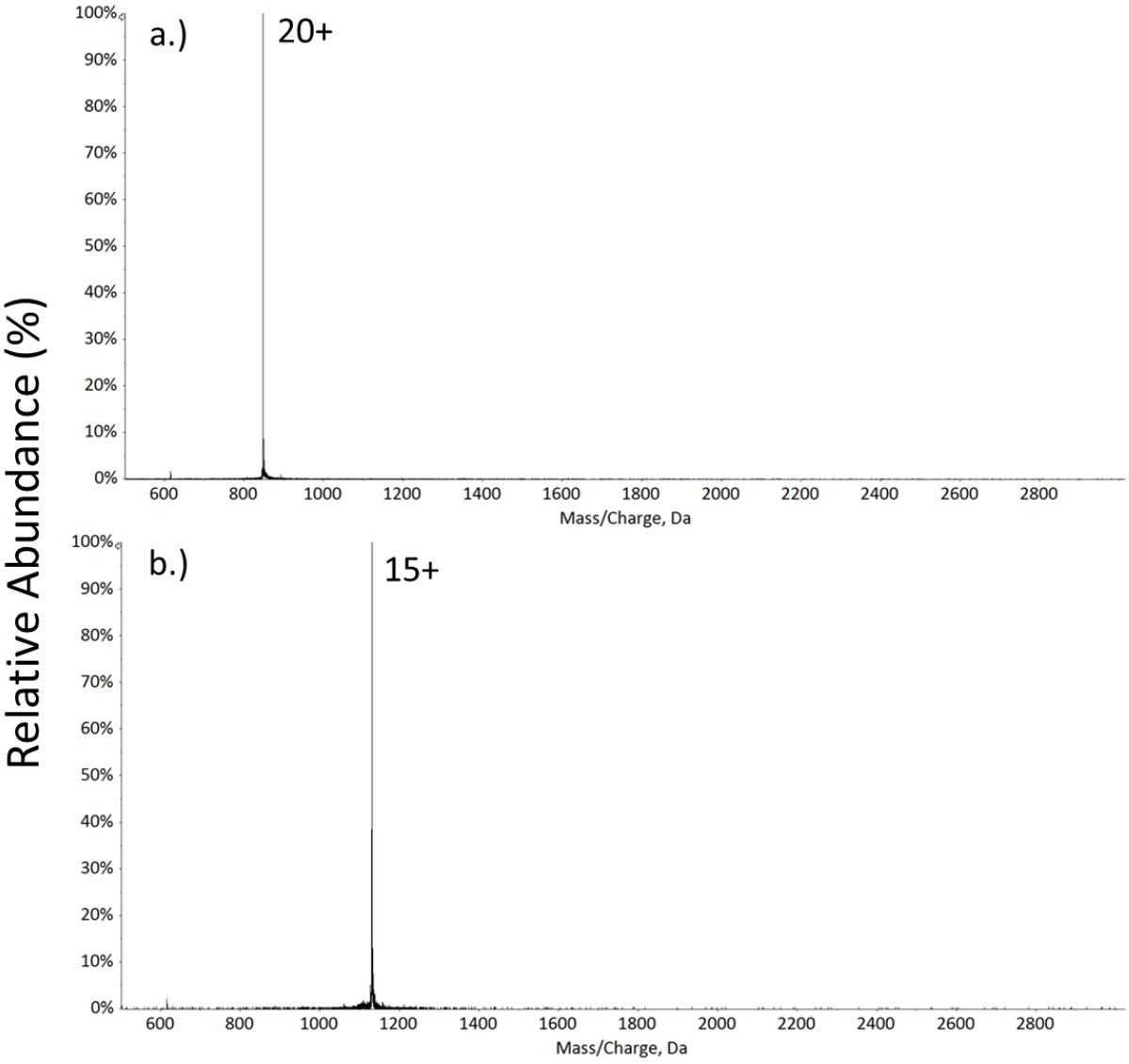

Figure 4.4 Shows the isolation of the a.) 20+ charge state and b.)15+ charge state of apo-myoglobin

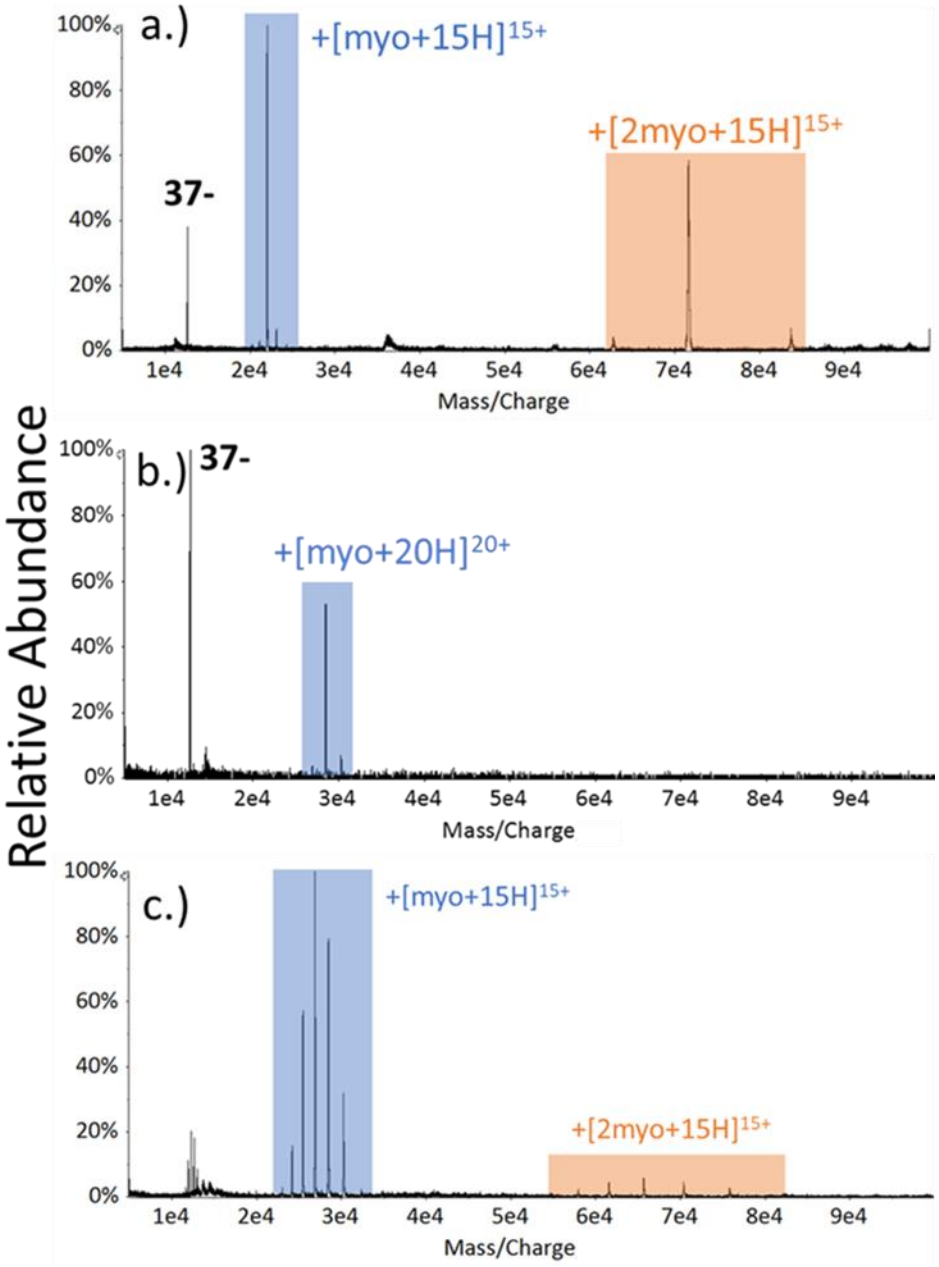

Figure 4.5 Shows the ion/ion reaction between a.) the 37- charge state of β-Galactosidase and [myo+15H]15+b.) the 37- charge state of β-Galactosidase and [myo+20H]20+c.) the entire charge state envelope of β-Galactosidase and [myo+15H]15+

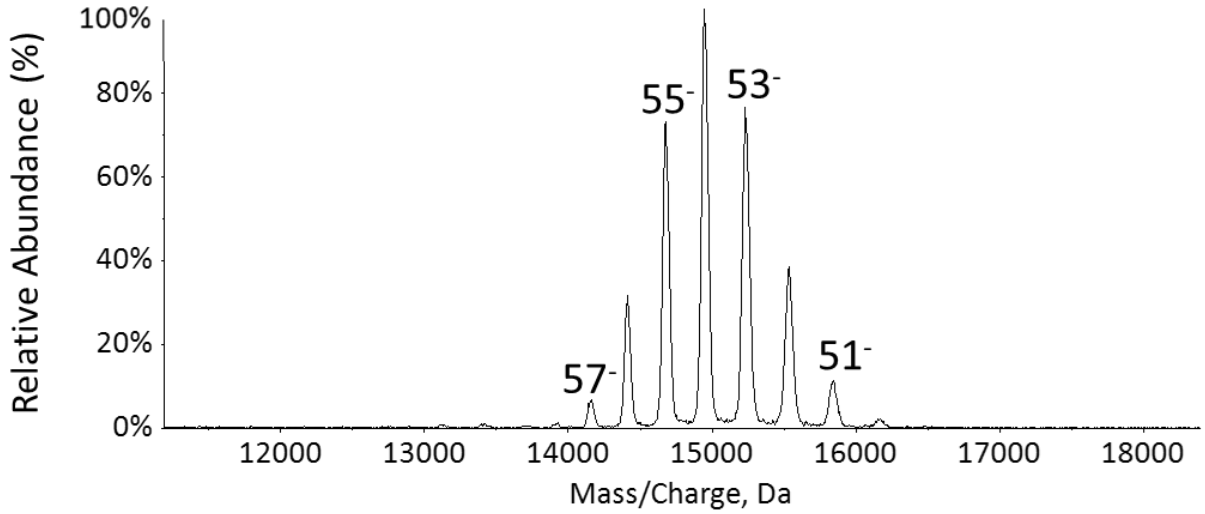

Figure 4.6 A mass spectrum of GroEL chaperonin sprayed in the negative mode showing charge states from 57- to 50-

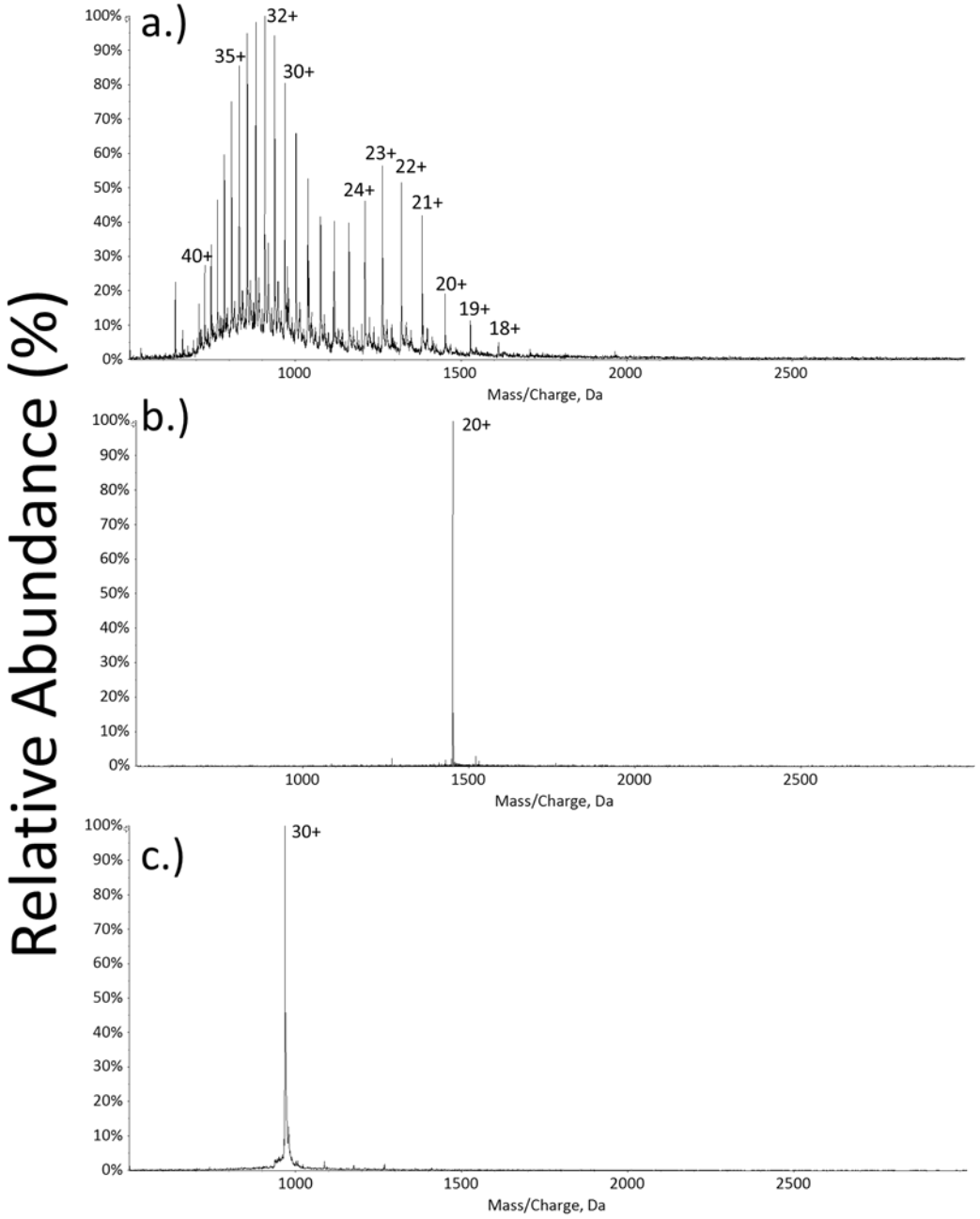

Figure 4.7 Shows the a.) MS spectrum of carbonic anhydrase under denaturing conditions and the rF/DC isolation of the 20+ charge state and c.) the 30+ charge state.

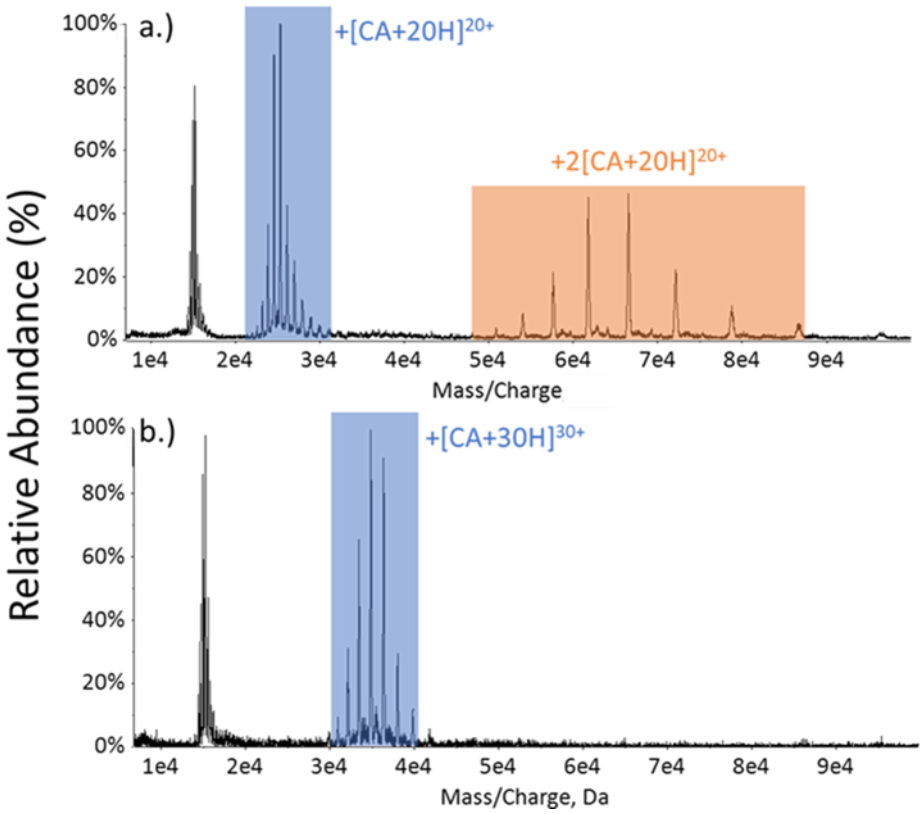

Figure 4.8 Shows a MAMA-MIA reaction between the charge state envelope of GroEL and a.) [CA+20H]20+b.) [CA+30H]30+

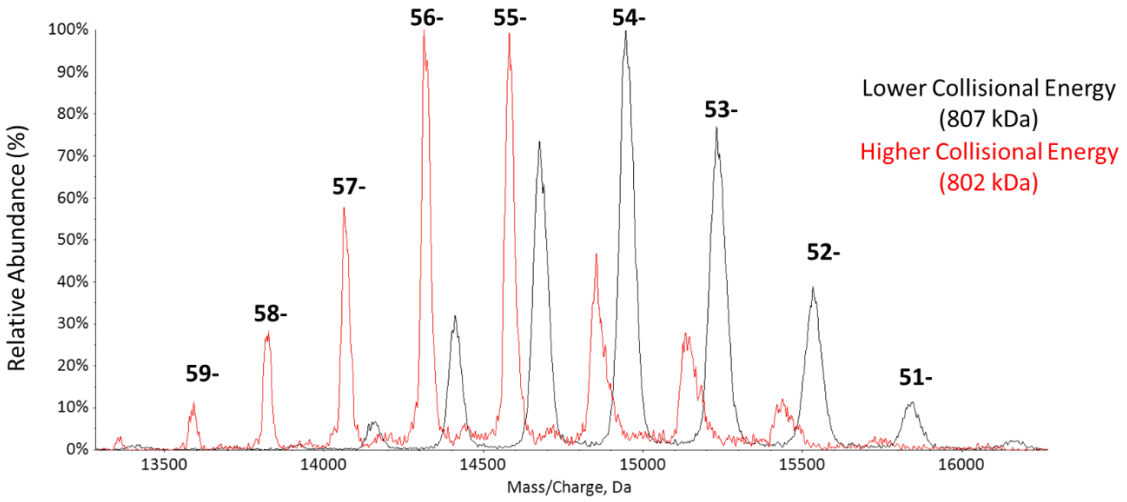

Figure 4.9 A overlay of mass spectra of GroEL chaperonin sprayed under negative mode obtained under low collisional energy upon injection (black) and high collisional energy (red)

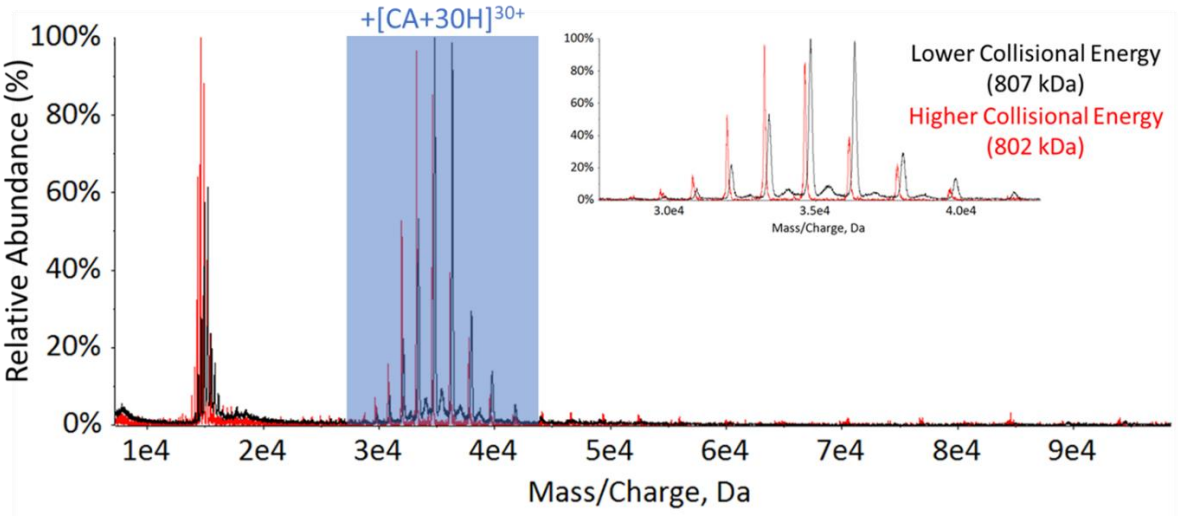

Figure 4.10 4.10 MS spectrum of a MAMA-MIA reaction between GroEL and [CA+30H]30+ after changing increasing collisional energy with ion transmission (red trace) compared to previous conditions (black trace). Inset shows a zoomed view of the first adduction

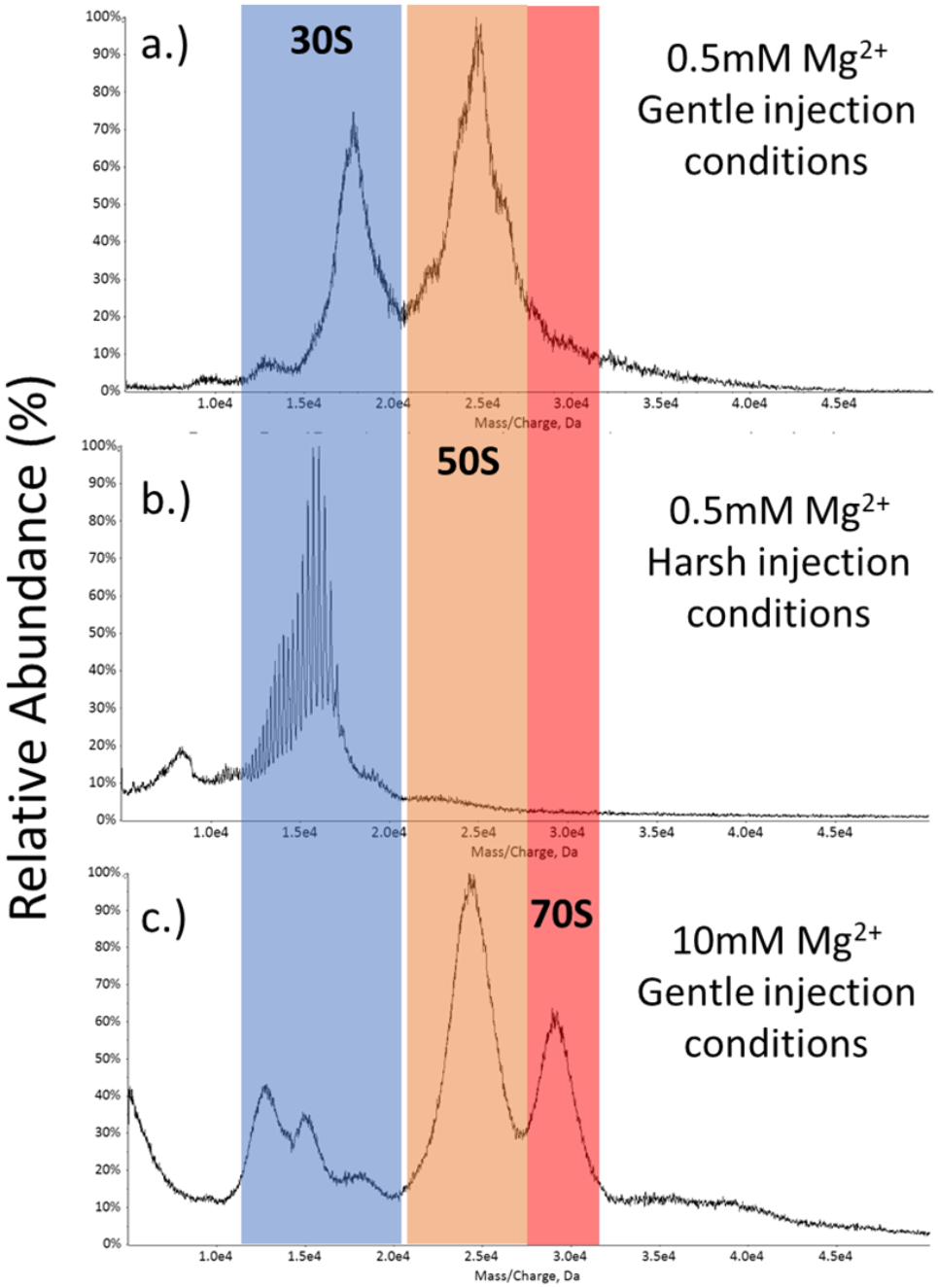

Figure 4.11 Shows the MS spectrum of ribosomal proteins under native conditions with a.)"gentle" injection and transfer conditions, b.) “harsh” injection and transfer conditions to drive off adducts, and c.) with 10 mM Mg2+ to maintain the intact 70S complex

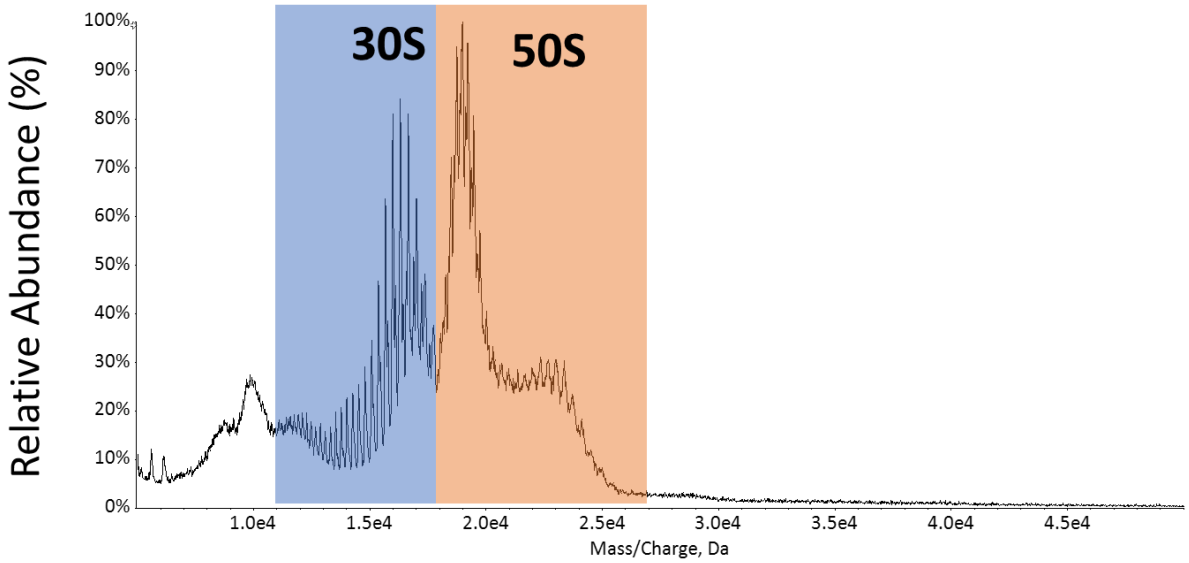

Figure 4.12 Shows a MS spectrum taken optimal conditions with ion desolvation allowing for observation of various components and charge states

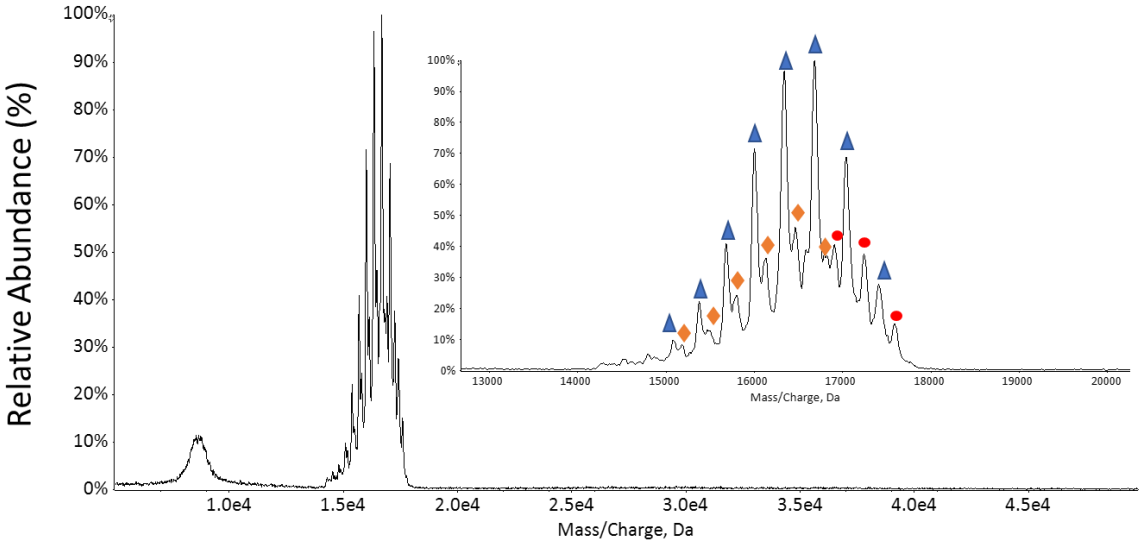

Figure 4.13 Shows the SWIFT isolation of the 30S ribosome. The insert shows a zoomed spectrum of the isolated distributions with multiple components.

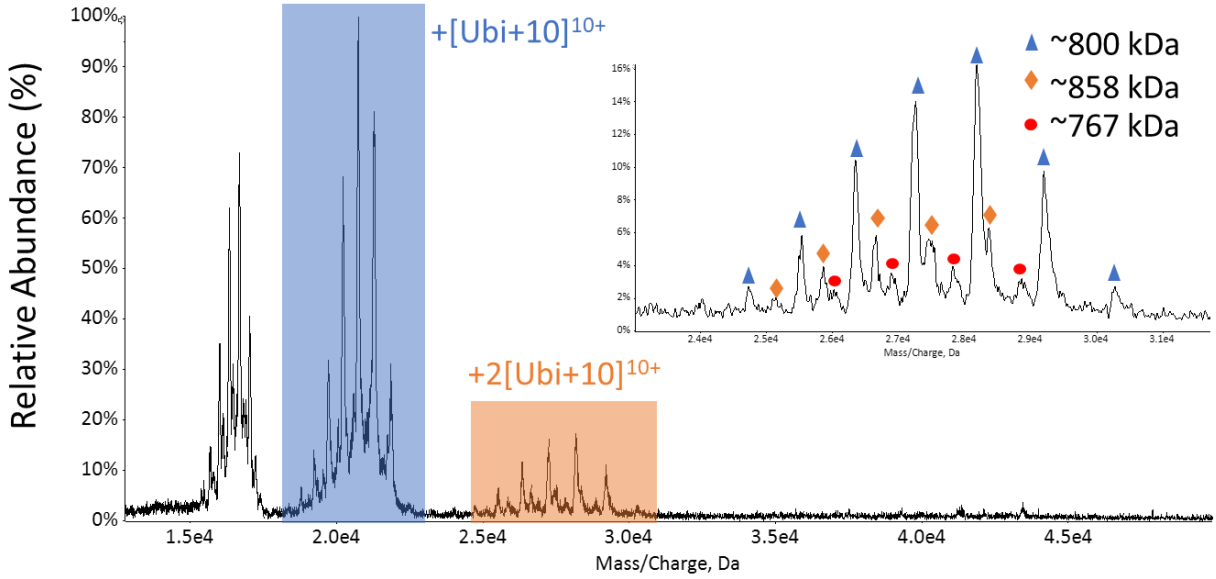

Figure 4.14 Shows the MAMA MIA reaction between the isolated charge state envelope of 30S and 10+ charge state of ubiquitin denoted as [Ubi+10]10+showing 2 attachments with the second attachment separating the three components denoted as 800 kDa, (blue triangle) 85

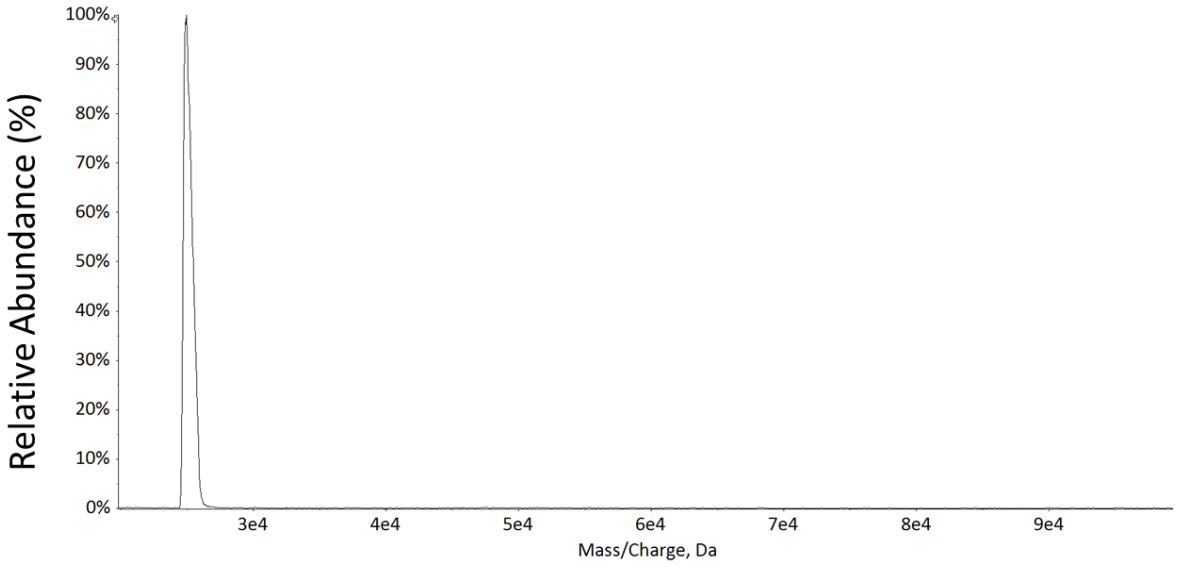

Figure 4.15 Shows the SWIFT isolation of the unresolved 50S ribosome under gentle conditions.

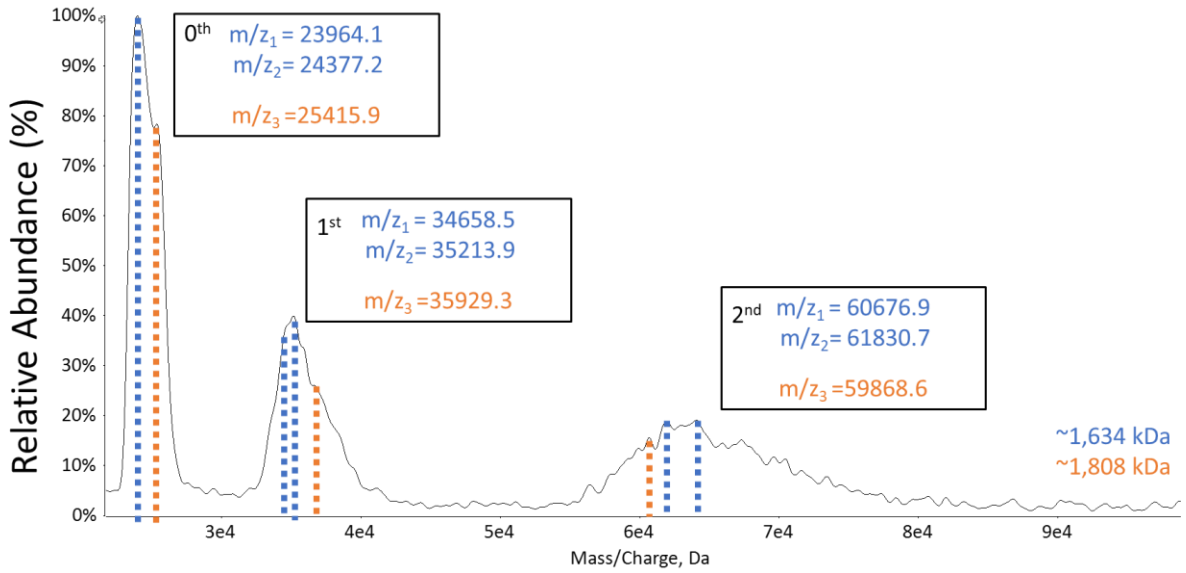

Figure 4.16 Shows a MAMA MIA reaction between an isolated distribution of the 50# ribosome and [CA+20H]20+ showing features give mass estimates of 1,634 kDa (blue) and 1,808 kDa (orange)

CHAPTER 5. CHARGE INVERSION OF LARGE PROTEIN COMPLEXES VIA MASS ANALYSIS OF MACROMOLECULAR ANALYTES VIA MULTIPLY-CHARGED ION ATTACHMENT(MAMA-MIA)

Gas-phase charge inversion reactions have been shown to assist in the analysis of many different analytes. Previously we have shown a method that drastic reduces of charge of native complexes in both positive mode and negative mode for mass determination coined (MAMA-MIA). In the negative MAMA-MIA reaction, highly charged reagents require fewer attachments and can charge invert native complexes. Here we show charge inversion of negative native complexes via ion attachment. Using two native protein complexes we show charge inversion of both systems using myoglobin and carbonic anhydrase. Demonstrate the versatility of ion/ion reactions This method allows for positive mode analysis and the be correlated to negative mode spectra which can be useful for wide m/z calibration.

5.1 Introduction

Gas-phase charge inversion reactions have been shown to assist in the analysis of many different analytes.[65, 80–84] Typically, analytes are injected under the polarity that provides the highest ionization efficiency. Once ionized analytes are stored within the mass spectrometer and a reagent with higher overall charge is sequentially injected. Once both analyte and regent are mutually stored an ion/ion reaction can occur that can change the polarity of the analyte. This allows for the analysis to occur in a polarity more analytically beneficial. Previous experiments have shown benefits such as structural elucidation, signal improvement, and isomeric separation.[70]

Recently ion/ion reactions have been utilized for mass determination of poorly resolved large native protein complexes by significant charge reduction. The method has been coined MAMA-MIA as an acronym of Mass Analysis of Macromolecular Analytes via Multiply charged Ion Attachment.[85] This method reduces spectral overlap allowing for mass determination by reacting an isolated distribution of the protein complex with a smaller multiply charged protein. The small protein will attach to the complex causing a shift in mass and reduction in overall charge.

This results in large shift in m/z and allows one to determine the original mass of the complex. This ion/ion reaction was also performed by spraying the native complexes under negative conditions. This allow regent protein ions to be sprayed in the positive mode under denaturing conditions. This significantly increases the charge state of the reagent ion allowing reduction of 30+ charges in one attachment. An additional benefit is that negative native complexes have lower average charge states compared to positive counterparts. This presented a challenge as the number density of the reagent was sufficient to push the m/z of the precursor outside the range of the mass spectrometer. Optimization of the concentration and injection conditions of the reagent ion were necessary to prevent signal loss for mass determination. Interestingly, when performing this reaction with the number density sufficient to eliminate the signal, native complexes can be observed by changing the polarity of the instrument to positive mode. In this work, we show the charge inversion of large native protein complexes from negative mode via ion attachment of denatured proteins. This experiment allowed for negative mode calibration at higher m/z values by comparing the charge inverted spectrum and a negative MAMA-MIA spectrum

5.2 Experimental

5.2.1 Materials

Sample preparation for native mass spectrometry of bio-complexes.

Beta galactosidase was purchased from Sigma Aldrich. The lyophilized solid was reconstituted in a 150 mM ammonium acetate (Sigma Aldrich) buffer to create a stock solution at a concentration of 10 µM (calculated by using the mass of the tetramer). The sample underwent adduct removal, via centrifugation, a minimum of four times with the same buffer adjusted to pH 7 using a 10 kilodalton (kDa) molecular weight cutoff (MWCO) Amicon Ultra 0.5 mL filter (Millipore Sigma). The recovered sample (17 µL) was diluted with the same buffer to achieve the same original concentration from the stock solution. GroEL (Sigma Aldrich) lyophilized powder preparation was described before in detail [85]

Reagent preparation

Myoglobin, carbonic anhydrase, proton sponge and cesium iodide were purchased from Sigma Aldrich. The lyophilized solid was reconstituted in 50:50 H_2O: Methanol with 1-5% glacial acetic acid at 10 µM concentration. Denaturing conditions were used to ensure higher charge state formation. Cesium iodide and proton sponge were dissolved in water at concentration of 1 mg/mL

5.2.2 Mass Spectrometry

All experiments were performed on a TripleTOF 5600 hybrid QqTOF mass spectrometer (SCIEX, Concord, ON, Canada) which was previously modified for ion/ion reactions.[86] Alternatively-pulsed nano-electrospray ionization (nESI) allows for sequential injection of multiply deprotonated protein complexes and multiply protonated reagent proteins.[87] Deprotonated analyte protein complexes were sprayed under native conditions and isolated in q2, using stored waveform inverse Fourier transform (SWIFT) isolation. Reagent proteins were isolated in Q1. The reagent proteins were sprayed under denatured conditions and were transferred to q2 for mutual storage with analyte protein complexes. The ions were stored for 5-50 milliseconds in q2 for gas phase ion/ion reactions.[42] Mass analysis was performed using time-of-flight (TOF).

5.3 Results and Discussion

5.3.1 Cesium iodide for instrument calibration

Optimization of instrument parameters and solution conditions are vital to method development of gas-phase ion/ion reactions. It is also critical to maintain instrument calibration in both polarities are all applicable m/z values. As the McLuckey group explores larger biomolecules, we ae continuously pushing the limits of our instruments. A recent example of this is the wide mass to charge range needed for the MAMA-MIA reaction, where data can fall between 5,000 and 100,000 m/z. This raised a question of how well our instrument is calibrate these high m/z values?

CsI clusters were analyzed over these wide ranges in both positive mode and negative mode to determine mass accuracy.[86] In positive mode, clusters reached m/z values approaching 20,000 m/z engulfing the m/z values where native complexes and early MAMA-MIA products appeared. This allowed for confirmation of mass accuracy in the positive mode for the entire mass range. In

the negative mode the CsI cluster did not exceed m/z of 8,000 which is lower than the m/z of the native complex of pyruvate kinase. The spectrum of CsI taken in the negative mode is shown in **Figure 5.1**. This spectrum shows the need of an accurate measurement at higher m/z in the negative mode. Previously we showed proton transfer reactions as method to determine instrument limitations. In **Figure 5.2** I show ion/ion reaction between β-galactosidase and proton sponge. In this spectrum multiple proton transfer reactions with charge reduced peaks reaching an upper limit of 60,000. Unfortunately, attachment ions in the MAMA-MIA reaction can surpass this limit in the negative mode. Serendipitously when performing the MAMA-MIA reaction, the relative abundance of the 2nd attachment peak was significantly higher than the previous attachment and precursor. Due to the large disparity, it was suggested to check the positive mode while performing this reaction. Conveniently, the negative native complex had underwent a third and possible fourth attachment. This is shown in **Figure 5.3** where the entire charge state envelope of β-galactosidase is reacted with the 20+ charge state of myoglobin (denoted as myo) with detection in the positive mode. This spectrum shows a wide range of charge states in the positive mode. Using this spectrum and the negative mode MAMA-MIA spectrum shown in the previous chapter calibration was performed.

This experiment was repeated with a larger native complex GroEL (~800 kDa) and with a more highly charged reagent, 30+ charge state of carbonic anhydrase. This is shown in **Figure 5.4** where the partial charge state envelope of GroEL after two attachments and the entire envelope after three attachments are observed. The third attachment is like due to the presence of $[2CA+30H]^{60+}$species. This is shown in the **Figure 5.5** which shows the MS spectrum of carbonic anhydrase where small dimer (shaded in blue) can be observed. This dimer population is likely what leads to the third attachment.

This experiment shows that large native complexes can be charge inverted and these reactions can be used for instrument calibration even across polarity and wide m/z ranges.

5.4 Conclusions

In conclusion, charge inversion of negatively sprayed native complexes is possible via ion attachment. The resulting ions produced can be altered by changing the charge state of the reagent to influence product ion m/z. This method would be most beneficial to frequency-based instruments such as orbitraps which is m/z limited to several tens of kilodaltons.[88] This method

could be applied to reduce the m/z to within operating range of an orbitrap for high resolution analysis.

5.5 References

1. Betancourt, S.K., Canez, C.R., Shields, S.W.J., Manthorpe, J.M., Smith, J.C., McLuckey, S.A.: Trimethylation Enhancement Using 13C-Diazomethane: Gas-Phase Charge Inversion of Modified Phospholipid Cations for Enhanced Structural Characterization. Anal. Chem. 89, 9452–9458 (2017). https://doi.org/10.1021/acs.analchem.7b02271

2. Shih, M., McLuckey, S.A.: Ion/ion charge inversion/attachment in conjunction with dipolar DC collisional activation as a selective screen for sulfo- and phosphopeptides. Int. J. Mass Spectrom. 444, 116181 (2019). https://doi.org/10.1016/j.ijms.2019.116181

3. Stutzman, J.R., McLuckey, S.A.: Ion/Ion Reactions of MALDI-Derived Peptide Ions: Increased Sequence Coverage via Covalent and Electrostatic Modification upon Charge Inversion. Anal. Chem. 84, 10679–10685 (2012). https://doi.org/10.1021/ac302374p

4. Stutzman, J.R., Luongo, C.A., McLuckey, S.A.: Covalent and Non-covalent Binding in the Ion/Ion Charge Inversion of Peptide Cations with Benzene-disulfonic Acid Anions. J. Mass Spectrom. JMS. 47, 669–675 (2012). https://doi.org/10.1002/jms.2968

5. Randolph, C.E., Shenault, D.M., Blanksby, S.J., McLuckey, S.A.: Localization of Carbon–Carbon Double Bond and Cyclopropane Sites in Cardiolipins via Gas-Phase Charge Inversion Reactions. J. Am. Soc. Mass Spectrom. 32, 455–464 (2021). https://doi.org/10.1021/jasms.0c00348

6. Randolph, C.E., Shenault, D.M., Blanksby, S.J., McLuckey, S.A.: Structural Elucidation of Ether Glycerophospholipids Using Gas-Phase Ion/Ion Charge Inversion Chemistry. J. Am. Soc. Mass Spectrom. 31, 1093–1103 (2020). https://doi.org/10.1021/jasms.0c00025

7. Prentice, B.M., McLuckey, S.A.: Gas-phase ion/ion reactions of peptides and proteins: acid/base, redox, and covalent chemistries. Chem. Commun. 49, 947–965 (2013). https://doi.org/10.1039/C2CC36577D

8. Abdillahi, A.M., Lee, K.W., McLuckey, S.A.: Mass Analysis of Macro-molecular Analytes via Multiply-Charged Ion Attachment. Anal. Chem. 92, 16301–16306 (2020). https://doi.org/10.1021/acs.analchem.0c04335

9. Xia, Y., Chrisman, P.A., Erickson, D.E., Liu, J., Liang, X., Londry, F.A., Yang, M.J., McLuckey, S.A.: Implementation of Ion/Ion Reactions in a Quadrupole/Time-of-Flight Tandem Mass Spectrometer. Anal. Chem. 78, 4146–4154 (2006). https://doi.org/10.1021/ac0606296

10. Xia, Y., Liang, X., McLuckey, S.A.: Pulsed dual electrospray ionization for In/In reactions. J. Am. Soc. Mass Spectrom. 16, 1750–1756 (2005). https://doi.org/10.1016/j.jasms.2005.07.013

11. Xia, Y., Wu, J., McLuckey, S.A., Londry, F.A., Hager, J.W.: Mutual storage mode ion/ion reactions in a hybrid linear ion trap. J. Am. Soc. Mass Spectrom. 16, 71–81 (2005). https://doi.org/10.1016/j.jasms.2004.09.017

12. Hecht, E.S., Scigelova, M., Eliuk, S., Makarov, A.: Fundamentals and Advances of Orbitrap Mass Spectrometry. In: Encyclopedia of Analytical Chemistry. pp. 1–40. American Cancer Society (2019)

5.6 Figures

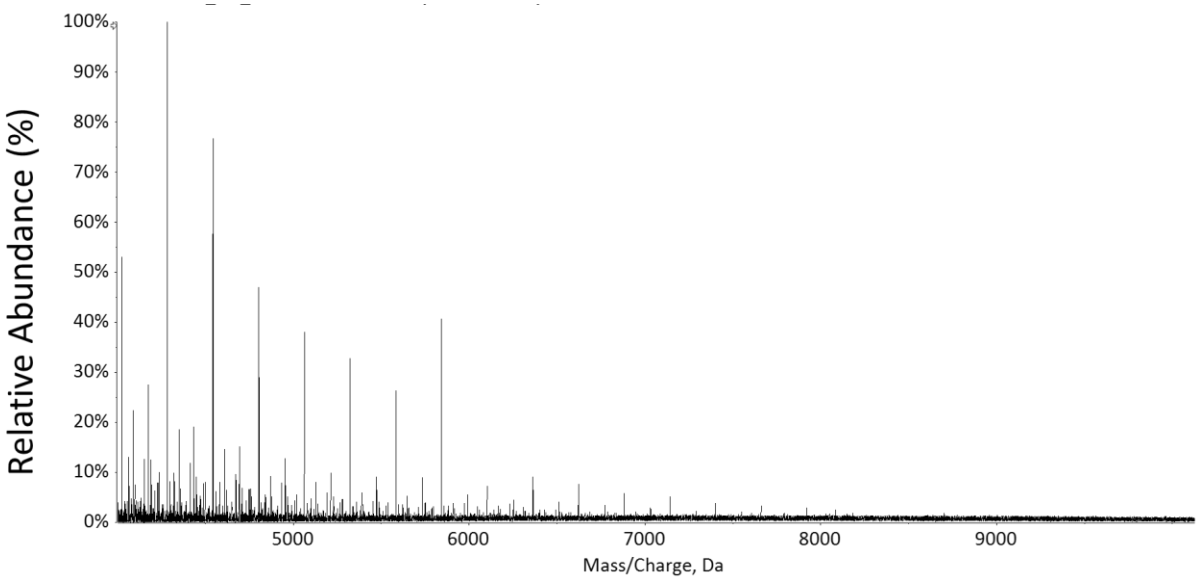

Figure 5.1 A MS spectrum of CsI in the negative mode

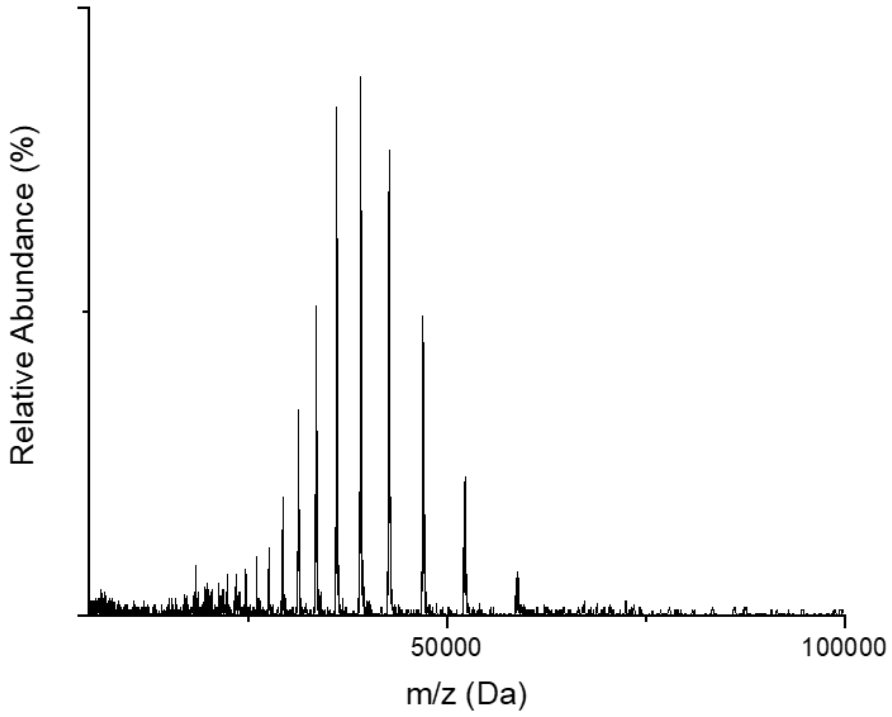

Figure 5.2 A spectrum showing a proton transfer reaction between beta galactosidase and proton sponge

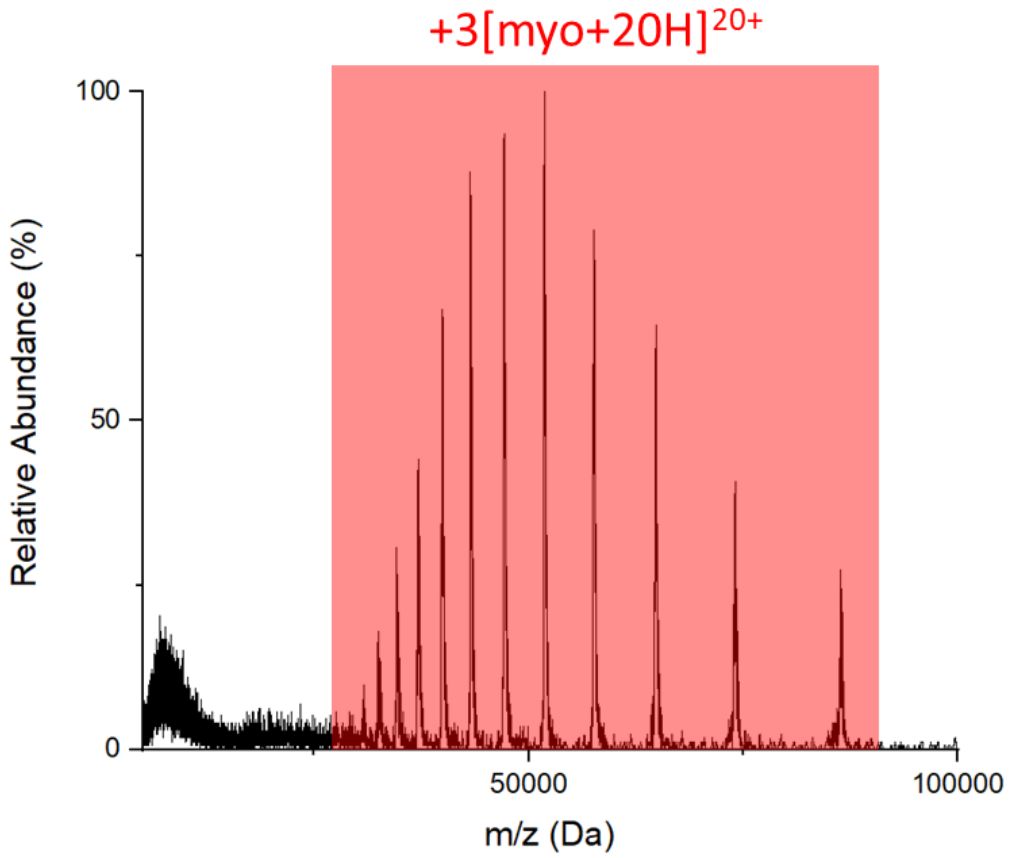

Figure 5.3 A spectrum showing the entire charge state charge inverted Beta Galactosidase after three attachments (shaded in red) of [myoglobin+20H]$^{20+}$

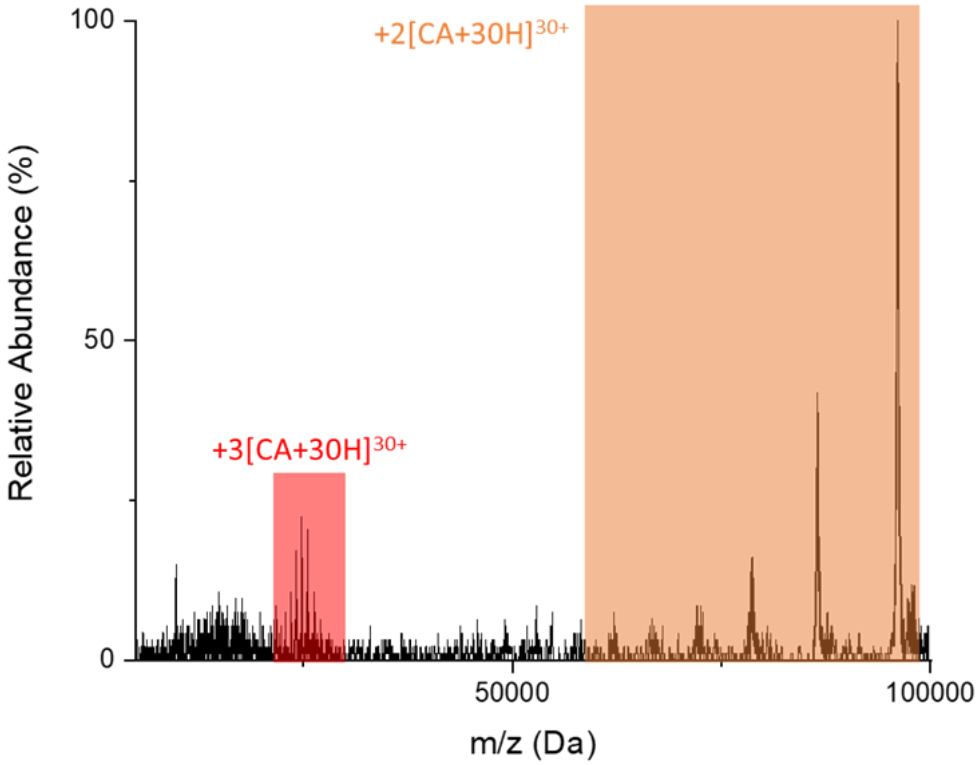

Figure 5.4 A spectrum showing charge inverted GroEL after two (shaded in orange) and three attachments (shaded in red) of [carbonic anhydrase+30H]$^{30+}$

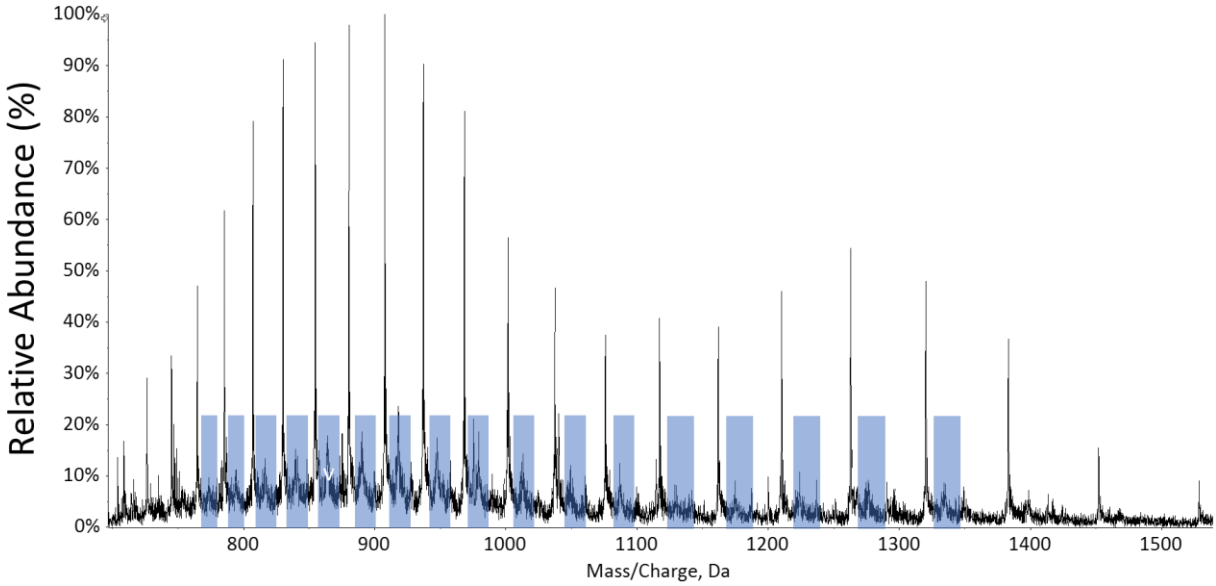

Figure 5.5 Shows the MS spectrum of carbonic anhydrase with dimer peaks shaded blue

LIST OF PUBLICATION

Pitts-McCoy, A. M.; Harrilal, C. P.; McLuckey, S. A. Gas-Phase Ion/Ion Chemistry as a Probe for the Presence of Carboxylate Groups in Polypeptide Cations S.A. *J. Am. Soc. Mass Spectrom.* **2019**, 30: 329.

VITA

Education

Purdue University West Lafayette, IN

Doctor of Philosophy, Chemistry Aug 2016 – May 2021

PI: Scott A. McLuckey

Thesis title: *Development of Gas-Phase Ion/Ion Reactions for Crosslinking and Structural Elucidation of Proteins and Peptides*

- Developed novel gas-phase ion/ion reactions to characterize the structures of small peptides and proteins using mass spectrometry. Performed numerous fragmentation/activation studies on proteins with masses ranging from sub kDa to MDa. This work allows for mass assignment of native protein complexes, charge reduction to deconvolute spectra, and high mass instrument calibration.

- Developed gas-phase ion/ion methods using click chemistry reagents to locate salt bridged structures in peptides and proteins on modified Sciex 4000 triple quadrupole and Sciex 5600 TripleTOF platforms. Worked to bring new technologies to these platforms to expand capabilities for more complex experiments. Mentored younger students by teaching instrumentation, experimental design, and troubleshooting skills. Led collaboration with several groups to analyze unique and challenging protein and peptide samples.

Chicago State University Chicago, IL

Bachelor of Science, Chemistry (ACS)

PI: Kristy Mardis, Robert LeSuer Aug 2013 – Dec 2015

Research Experience

S.C. Johnson Racine, WI)

RD&E Intern Managers: Christine Casper; Deborah Parker Jun 2020 – Aug 2020

- Worked with a team of scientists to quickly gain an enhanced understanding of a complex problem preventing a product launch. Drafted an annotated bibliography accumulating literature and discussing possible solutions. Virtually advised an associate level chemist, developed hypotheses to test, and designed relevant experiments.

- Employed Hansen Solubility Parameters in Practice Software (HSPIP) software to obtain the physical properties of compounds of interest and added these components to a shared database for internal use. This database can be used to search for compounds with specific properties or functional groups

University of Sao Paulo Sao Paulo, BR

Research Student PI: Claudimir Do Lago May 2016 – Aug 2016

- Evaluated a novel detection method, Capacitively Coupled Contactless Conductivity Detector (C^4D) capillary electrophoresis mass spectrometry, by demonstrating the separation and detection of isometric sugars. Worked to evaluate the performance of a stand-alone capillary electrophoresis C^4D platform. Collaborated with multiple scientists at undergraduate and graduate levels to learn and understand research performed in the lab and its significance.

- Wrote and presented a final report containing compiled results, broader impacts, and my suggestions for future directions.

Argonne National Laboratory Lemont, IL

Science Undergraduate Laboratory Internship Intern PI: Maria De La Cinta Jan 2016 – May 2016

- Prepared and tested oil samples of various viscosities containing various nanoparticle composition. The obtained data was used to model the amount of protection from wear to engines. This work was performed in the materials division within a tribology group working to incorporate nanoparticles to form protective films.

- Utilized microscopy techniques to visualize the nanoparticle protective films that formed under stress. This stress was induced utilizing a metal ball sliding along a metal flat system with an oil sample in between. This allowed for measurement of the amount wear on the ball and the flat independently and determine the effectiveness of the sample.

Chicago State University Chicago, IL

Minority Biomedical Research Support – Research Initiative for Scientific Enhancement Research Student PI: Kristy Mardis Aug 2014 – Dec 2015

- Investigated a novel Ni catalyst system to predict the catalytic reactivity of hydrogen oxidation using Density Functional Theory (DFT) models. Built and accessed computational models using PQSMol Software on a Linux based system.

- Presented data to supervisor on a weekly basis, as well as presenting project at Annual Biomedical Research Conference for Minority Students (ABRCMS). Data and methods were included in a publication listed below

University of Illinois at Chicago Chicago, IL

Undergraduate Research Student PI: Brian Chaplin June 2015 – Aug 2015

- Studied a novel titanium superoxide material as a reactive electrochemical membrane to remove nitrate from water sources as a potential filtration system.

- Analyzed water samples daily to determine the concentration of nitrate after diffusion through the membrane. Data was compiled and presented at the end of internship to peers.

Publications

- **Pitts-McCoy, A. M**.; Harrilal, C. P.; McLuckey, S. A. Gas-Phase Ion/Ion Chemistry as a Probe for the Presence of Carboxylate Groups in Polypeptide Cations S.A. *J. Am. Soc. Mass Spectrom.* **2019**, 30: 329.

- Niklas, J.; Westwood, M.; Mardis, K. L.; Brown, T. L.; **Pitts-McCoy, A. M.**; Hopkins, M. D.; Poluektov, O. G. X-Ray Crystallographic, Multifrequency Electron Paramagnetic Resonance, and Density Functional Theory Characterization of the $Ni(P^{Cy}{}_2N^{tBu}{}_2)_2^{n+}$ Hydrogen Oxidation Catalyst in the Ni(I) Oxidation State. *Inorg. Chem.* **2015**, *54* (13), 6226–6234.

Teaching Experience

Purdue University

STEM Boot Camp Teacher — June 2017 – Aug 2017

- Designed and taught an introductory class for incoming freshman to prepare them for college level chemistry courses.

Teaching Assistant (CHEM 112, CHEM 115) — Aug 2016 – May 2017

- Taught four recitation and laboratory sections of general chemistry.
- Utilized interactive presentations to assist students with visualization of difficult material. Promoted a safe laboratory environment for students and myself

Chicago State University

Learning Assistant (General Chemistry II) — Aug 2015 – Dec 2015

- Assisted professors in conveying general concepts to students during classes, led study sessions to assist students understanding.
- Provided in-depth suggestions on class activities by reviewing them prior to class to ensure that match students ability and were easy to understand.

Center for STEM Education and Research Student Peer Mentor — Aug 2014 – Dec 2014

- Tutored five to seven students per week for approximately fifteen hours in several subjects including General Chemistry, Organic Chemistry, and Physics.
- Assisted students in understanding as well as retention of major concepts present in these courses.

Presentations

1. **Anthony Pitts-McCoy,** Kwame Brown, Scott A. McLuckey (2019) *Gas-phase Crosslinking of Non-Covalent Protein Complexes via Ion/ion Reactions,* 46th Annual Meeting of the National Org' for the Professional Advancement of Black Chemists and Chemical Engineers (NOBCChE), St. Louis, MO November 18-22nd

2. **Anthony Pitts-McCoy,** Christopher Harrilal, Scott A. McLuckey, Timothy Zwier (2018) *A Gas Phase Ion/ion Reaction Sensitive to the Presence of Zwitterions,* 16th Annual American Society for Mass Spectrometry (ASMS) Conference, San Diego, CA, June 3-7.

3. **Anthony Pitts-McCoy,** Ana Paula Castro, Lun Guo, Brian Chaplin (2015) *The study of nitrate removal from water using Ti_2O_7 reactive electrochemical membrane, 1*5th Annual Biomedical Research Conference for Minority Students (ABRCMS), Seattle, WA, November 11–14.

4. **Brown, Tiara, Pitts-McCoy, Anthony**, Niklas, J., Poluektor, O. and Mardis, K.L (2015) *Influence of ligand substitution on electronic properties in bis(diphosphine) nickel (I) catalysts used in hydrogen catalysis,* Division of Catalysis Science & Technology PAPER ID: 2140406, 249th ACS National Meeting, Denver, CO, March 22-26.

5. **Anthony Pitts-McCoy**, Kristy Mardis, Tiara Brown, and Jeremy Webb (2014) *Computational Investigation of the Effect of Ligand Substitution on the EPR Properties of a Nickel Catalyst*, 14th Annual Biomedical Research Conference for Minority Students (ABRCMS), San Antonio, TX, November 12-15.

Leadership

(Alliance for Graduate Education and Professoriate) AGEP Scholar

- Mentored an incoming graduate student and matriculating undergraduate student
- Host several professional development workshops for undergraduate students

Chemistry Diversity Initiative (CDI) (Purdue University)- University Recruitment Co-Chair

- A member of an initiative to increase diversity of Chemistry Department at Purdue.
- Increase exposure of graduate school to underrepresented minorities through visits at undergraduate institutions and offering mentorship to incoming minority students to improve retention.

- Leading recruitment efforts to expose students at minority serving institutions to the benefits of a graduate career at Purdue University in chemistry.

Vice President of Student Lead Chapter (Chicago State University)

- Organized meetings, volunteer opportunities and fundraisers to maintain student led chapter
- Compiled departmental resources available to students

"Applying to Graduate School and Choosing the Right Institution" Panel led at Chicago State University in Chicago, IL

Awards

Special Diversity and Inclusion in Chemistry Award	April 2019
ACS Division of Analytical Chemistry Undergraduate Award	January 2016
1st Place Poster Presentation, Center for Science Technology Engineering and Mathematics Education (STEM) and Research	January 2015

Memberships

American Chemistry Society (ACS) - *Student Member*

American Society of Mass Spectrometry (ASMS) -*Student Member*

National Org' for the Professional Advancement of Black Chemists and Chemical Engineers (NOBCChE) *Student Member*